ČESKÉ VYSOKÉ UČENÍ TECHNICKÉ V PRAZE

FAKULTA STROJNÍ

ÚSTAV AUTOMOBILŮ, SPALOVACÍCH MOTORŮ A KOLEJOVÝCH VOZIDEL

DISERTAČNÍ PRÁCE

1-D Model of Roots-type Supercharger

Ing. Pavel Brynych

Doktorský studijní program: *Strojní inženýrství*

Studijní obor: *Dopravní stroje a zařízení*

Školitel: Prof. Ing. Jan Macek, DrSc.

Disertace k získání akademického titulu “doktor”, ve zkratce “Ph.D.”

Praha 2019

Declaration of Authorship / Prohlášení o autorství

I hereby certify that this thesis has been composed by me and is based on my own work, using only the literature and sources listed in the bibliography.

Prohlašuji, že jsem disertační práci vypracoval samostatně, s použitím odborné literatury a pramenů uvedených v seznamu, který je součástí této práce.

In Prague/ V Praze dne: ....

Signature / podpis autora

Acknowledgements

First, I would like to thank to Prof. Ing. Jan Macek, DrSc. for his guidance and support during my research work. I appreciate greatly his valuable advices and critical comments during our consultations and his critique of the manuscript, which improved the thesis substantially.

I would like to thank all of my colleagues at the Center of Vehicles for Sustainable Mobility in Roztoky under guidance of Ing. Vojtěch Klír, Ph.D. for their support during supercharger tests.

Additionally, I would like to thank to our partners at test cell in ČZ Strakonice for their effort during preliminary test.

I would also like to thank to Ing. Antonín Mikulec for his corrections in the manuscript of the thesis.

Finally, I would like to express my appreciation to my girlfriend and to my family for their support and patience.

Annotation

Keywords: supercharger, Roots-type supercharger, 1-D simulation, calibration, 3-D analysis, pressure indication in moving volume, pressure pulses frequency analysis

This thesis describes 1-D model of a Roots-type supercharger. The model is based on comprehensive 3-D geometrical analysis of the supercharger components using 3-D CAD software. 1-D unsteady model of irreversible changes respecting real gas features was applied. 1-D simulation model was built in commercial software GT-Suite/GT-Power using its solver and basic components. The model was calibrated to measured data at different operating conditions and may be used for further supercharger description and optimization. Values of the supercharger chamber pressure obtained during simulations were compared to measured data and analyzed by frequency analysis. Results of this analysis can be used as an input for supercharger NVH optimization.

Anotace

Klíčová slova: mechanicky hnané dmychadlo, Rootsův kompresor, 1-D simulace, kalibrace, 3-D analýza, indikace tlaku v pohybujícím se objemu, frekvenční analýza tlakových pulsací

Práce popisuje jednorozměrný model Rootsova dmychadla. Model byl postaven na základě obsáhlé prostorové analýzy součástí dmychadla s využitím software umožňující 3-D modelování. Poté byl použit 1-D nestacionární model nevratných změn respektující reálný plyn. 1-D model dmychadla byl postaven v komerčním 1-D simulačním nástroji GT-Suite/GT-Power s využitím jeho kódu a základních component. Model byl dale kalibrován na naměřená data v různých provozních režimech a může být použit pro další popis a optimalizace dmychadla a jeho chování. Průběh tlaku v pracovním objemu dmychadla získaný ze simulací byl porovnán s naměřeným průběhem a podroben frekvenční analýze. Výsledky této analýzy mohou být využity při optimalizaci hluku, kterým je provoz dmychadla doprovázen.

Contents

List of Figures

List of Tables

Nomenclature

Roman Symbols

Symbol	Meaning	Unit
A	Area (cross-sectional)	[m^2]
C	Skin Friction Coefficient	[1]
dx	Length of Mass Element	[m]
dp	Pressure Differential	[kPa]
D	Equivalent Diameter	[m]
e	Total Internal Energy	[J]
h	Heat Transfer Coefficient	[$W/m^2.K$]
H	Total Enthalpy	[J]
m	Mass of the Volume	[kg]
$\dot{m}$	Boundary Mass Flux into Volume	[kg/h]
n	Supercharger Speed	[rpm]
p	*P*ressure	[kPa]
s	Equivalent Speed	[rpm]
t	Time	[s]
T	Temperature	[K]
u	Velocity at the Boundary	[m/s]
V	Volume	[m^3]

Greek Symbols

Symbol	Meaning	Unit
α	Angular Position	[deg]
γ	Clearance Ratio	[1]
η	Efficiency	[1]
ρ	Density	[kg/ m^3]

Subscripts

Symbol	Meaning
c	Clearance
e	Equivalent
f	Skin Friction
g	Inter-teeth Gap
p	Pressure Loss
s	Heat Transfer Surface

Acronyms

Acronym	Meaning
1-D	One-dimensional
3-D	Three-dimensional
AVL	Anstalt für Verbrennungskraftmaschinen
CAD	Computer Aided Design
CO	Carbon Monoxide
CVT	Continuously Variable Transmission
EGR	Exhaust Gas Recirculation
FC	Frequency Converter
HCCI	Homogeneous Charge Compression Ignition
NO_x	Nitrogen Oxides
NVH	Noise, Vibration and Harshness
PCCI	Partially Premixed Charge Compression Ignition
PID	Proportional-Integral-Derivative Controller
VGT	Variable Geometry Turbine
VNT	Variable Nozzle Turbine
SpCCI	Spark Controlled Compression Ignition
TSI	Turbocharged Stratified Injection

1 Introduction

Today, passenger car engine design follows approach of downsizing, downspeeding and the reduction of number of engine cylinders. Superchargers alone or their combination with turbochargers can fulfill low-end requirement on engine torque for such engines. Moreover, low temperature combustion of lean mixture at low engine loads is becoming popular (HCCI, PCCI) requiring high boost pressure of EGR/fresh air mixture at low exhaust gas temperature, which poses high demands on turbocharger efficiency.

Globally, there are many different types of devices, which can be used for boosting of an internal combustion engine [1]. A turbocharger is the most spread solution today. It uses exhaust gas enthalpy to drive the turbine wheel set on a common shaft with a compressor wheel. The turbocharger may be controlled by by-pass (wastegate), where a part of exhaust mass flow is not lead to the turbine wheel but flows through a parallel piping of the engine. More sophisticated solution is application of variable nozzle turbine (VNT) also called variable geometry turbine (VGT). The swallowing capacity is automatically varied according to engine load at this device. This allows turbine power to be set, providing sufficient energy to drive the compressor at the desired boost level according to engine operating condition. This is achieved by varying the area of nozzle – a set of guide vanes that control the exhaust gas flow through the turbine. The advantage of VGT in comparison to the wastegated turbine is improved transient response, increased useful engine operating speed range and reduced fuel economy due to higher turbine efficiency. Under development is electrically assisted turbocharger which would couple the advantages of a supercharger i.e. fast response at low engine speed and the advantages of a turbocharger.

A supercharger is the next possible solution for combustion engine boosting. The supercharger is a compressor typically driven directly from the engine crankshaft via belt or a gear drive. There are two main categories of mechanically driven superchargers, centrifugal and positive displacement devices. Centrifugal supercharger is centrifugal compressor with very high step up gear ratio. The reason for that is that centrifugal compressor works at much higher speeds than an internal combustion engine. A system with continuously variable transmission (CVT) for better

control of supercharger speed has been developed and tested but it has been put aside of practical use because of very poor mechanical efficiency and thus very high input power [2].

2 Overall Survey

2.1 Roots-type Supercharger

The Roots-type supercharger is the most famous representative of positive displacement, two-rotor blowers with outer compression [3]. Roots blowers, invented by G. Jones in Birmingham, England in 1848, were re-invented in 1854 by the P.H. & F.M. Roots of Connersville, Indiana, now bearing their name [4]. They became well known ever since Gottlieb Daimler filed the first supercharger patent in the late 19th century, making Roots the oldest and most widely used supercharger in automotive engines until turbocharger took its place. However, Roots superchargers are still popular for many different types of 2-stroke and 4-stroke cycle engines, both gasoline and diesel.

The charge is delivered to the inter-teeth space at pressure in charger inlet and its compression occurs after the inter-teeth volume (positive displacement chamber) is connected to outlet piping [3]. At that moment, the delivered gas is compressed by an abrupt pressure increase caused by backflow of gas compressed during previous cycles. The chamber volume change needed for gas suction from inlet and delivery to outlet port is ensured by insertion of opposite rotor tooth into positive displacement chamber, which is ensured by rotation of two rotors with parallel axes in two intersecting cylinders machined in supercharger body (***Figure 2-1***). The rotors are separated from the cylinder wall by small clearance (in the range of 0.0015R – 0.0025R, where R is equals to rotor radius). Since there should be no meshing contact between rotors, two high-precision gears are used for synchronization of movement of rotors. Rotors rotate in opposite direction and control timing of flows by connecting positive displacement chamber to inlet and outlet ports. These ports are sized as a result of compromise – they should have large cross section to enable entering and expelling of gas without high pressure losses on one side and avoiding the inlet and outlet port connection and backflow occurrence at the other side.

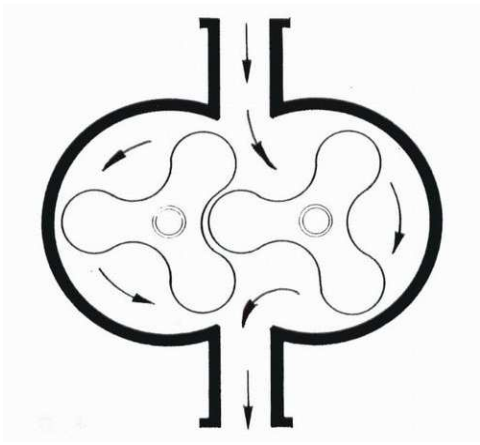

Figure 2-1: *Roots-type blower process [5]*

Because of absence of rotors contact, no lubrication is needed, which is a great advantage of this blower type for purposes, where the transport of clean gas without any contamination is needed. Additional advantage of the Roots blower is its reliability and durability due to simple design. The disadvantages are caused by low isentropic efficiency due to abrupt compression in inter-teeth space and internal leakages. The abrupt compression causes high noise. Moreover, the internal compression in inter-teeth gaps, while both teeth lobes are in contact in meshing zone, can cause additional power consumption. This phenomenon is well-known from gear pumps.

Smoother compression can be realized if helical gears and greater number of teeth are used instead of spur gears. In this case, movement of teeth contact in axial direction can change the volume of inter-teeth gap compressing the gas while both inlet and outlet ports are still closed. Therefore, a large amount of development work was devoted in the past to screw supercharger (Lysholm compressor) with continuous compression [6][7][8]. Since the screw type has internal compression different from the roots type, the screw type shows high efficiency at high pressure ratio. However, it shows significant power loss when pressure is not required. Such a parasitic loss becomes larger with increasing built-in pressure ratio. But several solutions how to minimize power loss are available. A clutch can be used for example to shut-off the compressor at the moment when pressure is not needed. More convenient solution is a variable speed system (VSS), which aims to limit the loss by reducing supercharger speed when the boosting is not required. However, at high

speeds the belt slip causes poor speed control and large friction loss (about 10% reduction of the maximum total adiabatic efficiency). Another popular control method for effective reduction of driving work at an industrial screw compressor is the variable geometry system (VGS) which releases a certain portion of inlet air before start of compression. Discharge bypass system is simple with high reliability since the supercharger is set only at low built-in pressure ratio [8]. The main difference between the Roots and screw superchargers consists in internal compression between rotors of the screw compressor while Roots blower processed air like a pump only without any internal compression [9]. The operation of both machines is obvious from picture below (***Figure 2-2***). New concept of helical gear Roots-type compressor, used since 90's, combines features of both designs.

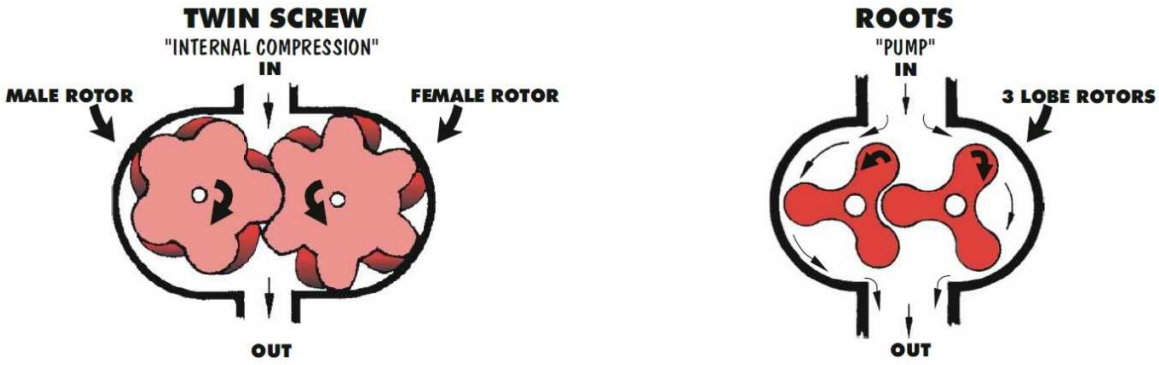

Figure 2-2: *Roots vs. screw compressor operation comparison [9]*

Air enters the screw supercharger through the top rear and is compressed internally between the rotors. The male rotor rotates clockwise while the female rotor rotates counter clockwise trapping and compressing air between them and "screwing" air to discharge (***Figure 2-3***).The shortest and smoothest path between two orifices (inlet and outlet) is always the best for optimum air flow. While at Roots blower air is pumped circumferentially between the supercharger case and rotors. All this surface area (rotors and case) coupled with the relatively long "torturous" air path creates more turbulence, friction, heat and pumping (power) losses than the screw compressor. That is why, the Roots is clearly not as efficient as the "screwer".

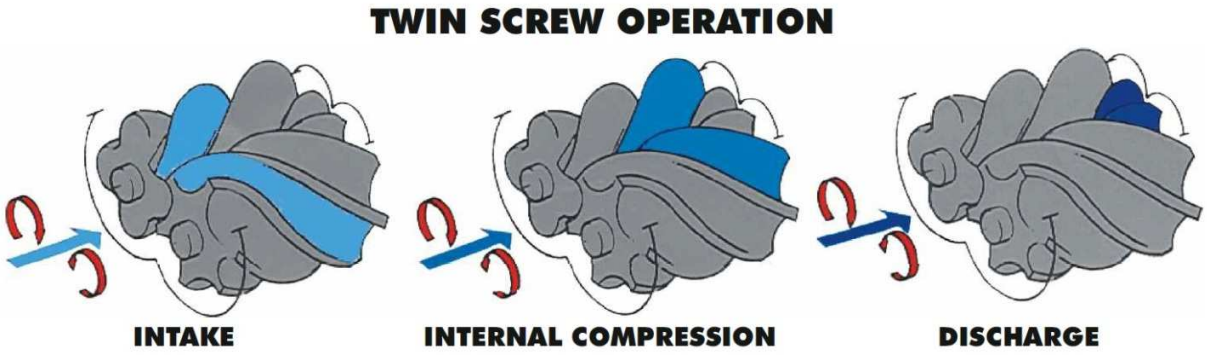

Figure 2-3: *Screw compressor operation [9]*

Concerning automotive use, production of the first cars using engines supported by Roots superchargers started in 1922 with 6/25 PS and 10/40 PS models at Mercedes-Benz company. These models have been later followed by the worldwide famous S, SS and SSK sport-models. In 1995 Mercedes-Benz started new period of using Roots superchargers on its engines [10]. A few years later, in 2008, Volkswagen brought its TSI (Turbocharged Stratified Injection) concept into the production. The TSI engines combine the benefits of both petrol and diesel power units. It is also the first engine using a combination of supercharger and turbocharger for boosting. That means the engine is charged by a supercharger in addition to the turbocharger depending on the torque requirements. The main advantage of using Roots-type supercharger instead of turbocharger are faster build-up of boost pressure, high torgue at low engine speed, only activated when required, no external lubrication and cooling is necessary. Disadvantage is the drive power required from engine crankshaft [11][12]. The Roots blower is very popular also in aftermarket and very often used as supercharger for internal combustion engines adapted for use in race cars.

2.2 Supercharging for New Combustion Processes

In the recent past, environmental problems have been taken up widely in the world and in the automobile industry as well. The demand for drivability is strong and compatibility of high power with low fuel consumption and clean exhaust gas is highly desired. As one of the suitable solutions, a supercharged engine has occurred in the market because of its fast load-change response and faster warming-up of a simple exhaust system unlike in the case of a turbocharged engine. There are big advantages of supercharged engines, especially in the case of small number of cylinders

since the non-uniform pressure pulses lower the turbine efficiency significantly if turbocharger is used.

Furthermore, new combustion processes of lean mixture at low temperature (Homogeneous Charge Compression Ignition – HCCI; Partially Premixed Charge Compression Ignition - PCCI) are elaborated deeply today with both diesel and spark ignition engines [13]. The main advantage of such combustion processes is very low emission of soot and NO_x whereas thermodynamic efficiency increases due to reduced heat transfer into cylinder walls during combustion and higher ratio of specific heats at constant pressure and volume due to lean mixture and low flame temperature. As is obvious from ***Figure 2-4***, the emissions of soot and NO_x are very low during combustion of a lean mixture at low temperatures. At HCCI, the mixture of fresh air, fuel and recirculated exhaust gases is ignited as a result of compression and heating of the mixture during the compression stroke. The combustion at low temperature decreases the heat transfer into the cylinder wall and thus increases the thermodynamic efficiency.

Should HCCI be implemented, a large amount of fresh air in engine cylinder at start of compression, i.e., high boost pressure, is needed due to lean mixture and massive EGR, required for ignition delay reduction. Mass of fresh air trapped in the cylinder should be much greater than in the case of a standard engine. Since cycle peak temperature is low, the exhaust gas temperature is reduced as well and the enthalpy head on turbocharger turbine is not sufficient to drive compressor unless a very high exhaust manifold back pressure is used. The exhaust manifold backpressure, needed to cover turbine power, increases pumping work and may eliminate the advantages of low-temperature combustion. Moreover, the mentioned low temperature combustion processes of lean mixture are used at low-end torque, where the boost pressure would be too low and a turbine needs closing the stator vanes, which results in reduction of turbine efficiency and increases all mentioned issues. For all these reasons, there is a need for a high efficient supercharger used separately or in combination with a turbocharger, which would cover the boost pressure lack of a turbocharger [14].

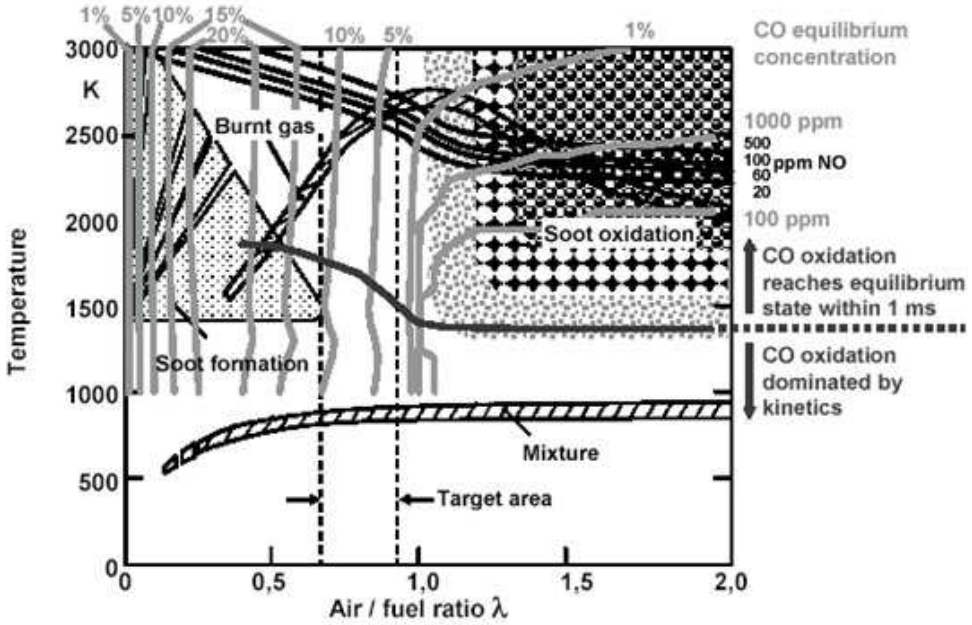

Figure 2-4: *Soot and NOx emissions depending on mixture richness and temperature of combustion [13]*

New engine released by Mazda Motor Corp. in 2018 called Skyactiv-X is using Spark Controlled Compression Ignition (SpCCI). The SpCCI system is the culmination of more than eight years of intensive development by Mazda to design a gasoline engine that embraces the economy and torque of a diesel with the high-revving capacity of a twin-cam gasoline unit, while delivering sub-60 g CO2/km emissions. Adding to the attraction, SpCCI requires relatively minimal investment in the engine bill of materials - electronic controls and a revised cylinder head comprise the major changes [15]. SpCCI's air-fuel mixture is created by two-phase, split injection on the intake and compression strokes. A strong swirl is created in the combustion chamber to create an intentionally uneven distribution of fuel density, with a lean mixture around the periphery for CI and a relatively rich air-fuel mixture around the spark plug in the center-conducive to creating the fireball. A key to Mazda's achievement for the production engine is an accurate control of the combustion process. The SpCCI engine uses pressure sensors in each cylinder to enable real-time temperature and pressure monitoring, in addition to other engine parameters. The engine-management system controls the twin electrically-variable camshafts, the new split-injection strategy that operates at

500 bar (7252 psi) and the air pump. The latter is a unique Roots-type device engineered by Eaton Corp. for the Mazda SpCCI application which helps to deliver enough air into the cylinder for generation of lean mixture. The supercharger is not engaged for achieving low-end torque or peak power but helps in generation of appropriate air-fuel mixture.

2.3 Roots-type Supercharger Acoustic Models

Supercharging of V6 or V8 engine may be provided by highly integrated module with a Roots-type blower placed inside the V (***Figure 2-5***) [16]. Next to the Eaton Roots-type supercharger (Generation 6, R1320) there is a one cross-flow intercooler per cylinder bank. The supercharger drive is coupled with engine crankshaft by way of torsion spring to improve dynamic response. Dealing with compressor acoustics is a prerequisite for meeting the noise requirements in the premium vehicle class. For the first time a model has been developed for simulating the highly complex compressor airflow in the rotor group. With the design of the rotors, the intake cross-sections and the blowholes that were finally selected, there are no significant pressure peaks at the outlet from the rotor. This leads to low primary excitation in the vehicle and reduces expenditure on secondary acoustic measures (***Figure 2-6***).

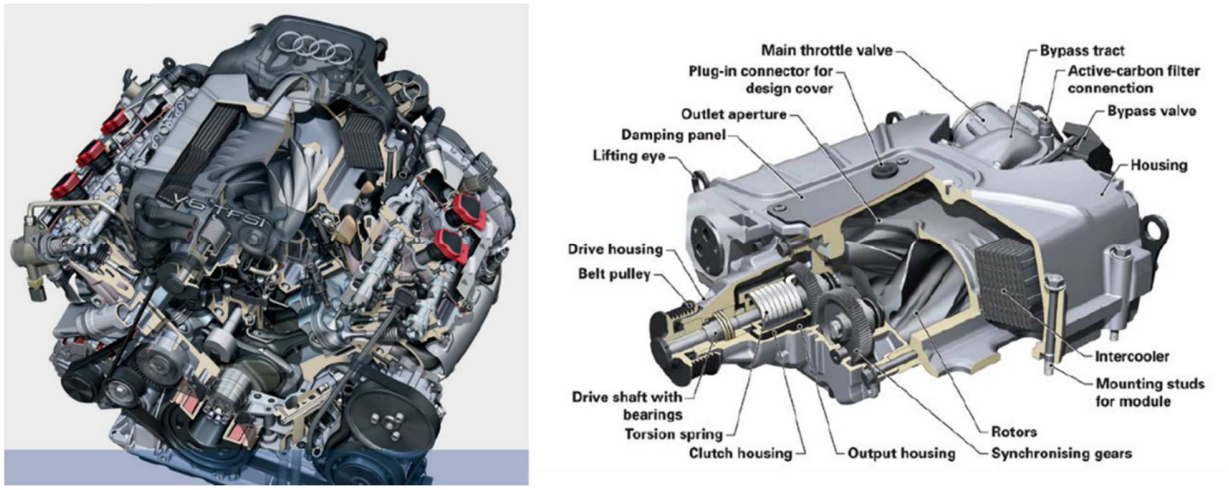

Figure 2-5: *Audi 3.0l TFSI engine and the highly integrated supercharger modul including supercharger itself, intercooler, by-pass valve and further accessories [16]*

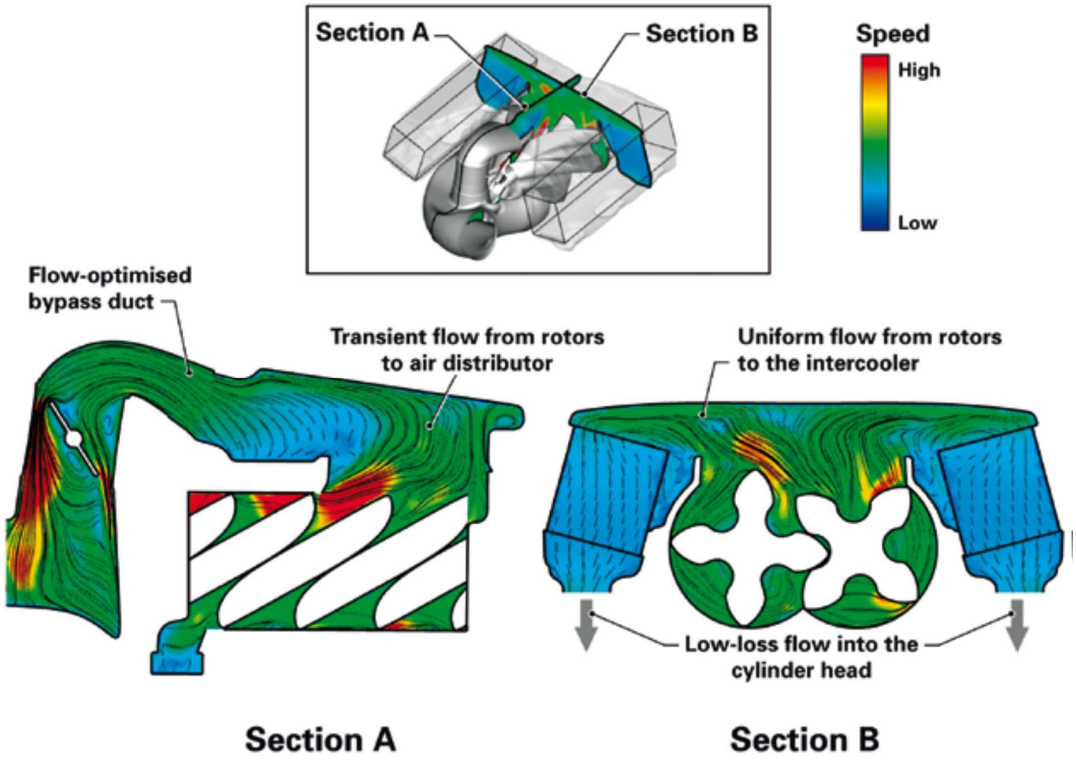

Figure 2-6: *Flow simulation in the supercharger module [16]*

Mechanical supercharger systems are widely regarded as problematic in terms of effective part-load consumption because of the required drive power of the compressor. This proved only partially true in the concept phase. By purposely positioning the main throttle valve upstream of the rotor unit, the effective specific fuel consumption can be significantly reduced. Throttling the supercharger unit results in a decrease in air density. This reduces the bypass mass flow while maintaining a constant volumetric flow through the compressor. The required drive power decreases (***Figure 2-7***). The comparative measurements relating to constant fuel consumption between the V6 twin-turbo and the V6 with mechanical supercharger indicated the same consumption figures with identical transmission configurations in the lower speed range. In the upper speed range the 3.0 l TFSI was actually more economical. The disadvantage of the V6 twin-turbo concept could only be offset by means of a modified supercharger design with a significant deterioration in responsiveness.

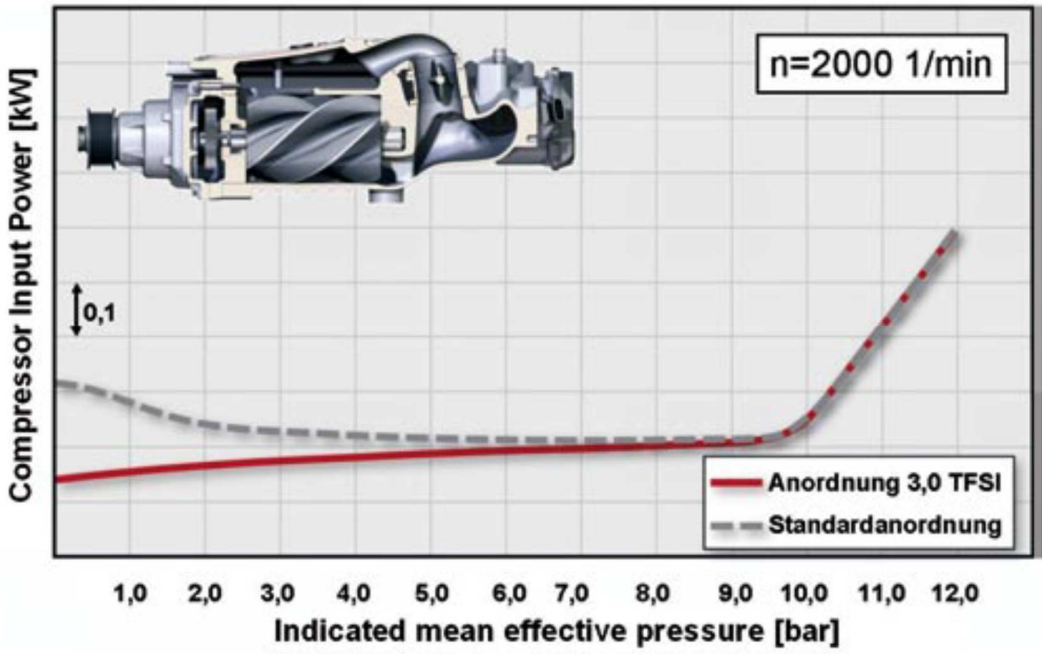

Figure 2-7: *Positioning of the main throttle valve upstream of the rotor unit in the Audi V6 3.0l TFSI [16]*

Mechanical supercharger is also a helpful tool for downspeeding a light duty diesel engine for a passenger car [17]. The twin sequential turbocharged engine had slightly lower full load BSFC values than the supercharged engines, but this slight penalty was easily overcome through vehicle downspeeding by matching performance of the twin turbo vehicle. Vehicle fuel consumption for the supercharger based boosting systems was 8-10% lower over the NEDC and 12-14% lower over the ARTEMIS (urban) cycle when compared to a twin sequential turbocharger boosting system on 1.6l inline-4 cylinder engine.

A huge amount of simulation and testing work have been devoted to limit the sound characteristic for Roots-type supercharger depending on its operating conditions [16]. It is well known that roots blowers inherently feature significant disadvantages with respect to noise generation [20]. The root cause being that the air, that is air trapped inside the volumes surrounding the lobes, is carried in discrete pulses. From this, a pulsation noise is generated at the inlet as well as the outlet port. The amplitude of these pulses is dependent of the size of the unit, number of lobes, rotation speed etc. and sound pressure levels larger than 150 dB can be observed at the outlet ports for high pressure

ratio load conditions. Here, the pressure ratio is defined as the ratio between the static pressure at the outlet and inlet ports. Installations in automobile applications require special treatment in order to meet the desired NVH refinement. Efficient countermeasures include fine tuning of the in- and outlet ports to reduce the strength of the sound source, passive silencer optimization to reduce sound level inside the surrounding ducts and material optimization or encapsulation to mitigate the radiated and transmitted sound. Careful tuning of Helmholtz passive style silencers based on multiple holes, slots and chambers is not suitable for modelling in 1-D when 3-D effects are present. A complete model, that is able to predict the final emitted sound, must include both the sound source and the propagation to be able to capture installation effects of the silencer elements. For the cases where only plane waves are considered the most simple source model that has the potential to represent a roots blower is the linear time invariant frequency dependent active one-port source model. The one-port assumption implies one-dimensional wave propagation and hence constant acoustical variables over the cross-section where the source is considered. A specific test bed in a semi anechoic environment developed for supercharger testing was used in the measurement campaign (***Figure 2-8***).

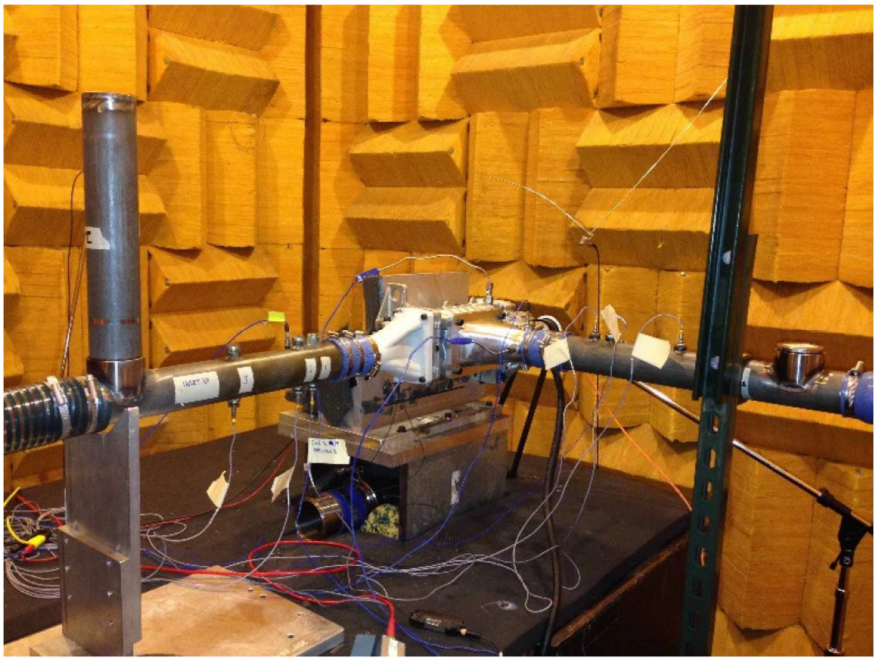

Figure 2-8: *Roots-type supercharger sound oriented measurement set-up [20]*

The acoustic load case that was chosen for the validation (side branch with length 0.63 m) was excluded in the computation of the source data (that was based on five acoustic load cases). The accuracy of the model is excellent, as can be seen in ***Figure 2-9***, and deviations are less than 1 dB in the entire speed range. It can be concluded that the linear time invariant one-port source model can be used for this specific roots blower with very good results.

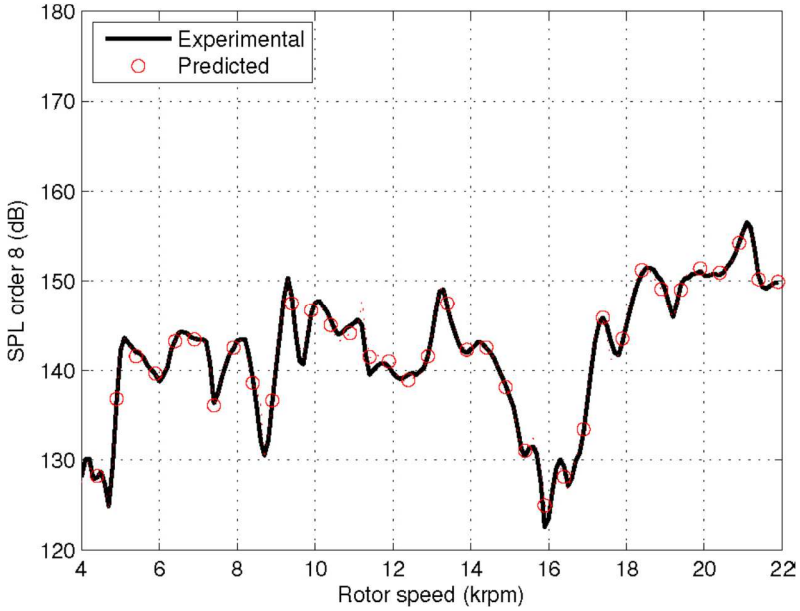

Figure 2-9: *Comparison of experimental and predicted sound pressure level at the inlet source position for the test set-up with acoustic load 6 on the inlet side at high boost conditions (pressure ratio 1.5) [20]*

Results published in the paper [20] show that it is possible to use a linear acoustic source model to represent a roots-type blower and that sound predictions can be performed with good accuracy.

Full system level modeling described in paper [21] is considered for dual boosting system of turbo-super configuration from an NVH perspective. The system level noise prediction is presented through one way Fluid Structural Interaction (FSI) simulation. For this full system, structural FE model (***Figure 2-10***) and duct model which is negative of the structural model is developed using acoustic FE in LMS Virtual Lab (3-D vibro-acoustic simulation tool). The results are then compared with the test data. This improved technique in intake acoustic modeling of a

supercharged engine is useful for accurate identification and ranking of noise radiating components in the full system considered from engine inlet to air box filter.

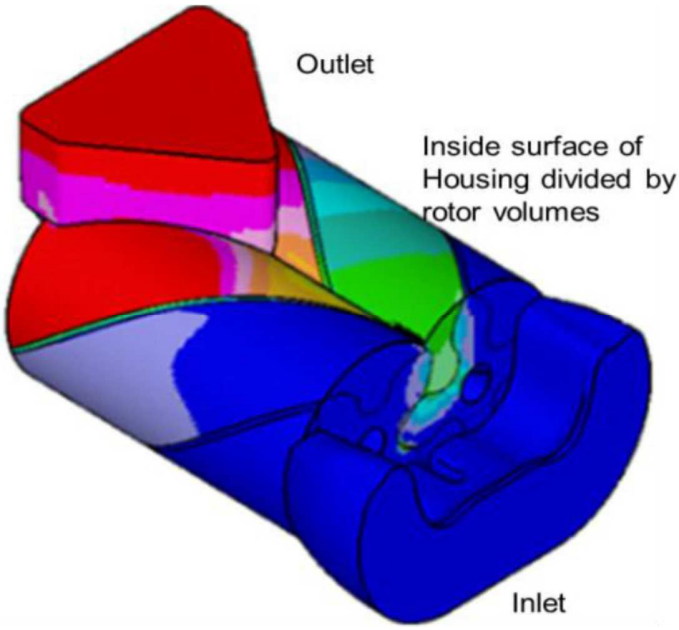

Figure 2-10: *Representation of supercharger volumes in FEM model [21]*

2.4 Leakage Model of Screw Supercharger

Detailed model is described depicting and analyzing leakage paths in a twin-screw supercharger in the reference [22]. This type of supercharger is very similar to the Roots one in this term. The leakages are determined by the clearances needed for the correct supercharger functionality. Several paths of leakage are present in the supercharger: across the contact line between the male and female rotors, across the sealing lines between the rotor tips and casing, through the blow hole, and through the clearance between the end plate and the rotor end face at the discharge end. As the supercharger performance is influenced more by the internal air leakages than by any other thermo-fluid aspect of its behavior, it is important to quantify the leakage rate through each leakage pathway [22] and after that to optimize rotor and housing design to minimize the leakage losses. CAD and CFD tools are used for the iterative process of design optimization (***Figure 2-11***).

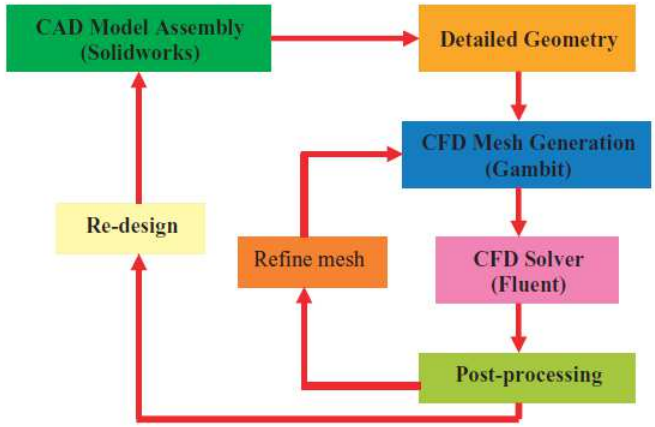

Figure 2-11: *CAD/CFD integration and optimization process [22]*

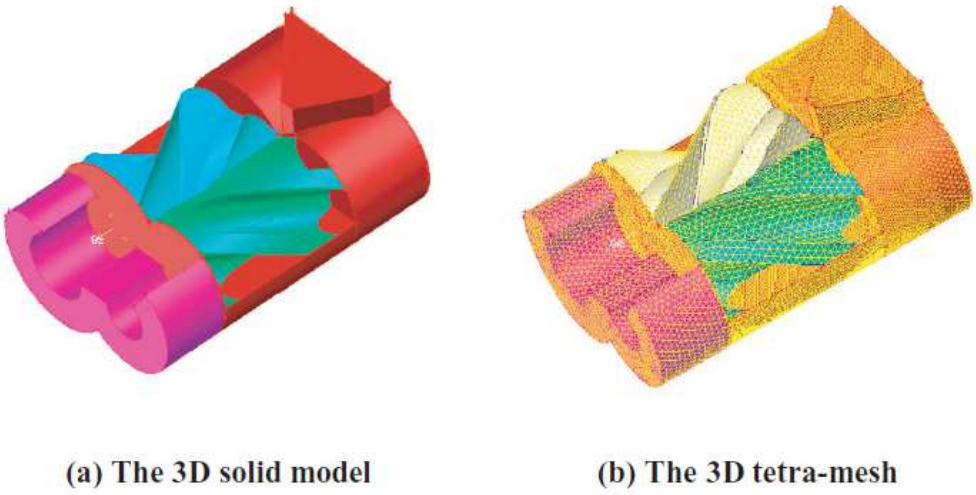

Figure 2-12: *3-D solid model and 3-D tetra-mesh of the supercharger [22]*

Leakage analysis is performed using the Fluent CFD package, which is employed to simulate the flow passage through the supercharger. The flow is simulated as a 3-D incompressible air using the Realizable k-ε turbulence model. ***Figure 2-13*** presents leakage flow behavior in the supercharger. ***Table 2-1*** presents the leakage flowrates through each leakage path in this model. The results show that Path 2 and Path 3 have a very important influence on the leakage distribution. Consequently, the improvement of a profile should concentrate on the following two aspects:

reducing the blowhole area by an asymmetric profile and reducing the leaking rates through Path 2 by optimizing the wrap angle of rotors.

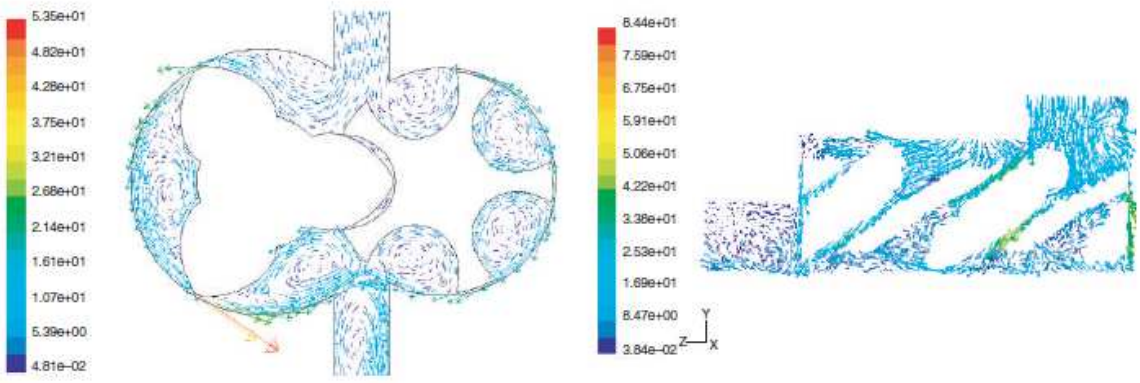

Figure 2-13: *Leakage flow behavior in the supercharger [22]*

Table 2-1: *Leakage flow rates through each leakage pathway in a supercharger [22]*

Leakage pathways	Leakage flow rate (kg/s)	%
Contact line (Path 1)	0.0015528	7.1
Sealing lines (Path 2)	0.0082927	37.8
Blowhole (Path 3)	0.0065058	29.6
End face (Path 4)	0.0055924	25.5

After the optimization of rotor design and taking into account above mentioned ideas, total leakage was reduced by 1,5% (absolutely). From this 1,5%, 1.2% is obtained by reducing the blowhole area and 0.3% is obtained by increasing the rotor wrap angle.

2.5 Supercharging of Two-Stroke Engines, Hybrids and Fuel Cells

Finally, two–stroke engines are being investigated increasingly due to their potentials in easy HCCI implementation, which may be reflected by reasonable efficiency and high specific power. In this case, there is a vital need to reach a positive pressure drop across the engine (i.e., the boost pressure higher than the backpressure) to allow two-stroke engine scavenging at low engine loads, where

exhaust gas temperature is low. Therefore, for the small two-stroke engines, the air system has to be supplemented by the mechanically driven supercharger and its power consumption is quite significant [13]. The supercharger is then coupled with turbocharger compressor in series and helps to cover the boost pressure drop in case of exhaust gas enthalpy decline. Moreover, unlike the pumping loop of a four-stroke engine, the work needed for reaching the positive pressure difference across the engine cannot be recuperated back to engine crankshaft but the supercharger power input has to be added to friction losses, changing thus gross brake power to the final net brake power. Thus, a sophisticated control of the turbocharger and supercharger is needed for that solution to limit the supercharger input power as much as possible and to use the turbocharger in a wide load-speed range. The comparison of indicated engine power and supercharger input power is plotted in ***Figure 2-14***. It is obvious that the supercharger power represents from 20% up to 30% of engine gross power. To minimize the supercharger power an efficient cooling of boosting air is needed also. Huge simulation and testing effort has been expended to car two-stroke diesel engine air loop optimization during the last eight years in the frame of two EU projects – Powerful (FP7), REWARD (H2020) [2], [13], [29].

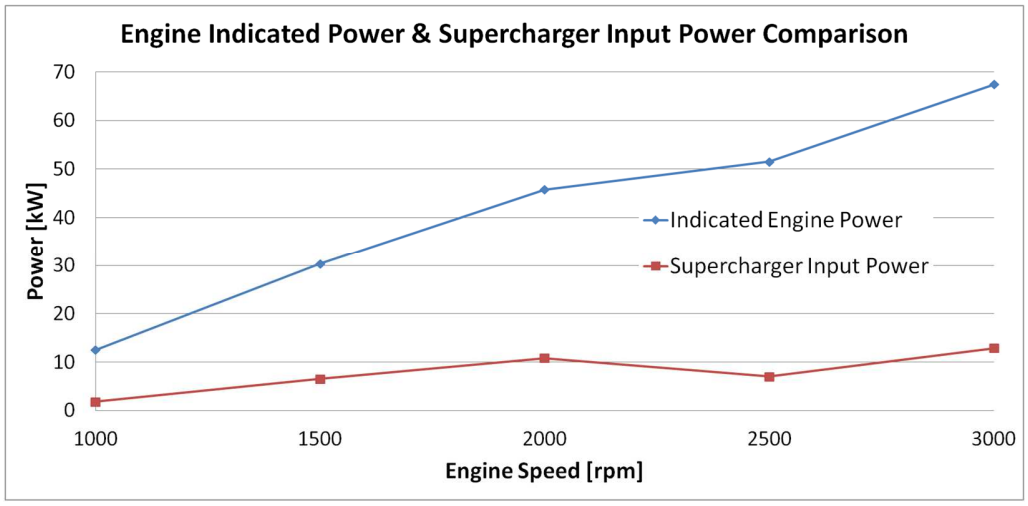

Figure 2-14: *Indicated engine power compared to supercharger input power in case of two-stroke diesel engine developed for small passenger car. The supercharger disposes of a shifted gearbox with two gear ratios, which are shifted depending on boost pressure need. [13]*

Concerning the global fight against climate changes a new concepts of car drives are investigated and developed. Especially hybridization of vehicle drives is increasing during a few last years. Different combinations of combustion engine and electrical motor are being more and more common. Roots-type supercharger may charge a combustion engine used as a range extender in a hybridized vehicle drive. Range extender is usually small high-loaded and thus highly boosted combustion engine used for driving electrical generator which charges electrical batteries used as a source of power for electrical motors. The engine is usually operating at only a few load points where efficiency of use of a supercharger may be optimized easily.

Next to hybrids using a battery as a stock of energy and source of power a hydrogen powered fuel cell vehicles are being investigated and functional solutions are already on the market [18]. The Roots-type supercharger serves there as a pump delivering air (oxygen) to the cathode of the fuel cell and may be used also as an expander (***Figure 2-15***), which may recuperate a part of compressor drive energy [19]. Eaton will modify the novel R340 Twin Vortices Series (TVS) roots-type supercharger for this application, which features slightly better performance than a centrifugal compressor/expander considering parasitic load, combined motor/motor controller efficiency, weight and volume. Roots-type compressor/expander system has a few issues. Plastic material used for rotors coating can potentially contaminate fuel. And the roots-type compressor has a limited pressure ratio and pulsation characteristics. Roots-type compressor/expander system has a potential to be competitive, but it needs further experimental development.

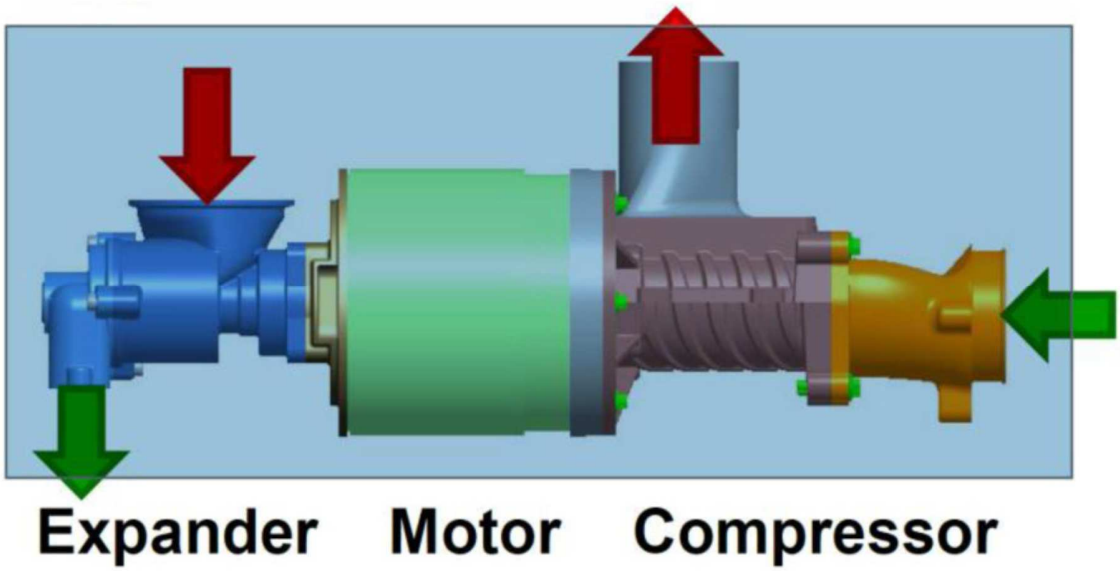

Figure 2-15: *Eaton Roots-type compressor/expander system [19]*

2.6 Thermodynamic Models of Roots-type Supercharger

VOLVO Car Group presented in 2015 1-D model of Roots-type supercharger [34]. The model is based on discretizing of inter-teeth gap into ten segments as shown in ***Figure 2-16***. Cross-sectional areas of each segment are integrated along the inter-teeth gap yielding its volume. System of volumes and orifices is implemented after that to build supercharger model in GT-Power (***Figure 2-17***). Simulation results obtained from the 1-D model are compared with measured values. As is obvious from ***Figure 2-18*** the model yields a good agreement with measured data.

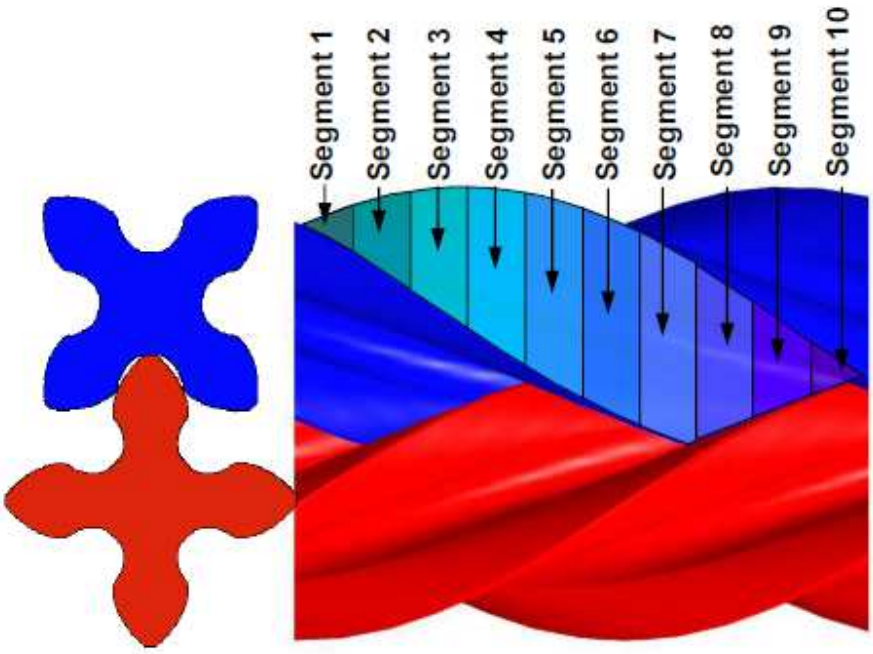

Figure 2-16: *Inter-teeth gap discretization [34]*

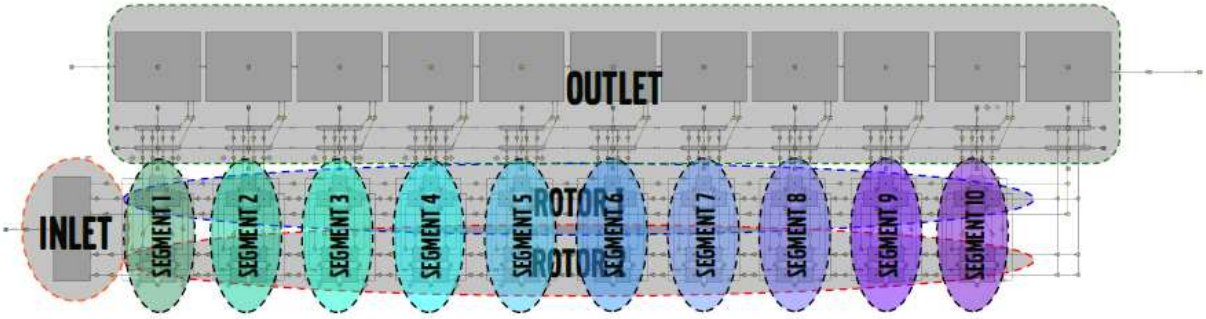

Figure 2-17: *Supercharger model in GT-Power [34]*

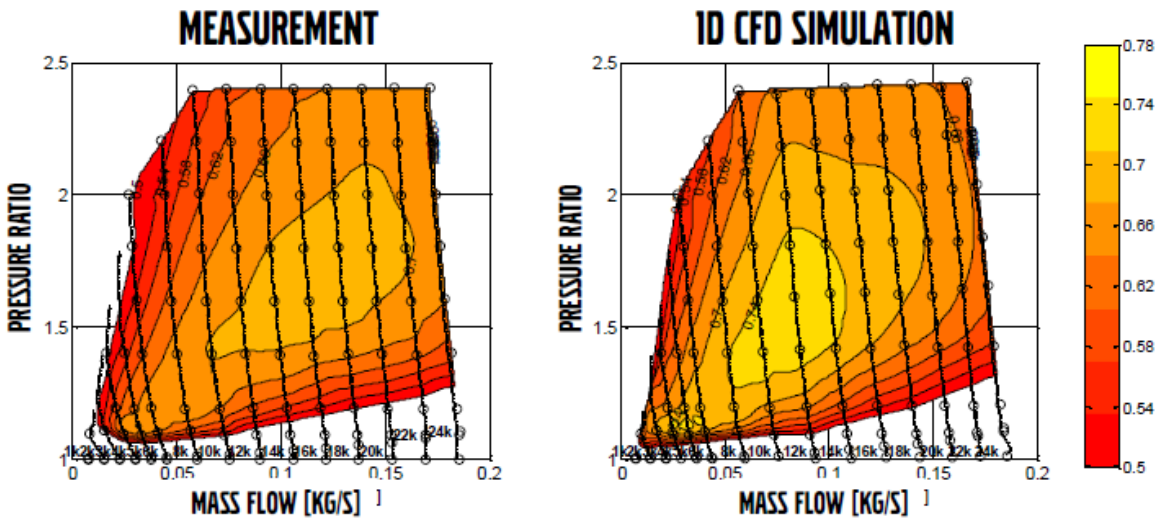

Figure 2-18: *1-D model results and measured data comparison [34]*

Eaton Corporation is one of the companies engaged in Roots-type supercharger development. They presented a paper summarizing the new TVS V-Series (Volumetric Series) supercharger in 2013 [23]. The work presented in this paper was driven by industry trends towards downsizing and downspeeding which highlighted the need for improving low speed volumetric efficiency to achieve the desired low speed engine torque and transient response. The way how to achieve that was increasing the helix angle (up to 160 deg). In that case approximately the same velocity of rotor mesh and velocity of incoming air eliminate acceleration or deceleration of the incoming air. TVS superchargers are targeted for two-, three- and four cylinder gasoline and diesel engines (0.5l up to 2.0l engine displacement) and ranging from 200 cc to 410 cc of displacement per revolution of the rotors. Three types of leakages in the supercharger are described below. Leakages are caused mainly due to clearances between rotor tips and rotor housing, between meshing rotors and between rotor end and the end plates (housing and bearing plate) (***Figure 2-19***, ***Figure 2-20***). Furthermore, rotor length to diameter ratio (L/d) is evaluated in this work with respect to the leakage, volumetric efficiency and rotor inertia point of view. Considering these three parameters L/d equal to 1.2 was chosen to be the design standard for the new V-series devices that would provide the best volumetric efficiencies over the broadest range of speeds and pressure ratios. Three-lobe rotors

possesses a good leakage area to displacement ratio, while reducing the magnitude of the pressure pulsations at the outlet and thus improving system acoustics.

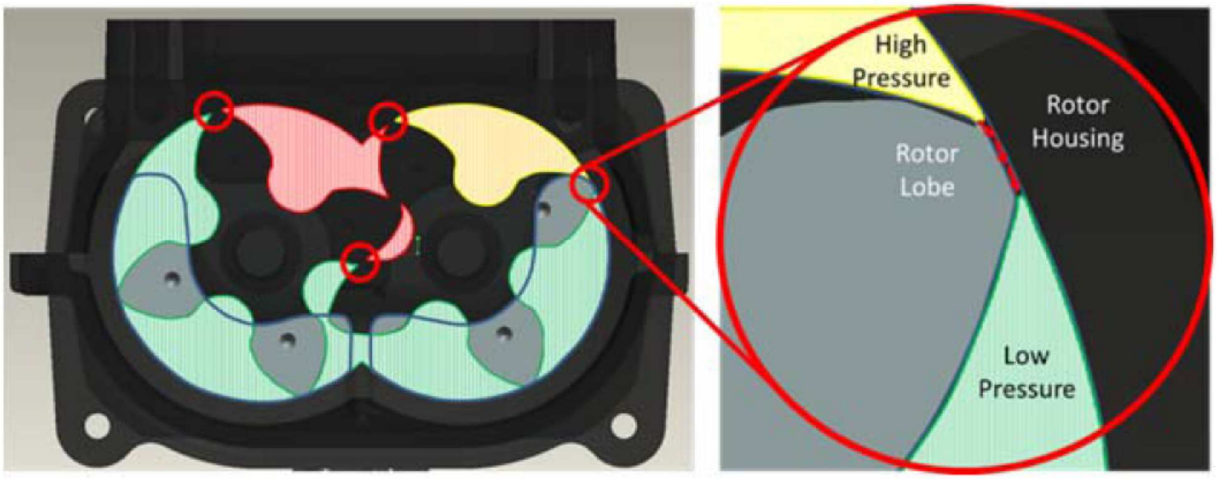

Figure 2-19: *Leakages in Roots-type supercharger caused by clearances between rotor and rotor housing and between meshing rotors [23]*

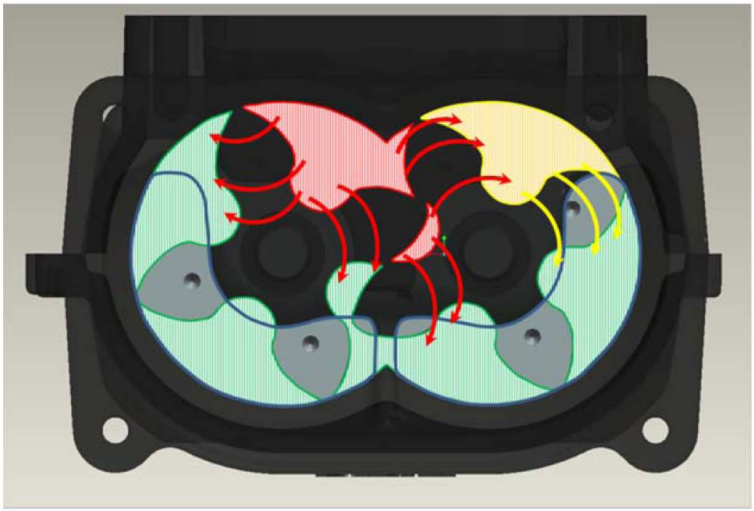

Figure 2-20: *Leakages caused by clearances between rotor ends and end plates (housing and bearing plate) [23]*

The final output of this optimization is the new TVS V-series model V250. The optimized design was then used to develop a model displacing 400 cc per revolution, the V400. Finally, 65%

isentropic efficiency islands are compared in ***Figure 2-21*** for the M24 (three-lobe design with 60deg of twist angle that displaces 393 cc), R410 and V400 units. Volumetric efficiency at pressure ratio of 1.6 is significantly higher for V400 compared to R410 in the whole speed range (***Figure 2-22***). Due to the higher rotor helix angle, the V400 has a much wider operating range than the M24, as the M24 thermal efficiency drops off in the upper portion of its speed range (***Figure 2-23***).

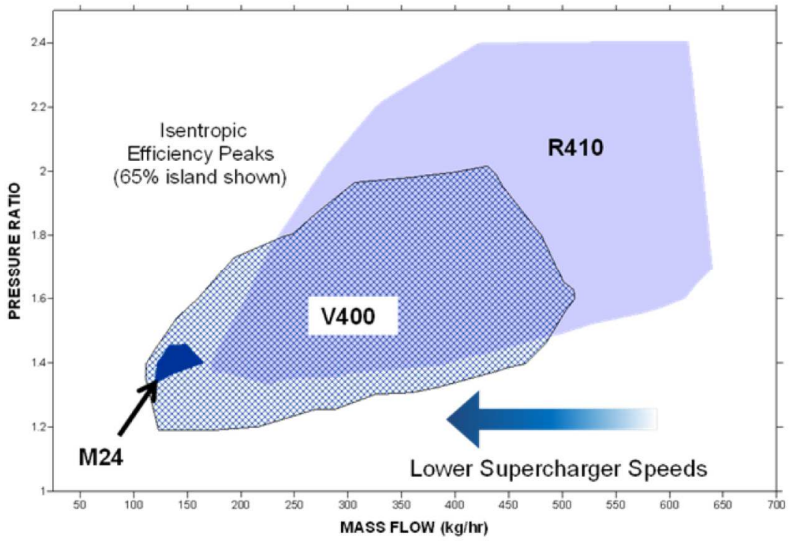

Figure 2-21: *Isentropic efficiency islands comparison for M24, R410 and V400 [23]*

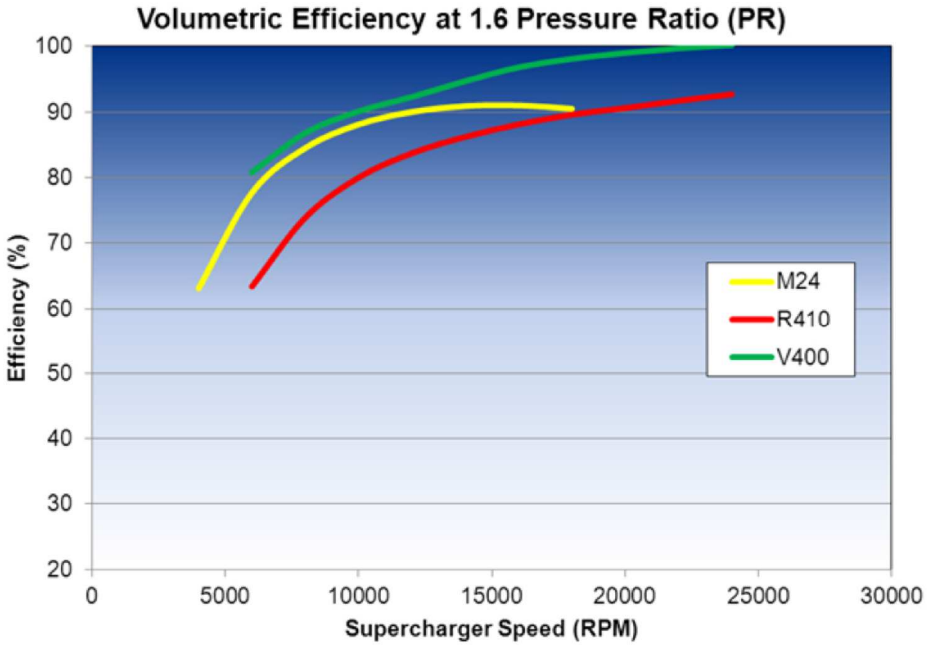

Figure 2-22: *Volumetric efficiency comparison for M24, R410 and V400 at 1.6 pressure ratio [23]*

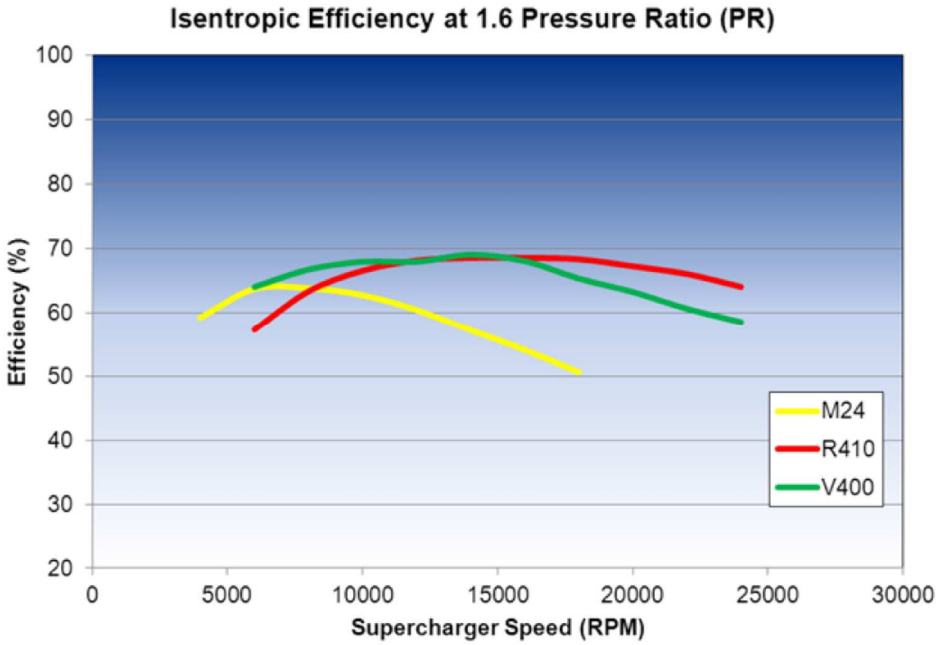

Figure 2-23: *Isentropic efficiency comparison for M24, R410 and V400 at 1.6 pressure ratio [23]*

Roots-type supercharger modeling and validation using 1-D model in GT-Power is described in [24]. All geometrical values (working chamber volume, inlet and outlet port areas etc.) of a supercharger with straight lobes on both rotors are calculated with help of code written in Matlab. In detail a model of leakages is presented in this work where radial and axial chamber to chamber clearances and radial and axial rotor to rotor clearances are respected. Moreover, axial clearances at both ends of rotors are taken into account in the model. These clearances are connected by holes in each of the lobe which lowers moment of inertia of the rotor. A restrictor of LEGRIS type is used to control supercharger outlet pressure.

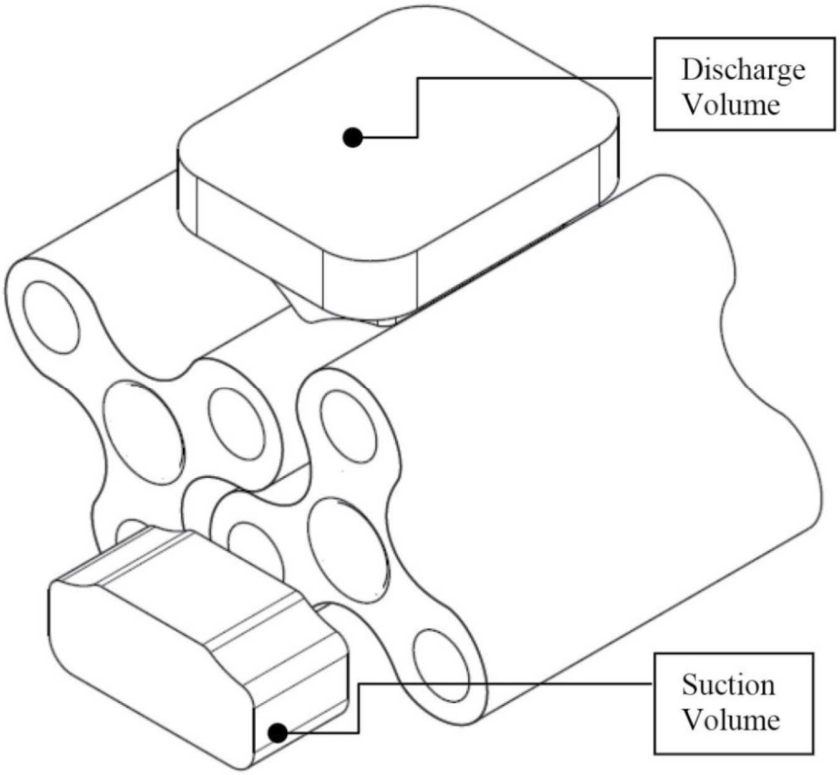

Figure 2-24: *Roots-type supercharger rotors with 3 straight lobes on each of them [24]*

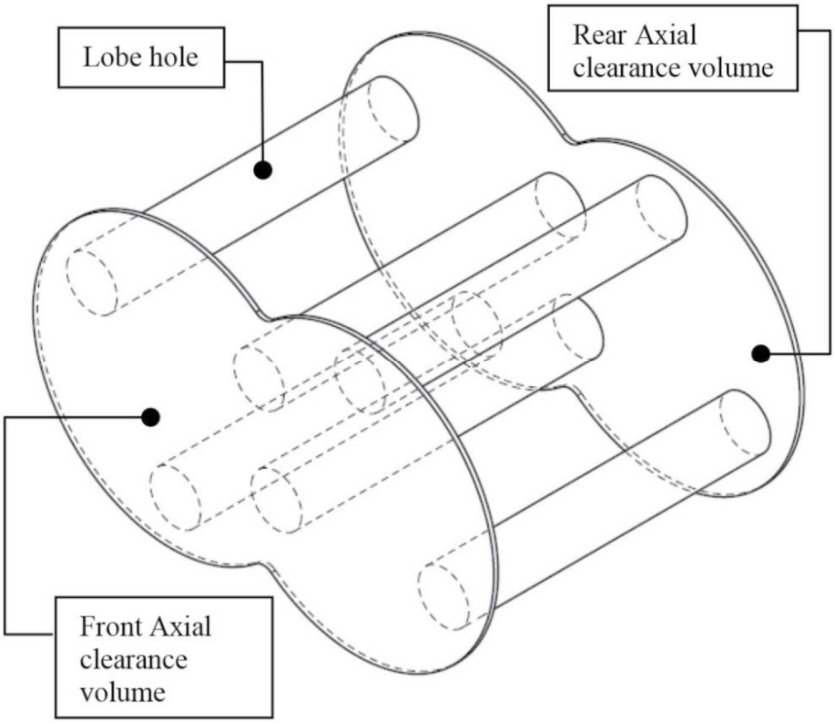

Figure 2-25: *Lobe holes connecting axial clearance volumes at each end of the rotors [24]*

Results yielded by the 1-D model in GT-Power are evaluated and compared to measured data. The accuracy of the validated model is about 90% in terms of mass flow rate and about 97% concerning discharger temperature. The strength of the model lies in its simplicity and ability to predict variation of mass flow rates with change of all design parameters. This makes it a perfect tool for making a decision about size of the supercharger considering the isentropic efficiency and mass flow rate requirements along with packaging constraints. Unfortunately, the model is able to respect only roots-type supercharger with straight lobes which is not the state-of-the-art solution in these days.

The model has been based on references on the author's SAE Paper [25] published in 2013. But the way the design data are transformed into the 1-D model is entirely different because spur gears can be described in analytical way easily.

2.7 Summary - Motivation for the Study

Internal combustion engines are currently under large pressure caused by emission regulations. A Roots-type supercharger is a device, which may help to improve engine torque at low speed and thus to reduce CO_2 emissions. Two-stroke engines are in renewed focus of engineers because of their high power density and natural internal gas recirculation. The need of positive pressure drop across an engine, which enables sufficient scavenging, may be covered by Roots supercharger. Globally, Roots-type supercharger can be used in different engine air loop configurations at two-stroke or four-stroke engines and may cover the boost pressure lack at various engine operation points, where boost pressure produced by a turbocharger compressor is not high enough to achieve the engine power target.

From the same reason (strict emission regulations), alternative powertrains are investigated massively during the last years. Roots-type supercharger used like an expander may be an effective part of a car powertrain using fuel cells as a source of power [19]. Roots-type superchargers are used in chemical and food industry, as well, where they deliver different gases, which may not be contaminated by undesired substances like oil [3].

Low-frequency noise custom to Roots-type supercharger operation needs to be limited. It brings new challenges in mufflers development and internal combustion engines packaging. A tool, which is able to find fast appropriate solution, would be appreciated.

The present situation calls for optimization of supercharger input power, aerodynamic parameters and the device acoustics. The papers focused on this issue are still rare, although the tools for optimization are available. There is no work published until now, which would represent a complex thermodynamic model of Roots-type supercharger with helical gears useable for both isentropic efficiency and noise optimization.

The abrupt compression, occurring after the outlet port is connected to the inter-teeth volume, reduces isentropic efficiency. Leakages may be significant, if there is too big clearance between tooth lobes and between rotor and supercharger body. The both types of clearances connect high and low pressure sides of a supercharger. Nevertheless, they are unavoidable, taking thermal

expansion into account. These features are common for both standard spur gear type and the type with helical gears.

Helical gears appeared first with Lysholm type of screw compressors. The advantage of smooth compression is compensated by the fixed built-in compression ratio, which cannot be used for lossless fitting of boost pressure to engine load requirements, until complicated variable port geometry is used.

If the boost pressure is higher than the one achieved by built-in compression ratio, the pressure difference is overcome in Roots-like abrupt compression by back-flowing gas. Nevertheless, skew position of gears and axial change of inter-teeth volume makes smoother air input or expelling possible. It is of advantage, especially if low number of teeth is used. The positive displacement chamber volume is larger with the same axial length of rotors, i.e., lower speed can be used for the same mass flow rate of gas. Both factors are important for noise reduction, as well. Therefore, the Roots-type helical gears superchargers have a large potential for engine implementation.

On the other hand, the relative leakage loss may increase due to long sealing contact curves with clearances. Aiming at limiting them, the both ports should be isolated by rotors in contact as long as possible. Then, the changes of chamber volume, after all lobes of meshing teeth are in contact and both ports are already closed, cause significant compression of rest gas in this volume, followed by leakage flow and expansion to low pressure. High local temperatures and additional efficiency losses are a result of it.

Therefore, the object of this work is to develop state-of-the-art computational tool for simulation of a Roots-type supercharger, where all these processes may be modeled and optimized using experience with implementation of advanced solver modules developed in 1-D codes for unusual purposes, e.g., [26] or [27]. The arbitrarily changed volume of virtual cylinders, describing inter-teeth volumes and variable connecting orifices simulating not only ports but also clearance leakages may be applied if appropriate geometric dimensions are investigated in suitable 3-D CAD software. The virtual manufacturing method can be used for description of meshing profiles. This procedure excludes complicated deduction of analytical formulae – yet spur gears are elaborated

in more details in [28] - for more general and rather difficult 3-D case, which is not described in literature sources known to the author.

Thermodynamic basics used for 1-D simulations in GT-Power are described in details in chapter **5.1 GT-Power**.

3 Goals of the Thesis

The main goal of this theses is to develop a 1-D mathematical model of a Roots-type supercharger, which represents the device with all significant phenomena, like shock-wise compression after the connection of outlet port to an inter-teeth space, leakages of delivered gas due to clearances, low-frequency noise etc.

The outputs of simulation are:

- the description of charger internal geometry, used for Eaton R- and M-types of Roots-type supercharger
- predicted mass flow rate
- predicted isentropic efficiency
- estimated pressure pulsation
- boundary conditions for design and 3-D simulations, which is outside of this thesis scope (e.g., the deformations of charger casings due to temperature field or the changes of axial clearance between rotors, etc.).

Plan of the Work:

- Geometrical model of helical gears using 3-D CAD model of Roots-type supercharge, e.g., inter-teeth gap volume, inlet and outlet port areas.
- Supercharger 1-D thermodynamic model; model development using basic modules in GT-Power simulation environment; the model performance is focused especially on:
    - Abrupt compression
    - Leakages due to clearances
    - Parameters definition for the following calibration.
- Pressure trace measurements and analysis.
- Model calibration and supercharger map prediction (pressure ratio and isentropic efficiency in dependence on mass flow rate and speed).

The following milestones should be achieved:

- test bed development,
- supercharger map measurement,
- calibration of the model for the prediction of flow-speed map,
- fast pressure indication in moving volume.

4 Geometrical Model of Helical Gears Roots-type Supercharger

The geometrical features of axially long helical gears can be determined easily using numerical elaboration in suitable 3-D CAD model. Therefore, the data needed for 1-D model were obtained from Catia V5 R19 and Autodesk Inventor for the current state.

The following models based on Eaton R-type supercharger in two sizes and one size of M-type are shown here as a demonstration of the method. Both R-type and M-type supercharger are Roots-type superchargers but they features with different design of rotors and inlet and outlet ports. As already published in [25], the design started with helical rotors (***Figure 4-1***). Each has four teeth with involute-shape lobes and four inter-teeth gaps. This geometry is used for Roots-type superchargers of newer generation. The absence of built-in compression, which is a main feature of Roots-type supercharger, can be found from phase diagram presented in ***Figure 4-3***, since during contact period of tooth lobes the volumes determined by tooth contact zones are opened to one of the ports. Gas is taken into the positive displacement chamber through inlet port positioned at casing face at the bottom of the ***Figure 4-1***, delivered along rotors and finally expelled through an outlet port located radially at the opposite side of a supercharger body due to the change of inter-teeth gap volume as the contact curve of teeth ***C*** moves backwards.

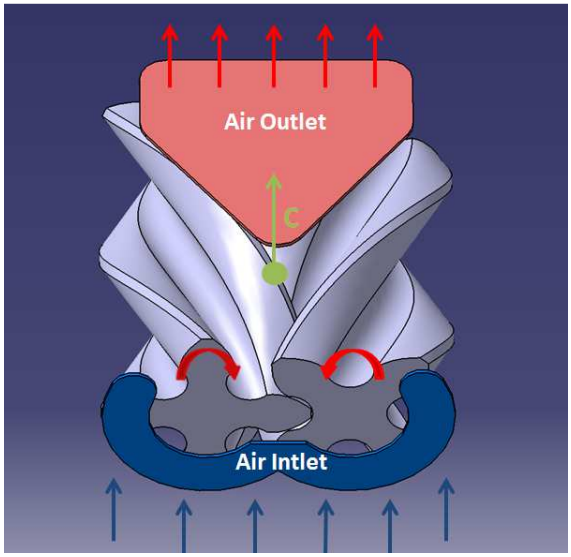

Figure 4-1: *CAD solid model of Roots-type R-type supercharger rotors with an inlet port (blue), an outlet port (red), direction of rotation and a movement of teeth contact curve C towards an outlet port [25]*

The main goals of the developed 3-D model are the determination of positive displacement chamber volume, port area and leakage flow clearances, all in dependence on rotor position. For this purpose, only one tooth on the first rotor and only one gap of the other one are sufficient (***Figure 4-2***). Their mutual position was investigated with the angle step of rotor position of 10 degrees. Initially, the tooth comes into the gap without a contact with the other lobe after passing the intersection of both addendum (tooth head) circles. Even without contact the entering tooth reduces the volume of chamber (e.g., ***Figure 4-4***). This position is followed by "contact" of lobes after the region of line of action is encountered. In reality, the contact of lobes is avoided but minimum clearance is fixed in this zone by accurate synchronization gears. After the angle of top land width is gone, the other pair of lobes starts the contact of both tooth lobes, closing the chamber by both lines of contact at lobes and by curves of "contact" of both top and bottom lands of opposite teeth. The contact curve ***C*** moves axially backward (towards outlet port - ***Figure 4-1***) and divides the volume of inter-teeth gap into two parts. The forward part increases, being connected to an inlet port. The backward part decreases being connected to an outlet port. From that reason, the

thermodynamic model of equivalent piston compressor should use double-acting pistons with leakages.

This situation extended to a pitch plane located in the zone of contact is shown in ***Figure 4-3***. The chamber volume is determined by both face planes and by cylindrical bores of supercharger body in "contact" with gear addendum cylinders and closed by lobe surfaces up to the teeth curves of contact. The contact points create space curves on the surface of lobes (lines of contact for involute lobes, curves for the undercut regions).

These chamber volume dependence on angle for helical gears was generated by 3-D CAD tools using developed script based on built-in algorithm. The whole teeth length contact lasts during 160 degrees (for R-type supercharger, 60 deg for M-type) of rotor rotation from its beginning at one rotor face until it ends at the other face. The teeth contact splits the inter-teeth gap volume into two positive displacement chambers. One of them – connected to inlet port – increases during the contact period and intakes low-pressure air. The other one delivers the air into outlet being reduced in its volume. The change of chamber volume is advanced at start and delayed at the end in comparison to the contact period, due to teeth entering or leaving the gap after passing inlet addendum cylinder intersection line or before passing outlet one. Before the teeth come into meshing the chamber volume is reduced by a tooth (***Figure 4-4***).

The other target of the 3-D CAD model was to determine inlet & outlet port areas. The inlet port with rotors was sketched as it is obvious from ***Figure 4-5***. Then, by rotating of rotors the free area of inlet port was determined stepwise. The outlet port area was investigated using the same methodology. The total outlet port area consists of radial and axial area, relative to the rotors (***Figure 4-6*** and ***Figure 4-7***).

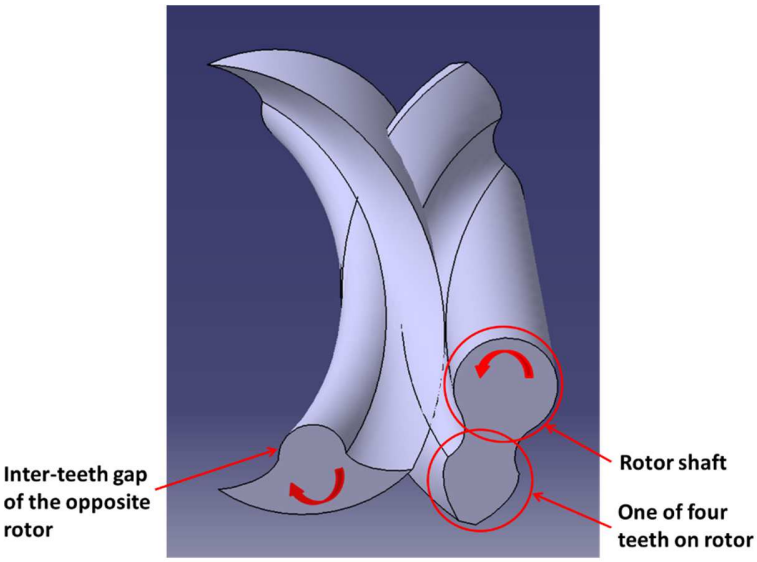

Figure 4-2: *Teeth meshing (right – a tooth with a part of a rotor body, left – inter-teeth gap of the opposite rotor). The lobes are in contact in the rear (upper) part of the figure expelling compressed air at the end of outlet period. Simultaneously, low-pressure air enters the increasing volume of the front (bottom) part of the inter-teeth gap still connected to the inlet port (**Figure 4-1**). The tooth acts in inter-teeth gap as a double-acting piston (R-type supercharger) [25]*

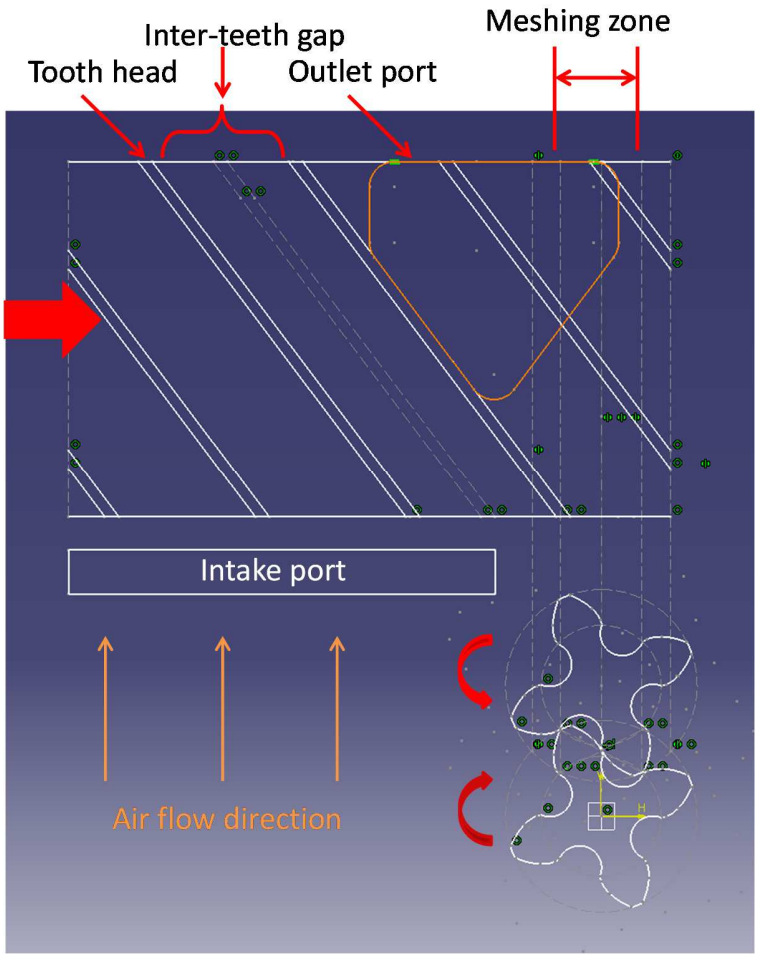

Figure 4-3: *Compressor rotor extended to a pitch plane in the zone of contact with marked both addendum circle intersection zone and teeth contact zone (meshing zone). The opposite lobes of single tooth are in contact with the angle shift caused by top land width. (R-type supercharger) [25]*

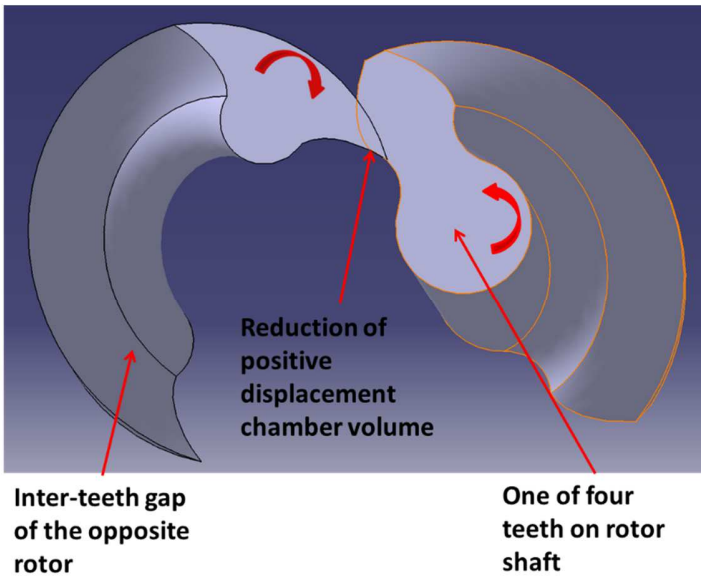

Figure 4-4: *Reduction of a positive displacement chamber volume due to a rotor tooth entering the gap before contact occurs (R-type supercharger) [25]*

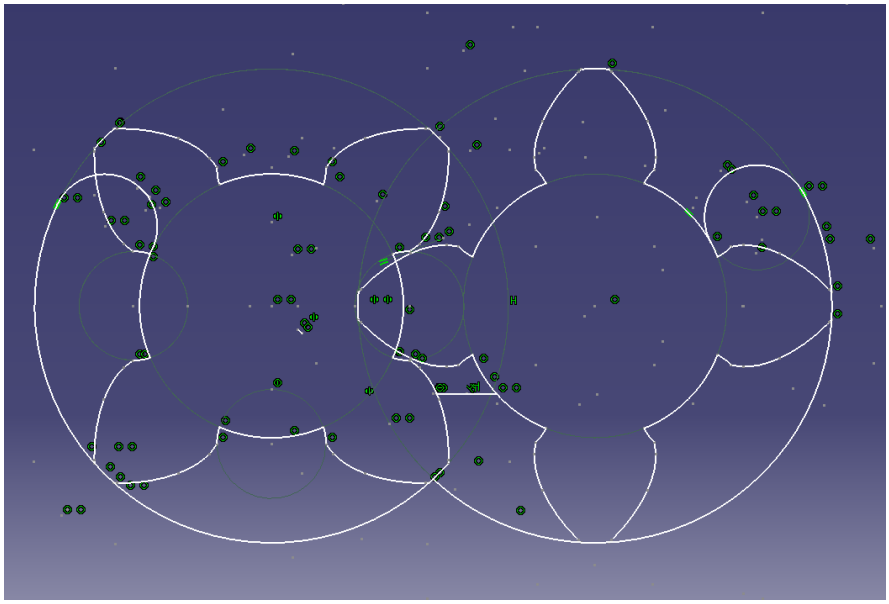

Figure 4-5: *Inlet port area sketch (the parts of teeth below the bottom limit of an inlet port are not drawn) (R-type supercharger) [25]*

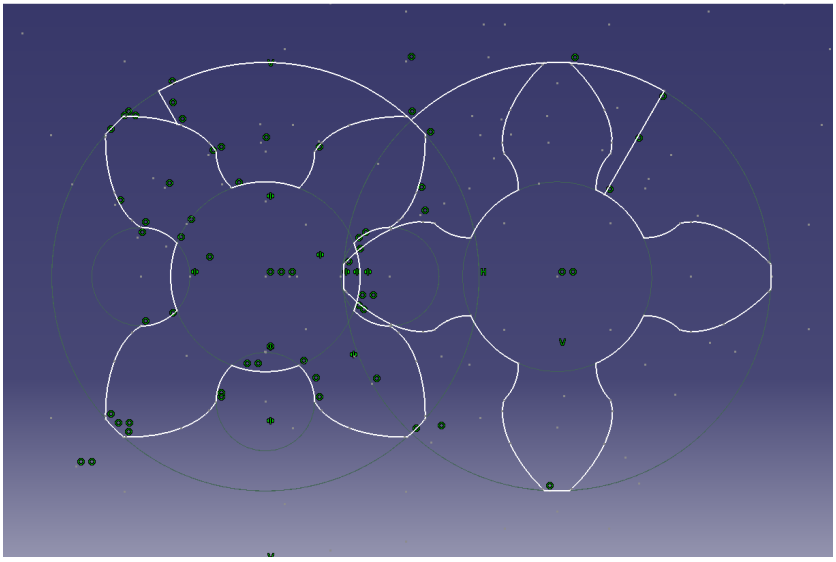

Figure 4-6: *Determination of axial outlet area from inter-teeth gap to outlet chamber connected to a radial outlet port (R-type supercharger) [25]*

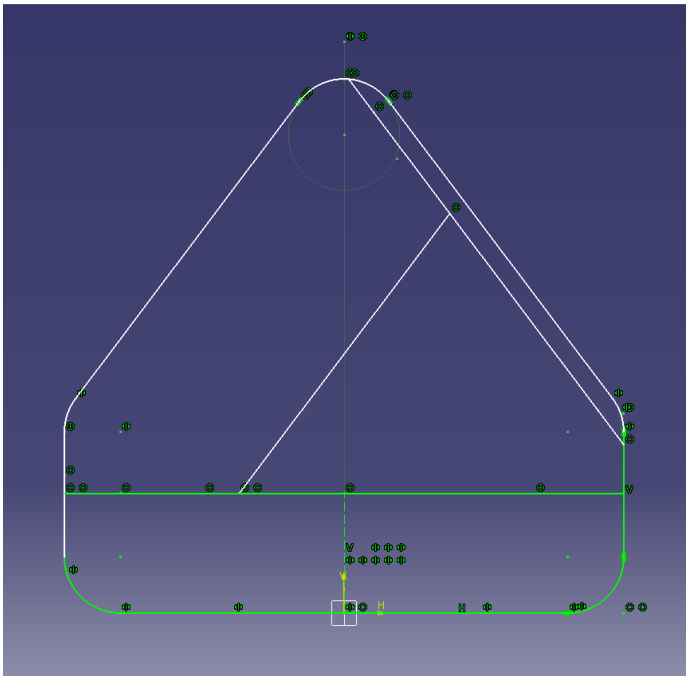

Figure 4-7: *Radial outlet port with two teeth extended by an axial outlet chamber (bottom part) (R-type supercharger) [25]*

The final chamber volume and inlet and outlet port areas with appropriate timing during one cycle are shown in ***Figure 4-8.*** As is obvious from chamber volume dependence on angle for helical gears, one cycle related to inlet face rotor position is more than 360 degrees (more than one rotor revolution), approximately 610 degrees for R-type supercharger. This means 360 deg for one revolution plus 160 deg for rotor twist (actually a shift between inlet and outlet timing) plus 90 deg for inter-teeth gap width (opening tooth is shifted 90 deg prior to the closing one). The fact that one cycle of the supercharger gap is 610 deg complicates the straight usage of gap volume and flow areas of inlet, outlet and connections in GT-Power model. Thus, when using GT-Power primarily developed for combustion engine simulations for modeling the supercharger all the angles have to be extended to get the cycle taking 720 deg. In fact, it means to multiply all the angles by multiplier 720/610. The extended values are compared to the original one in ***Figure 4-11***. In the same way the supercharger speed has to be increased in the model for each simulated point to save the comparability of time depending values, especially the mass flow rate. Based on that ***Equivalent speed*** is defined as:

$$s_e = \frac{720}{610} \times n_s \,, \tag{4.1}$$

where

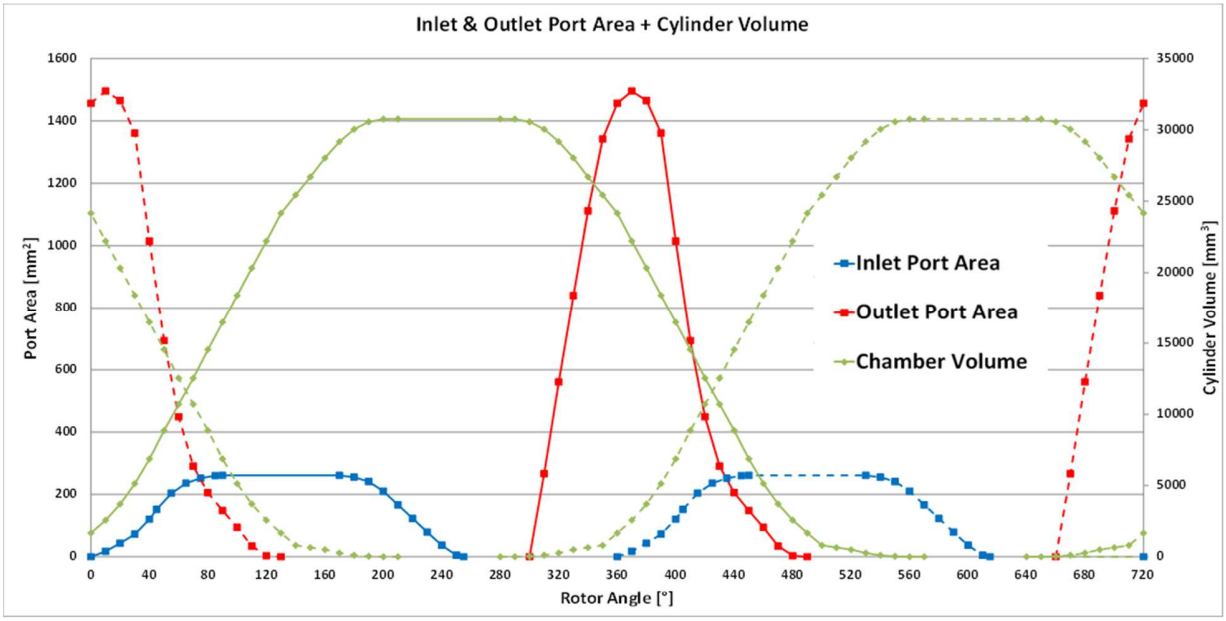

Figure 4-8: *Chamber volume and related inlet and outlet port areas (full lines) of chamber in consideration together with the chamber volume in the same inter-teeth gap separated by teeth contact with related inlet and outlet port areas (dashed lines) for the smaller one R-type supercharger [25]*

Next to inlet and outlet port there is another connection between inlet or outlet and inter-teeth gap volume. There is a small area between rotor tips and supercharger housing connecting neighboring inter-teeth gaps. It is caused by the rotor twist at both described and modeled supercharger types (Eaton R- and M-type). One gap is connected to the inlet or outlet through this small area even it is not connected to inlet or outlet by relevant port (***Figure 4-9***). This connection causes that the pressure increase in the gap is not abrupt after outlet port opening. The air flows through this connection from the gap opened already to the outlet to the gap, which is not opened to the outlet, makes the pressure increase gradual. The scheme of air flow from supercharger outlet into inter-teeth gaps is shown in ***Figure 4-10***. The gap number 1 is already opened to outlet through outlet port and the gap number 2 is not yet connected to outlet through outlet port. The air flow is streaming through the connecting flow area according to the red arrow direction. The same situation is then between gaps 2 and 3. The gap 4 is separated from gap 2 by the tooth 24, which is still in "contact" with supercharger casing along its length in this position (***Figure 4-9***).

Even though there is the connection between gaps, there is no straight connection between supercharger inlet and outlet. This fact is corresponding to the diagram in ***Figure 4-11*** where the connection to the inlet is closing at about 315 deg, the connection with outlet is opening a few degrees later.

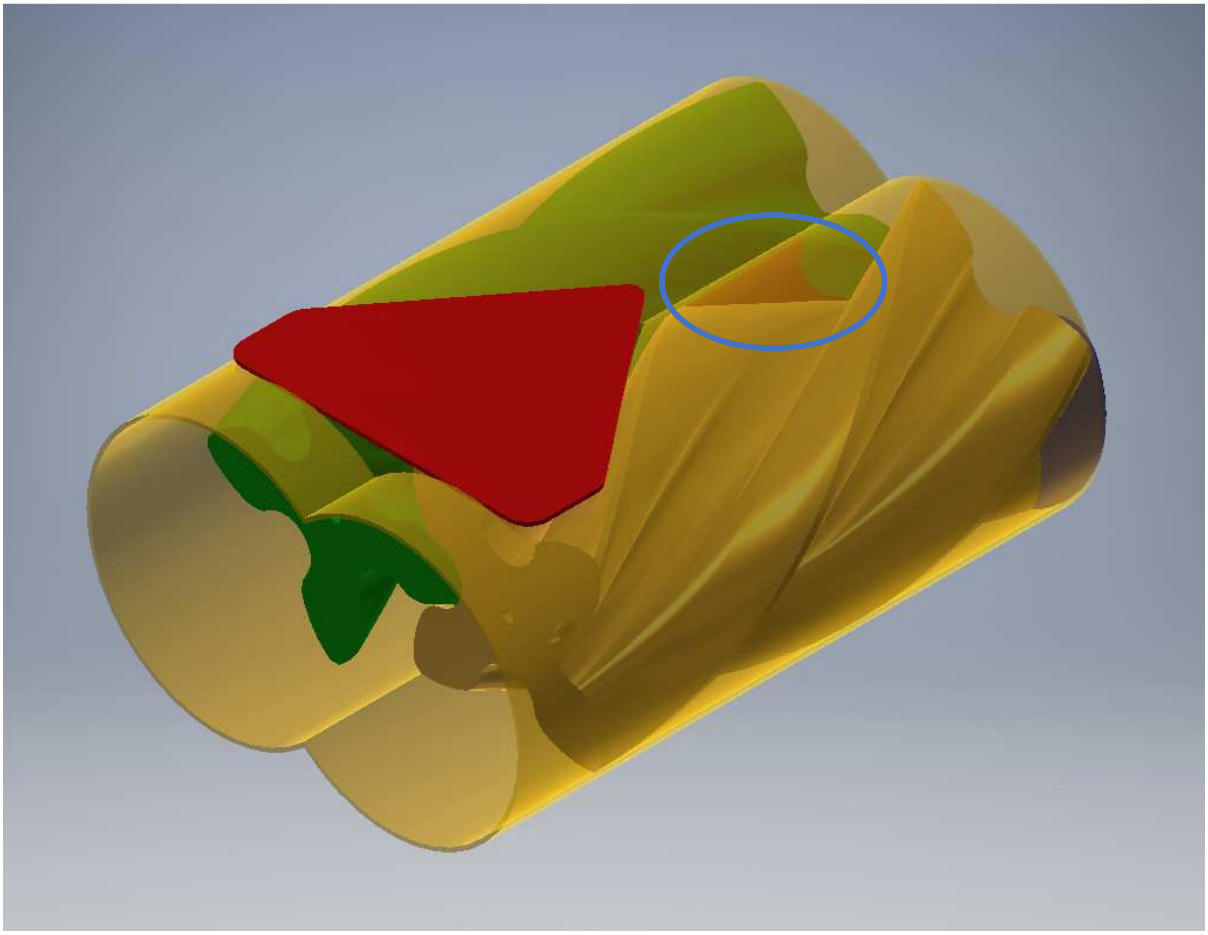

Figure 4-9: *Area (red triangle between rotors and intersection of the casing cylindrical walls – in blue circle) connecting inter-teeth gap already opened to the outlet (on green rotor) and one separated from the outlet (on yellow rotor) for R-type supercharger*

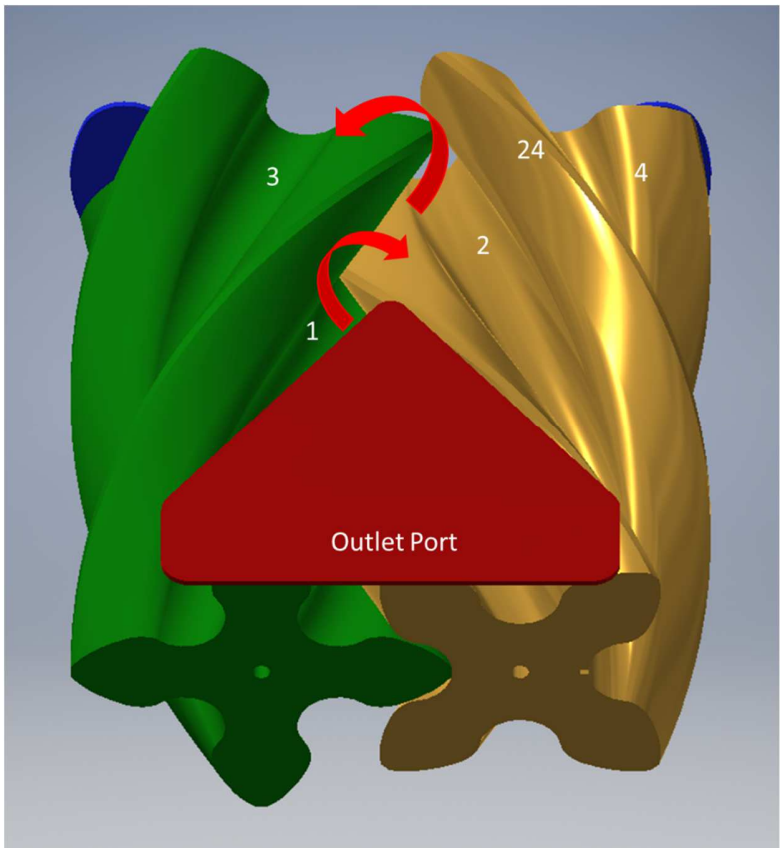

Figure 4-10: *Scheme of connections between supercharger volumes – connection of inter-teeth gaps with outlet event not opened to outlet port (R-type supercharger)*

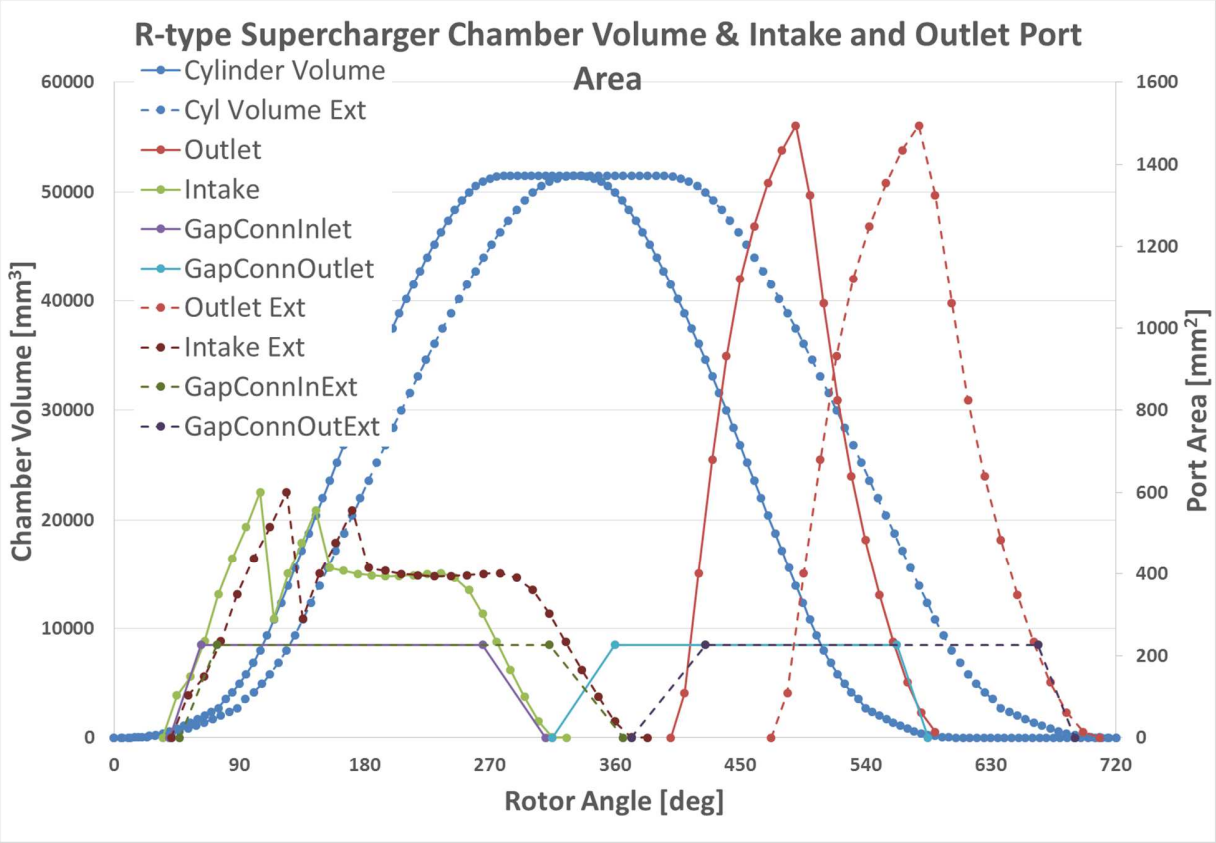

Figure 4-11: *Inter-teeth gap volume, related inlet and outlet port areas and gap connection areas for the real supercharger (cycle lasting 610 deg – full lines) and for the GT-Power model extended to 720 deg (dashed lines) (R-type supercharger)*

The above depicted 3-D analysis has been made also for the M-type supercharger (***Figure 4-12***). Due to the twist of M-type supercharger rotors for only 60 deg instead of 160 deg like in R-type supercharger case the whole working cycle takes only 540 deg, which means 360 deg of one rotation plus 60 deg of the rotor twist and 120 deg of inter-teeth gap width. The inter-teeth gap width results in 120 deg due to that M-type supercharger features with only three-lobes rotors (***Figure 4-12***). Based on this the equation $\boldsymbol{se}=\frac{\mathbf{720}}{\mathbf{610}}\times\boldsymbol{n_s}$, (**4.1**) for ***Equivalent speed*** calculation transforms as follows:

$$\boldsymbol{s_e}=\frac{\mathbf{720}}{\mathbf{540}}\times\boldsymbol{n_s}\,, \tag{4.2}$$

where s_e is equivalent speed used in 1-D model and n_s is real supercharger speed at test bed. Next to that, M-type supercharger synchronization gear includes a step up gear ration, which equals to 1.928. That means, rotor speed is 1.928 times higher than the supercharger pulley speed. To make the situation easier to read all the mentioned speeds below are speeds of rotor even if they are called supercharger speed, e.g. Much easier is the situation in case of R-type supercharger, where rotor speed equals to supercharger pulley speed, as mentioned above.

Moreover, M-type supercharger features with two small outlet ports, which open to outlet much ealier than the main outlet port. This fact is also obvious in ***Figure 4-13***, where outlet port area has a small constant value for a short time after outlet opened.

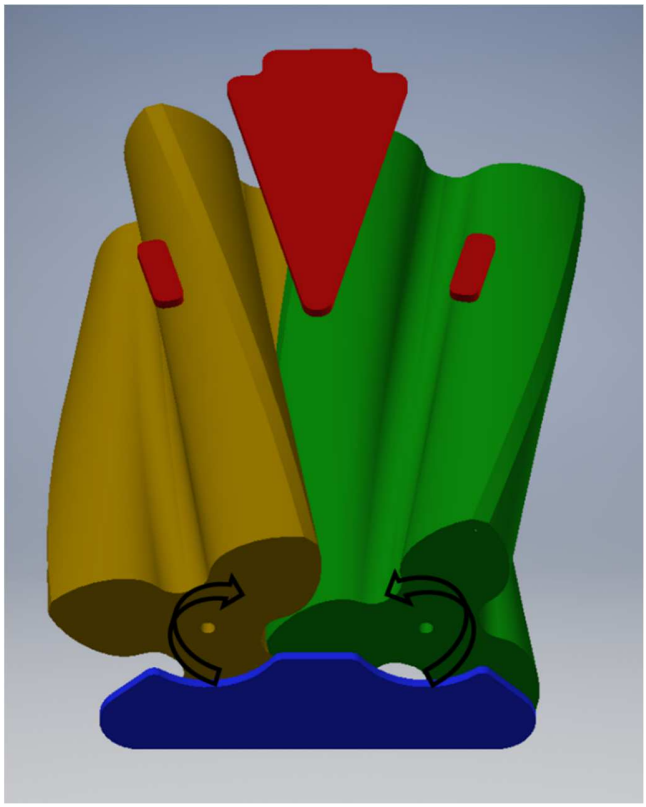

Figure 4-12: *3-D CAD model of M-type supercharger's rotors and inlet (blue) and outlet ports (red). Two small outlet ports open much earlier than the main outlet port. Black arrows show the direction of rotor rotation.*

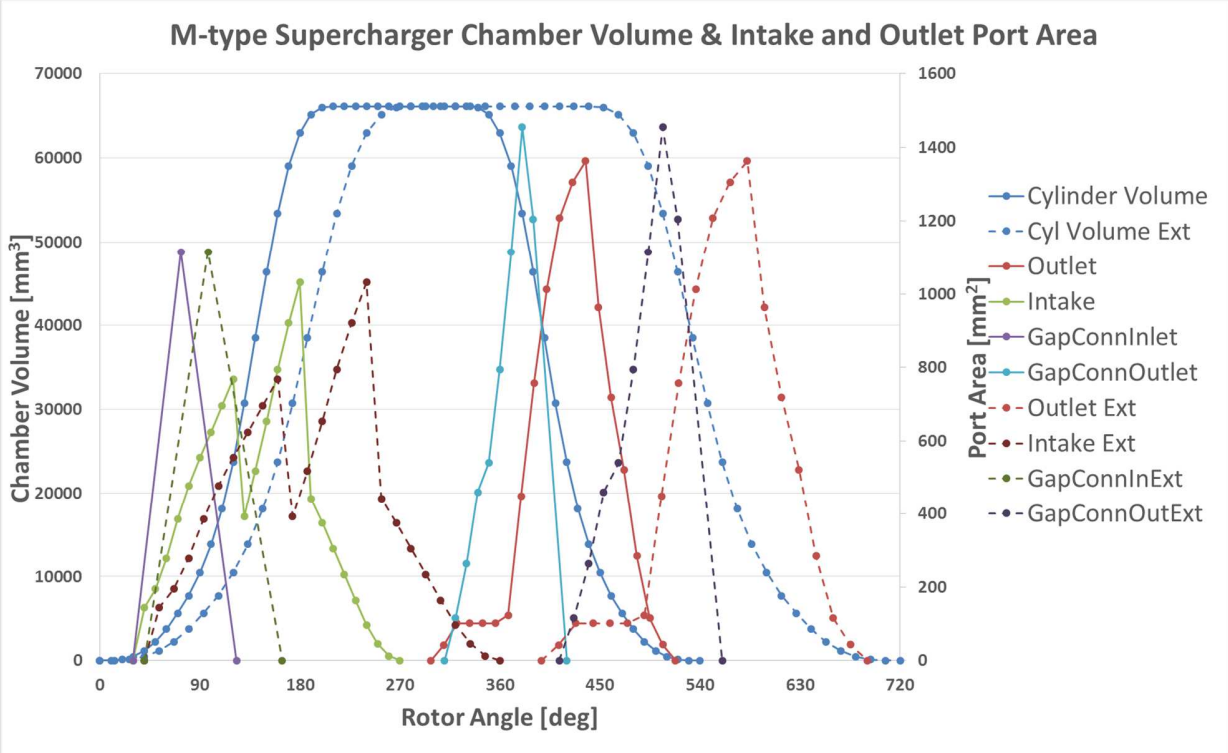

Figure 4-13: *Inter-teeth gap volume, related inlet and outlet port areas and gap connection areas for the real supercharger (cycle lasting 540 deg – full lines) and for the GT-Power model extended to 720 deg (dashed lines) (M-type supercharger)*

5 Supercharger Model in GT-Power

5.1 GT-Power

GT-Power is a part of GT-SUITE, which is a package of solvers developed by Gamma Technologies, Inc. and which is able to simulate the whole car powertrain from internal combustion engine over different types of electric or hybridized powertrains, gearbox and axes up to wheels under different steady-state operating conditions, transients or driving cycles. GT-Power is a one-dimensional solver that involves solution of Navier-Stokes equations [33], namely the conservation of continuity, momentum and energy equations. These equations are solved in one dimension. It means that all values of calculated quantities are averaged across the flow direction. The model in GT-Power consists of different basic components like pipes, orifices, flowsplits, cylinders, valves etc. The whole system is discretized into many volumes, where each flowsplit is represented by a single volume, and each pipe is divided into one or more volumes. These volumes are connected by boundaries. The scalar variables (pressure, temperature, density, internal energy, enthalpy, species concentrations, etc.) are assumed to be uniform over each volume. The vector (flow) variables (mass flux, velocity, mass fraction fluxes, etc.) are calculated for each boundary. This type of discretization is referred to as a "staggered grid" (***Figure 5-1***).

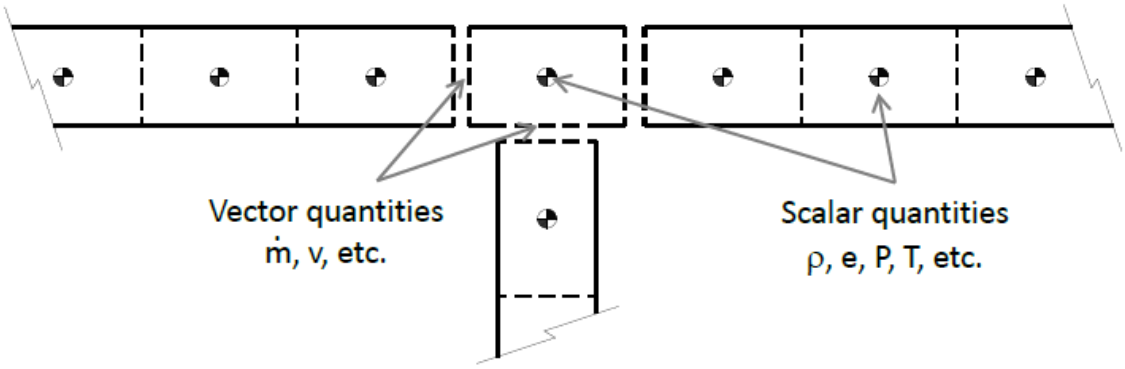

Figure 5-1: *Staggered grid approach – scalars calculated at centroid and vector (flow) quantities at boundaries [33]*

There are two options of time integration methods, which affect the solution variables and limits on time steps. The time integration methods include an explicit and an implicit integrator. The primary solution variables in the explicit method are mass flow, density and internal energy. The primary solution variables in the implicit method are mass flow, pressure and total enthalpy. The explicit method should be used when wave dynamics are important and in all other cases when the part simulating engine cylinder is used. Implicit method should be used when non-engine simulations of long duration are considered (exhaust system warm-up, e.g.). Explicit method has been chosen for presented simulations of Roots-type supercharger.

The conservation equations solved by GT-SUITE are shown below [33]. The left hand side represents the derivatives of the primary variables.

Continutity: $$\frac{dm}{dt} = \sum_{boundaries} \dot{m} \tag{5.1}$$

Energy: $$\frac{d(me)}{dt} = -p\frac{dV}{dt} + \sum_{boundaries}(\dot{m}H) - hA_s(T_{fluid} - T_{wall})$$ (explicit solver) (5.2)

Enthalpy: $$\frac{d(\rho HV)}{dt} = \sum_{boundaries}(\dot{m}H) + V\frac{dp}{dt} - hA_s(T_{fluid} - T_{wall})$$ (implicit solver) (5.3)

Momentum: $$\frac{d\dot{m}}{dt} = \frac{dpA + \sum_{boundaries}(\dot{m}u) - 4C_f\frac{\rho u|u|}{2}\frac{dxA}{D} - C_p\left(\frac{1}{2}\rho u|u|\right)A}{dx} \tag{5.4}$$

where:

$\dot{m}$	boundary mass flux into volume, $\dot{m} = \rho A u$
m	mass of the volume
V	volume
p	pressure
ρ	density
A	flow area (cross-sectional)
A_s	heat transfer surface area
e	total internal energy (internal energy plus kinetic energy) per unit mass
H	total enthalpy, $H = e + \frac{p}{\rho}$

h	heat transfer coefficient
T_{fluid}	fluid temperature
T_{wall}	wall temperature
u	velocity at the boundary
C_f	skin friction coefficient
C_p	pressure loss coefficient
D	equivalent diameter
dx	length of mass element in the flow direction (discretization length)
dp	pressure differential acting across dx

5.2 1-D Model of Roots-type Supercharger in GT-Power

Based on data from 3-D CAD model, 1-D model in GT-Power [32] was built assuming that each rotor tooth is a piston and each gap is a cylinder. The R-type supercharger is designed with two rotors having four teeth and four gaps. Moreover, each tooth works as a double-acting piston splitting the inter-teeth gap into two chambers as described above (***Figure 4-1***). Since GT-Power is a simulation tool developed primarily for simulations of machines, which use crank mechanism, as combustion engines, piston compressors, pumps, etc., frequency transformation needed to be performed, if simulation of other device is considered. GT-Power is quite rigid in using working cycle, which lasts 360 deg or 720 deg. That is why supercharger speed has to be fit to fixed angle duration of a cycle (360 or 720) keeping the time dependence of variable chamber volume, inlet and outlet ports areas, etc., as described in chapter 4. On the other hand, when comparing measured data with simulation results, data from GT-Power need to be transformed back to the correct angular speed and angle of rotor rotation to be comparable with the data measured at a real machine.

The modeled Roots R-type supercharger can be substituted by a piston compressor with sixteen cylinders (two rotors x four teeth & gaps on each rotor x each tooth-like double–acting piston) controlled by ports, orifices simulating connections between gaps and other orifices simulating leakages (***Figure 5-2***). Bore of cylinders was set to 35mm and the inter-teeth gap volume was controlled by changing of piston position in the cylinder according to ***Figure 4-11***. Flow areas of inlet and outlet ports were defined by the same approach - fixed valve diameter and variable valve

lift yielding the same area like the 3-D CAD model (***Figure 4-11***). Inlet and outlet valve diameters were set to 25mm and 100mm respectively. Discharge coefficients of both ports were set to reasonable values (0.9). Areas connecting inter-teeth gaps with inlet or outlet even though the straight connection through inlet or outlet port is missing were defined by poppet valves with certain diameter and variable valve lift corresponding to 3-D CAD model data. The discharge coefficients of these orifices were set to 0.8.

Considering M-type supercharger, it can be modeled as a piston compressor with twelve cylinders (two rotors x three teeth & gaps on each rotor x each tooth like double–acting piston). All other modeling principles remain the same like at the R-type supercharger.

In the current 1-D model, inlet and outlet piping of the supercharger is the same like at the test bed to get the similar pressure behavior caused by high frequency of inlet and outlet ports opening and closing. The supercharger pressure ratio i.e. ratio between inlet and outlet pressures is controlled by outlet throttle in the test bed configuration (***Figure 5-2***). Moreover, PID regulator is engaged for faster tuning of its diameter.

Clearance ratio has to be defined when using a cylinder and piston substituting inter-teeth gap and meshing tooth:

$$\boldsymbol{\gamma} = \frac{\boldsymbol{V_g + V_c}}{\boldsymbol{V_c}}, \tag{5.5}$$

where γ is the clearance ratio, V_g is the inter-teeth gap volume and V_c is the clearance volume. Even though there is no compression in supercharger inter-teeth gap (***Figure 4-11***), the clearance ratio is to be set in the model to reasonable value to define the cylinder. The clearance ratio was selected to be equal to 12 after sensitivity study during GT-Power model calibration (more details in **Chapter 7**).

Air compression occurs by a reverse flow from the outlet piping to the chamber during outlet port opening. Currently, the heat transfer during delivered gas compression is assumed to be able to calibrate isentropic efficiency to values obtained during testing (more details in **Chapter 7**).

The mass flow rate losses due to clearances between rotors and a supercharger casing (including leakages at rotors faces) are simulated by calibrated orifices connecting neighboring cylinders (***Figure 5-4***). In the same way the mass flow rate losses caused by leakage of rotor tooth (piston) dividing inter-teeth gap into two compressor chambers are simulated (***Figure 5-5***). Effective area of orifices simulating clearances was the object of calibration according to measured mass flow rate data and is described in details in **Chapter 7**. Both clearances (in the rotor – gap mesh and between rotor and supercharger casing) are changing its size depending on temperature. This fact is respected in the 1-D model by calibration of the clearances discharge coefficient. Moreover, to minimize clearances in the real device rotors are coated by a thin layer of tough synthetic resin. This thin layer is shaped appropriately during a few first supercharger revolutions without any damages to rotors or casing.

Summarizing above described calibration parameters, there are five quantities totally to be calibrated:

1. Clearance Ratio
2. Leakage Area
3. Leakage Area Discharge Coefficient
4. Supercharger Casing Wall Heat Transfer Coefficient
5. Supercharger Wall Temperature

The calibration process is described in details in **Chapter 7**.

In ***Figure 5-6***, the comparison of measured data and raw results from GT-Power model are shown for the R-type supercharger. The diagram should show that the model follows the trends of each speed line even if leakages and heat transfer are not taken into account. The model calibration will eliminate this fact that is why it is stated here. In ***Figure 5-7***, the comparison of measured data and raw results from simulation are shown for the M-type supercharger.

The 1-D model convergence criteria are set up as shown in ***Table 5-1***. The supercharger speed variation from cycle to cycle should be less than 0.1%, the same value is used for outlet

temperature. For mass flow rate should be the variation from cycle-to-cycle less than 1% and finally for outlet pressure less than 1kPa.

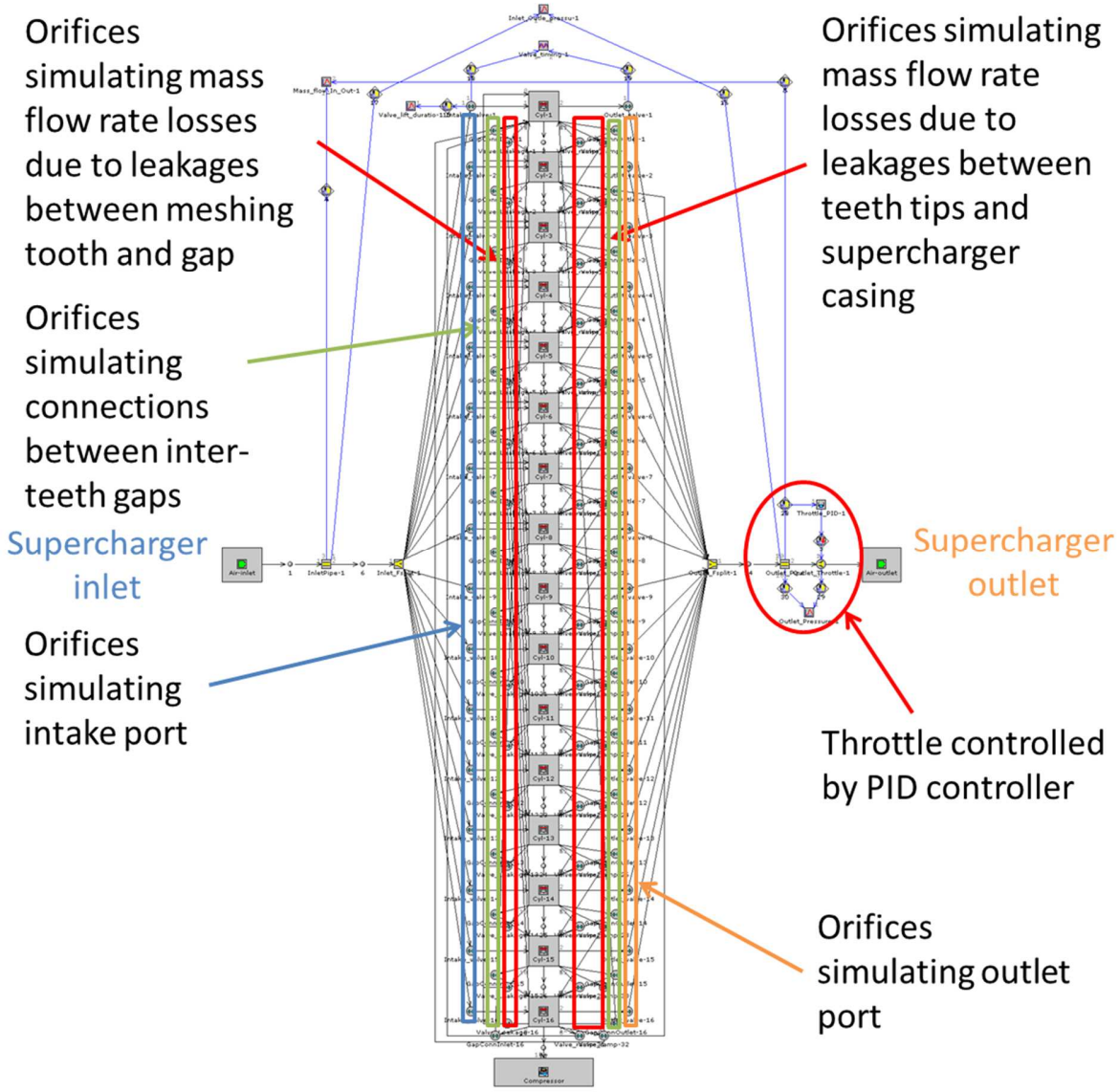

Figure 5-2: *GT-Power model of a Roots-type supercharger (R-type supercharger)*

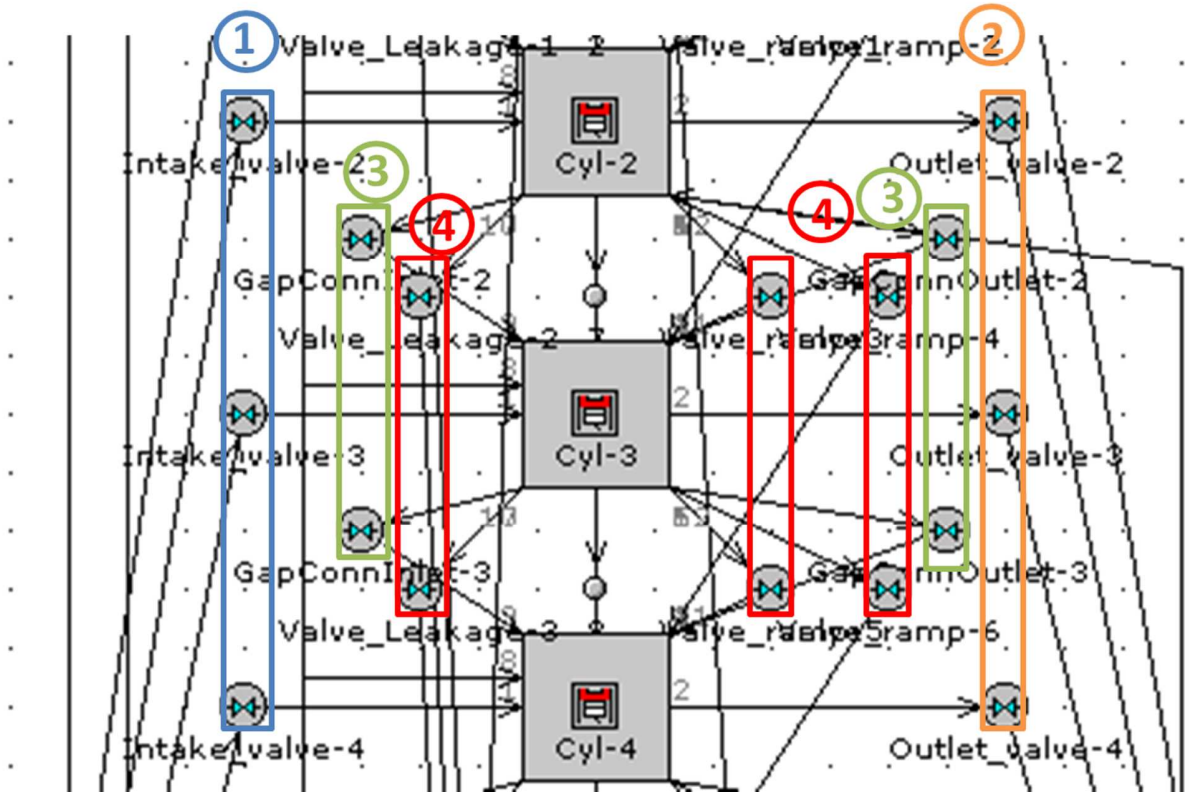

Figure 5-3: *GT-Power model detailed view – inlet 1 and outlet 2 ports, areas connecting neighboring "cylinders" due to the rotor twist 3, orifices 4 represents clearances either in rotor mesh or between rotors and supercharger casing.*

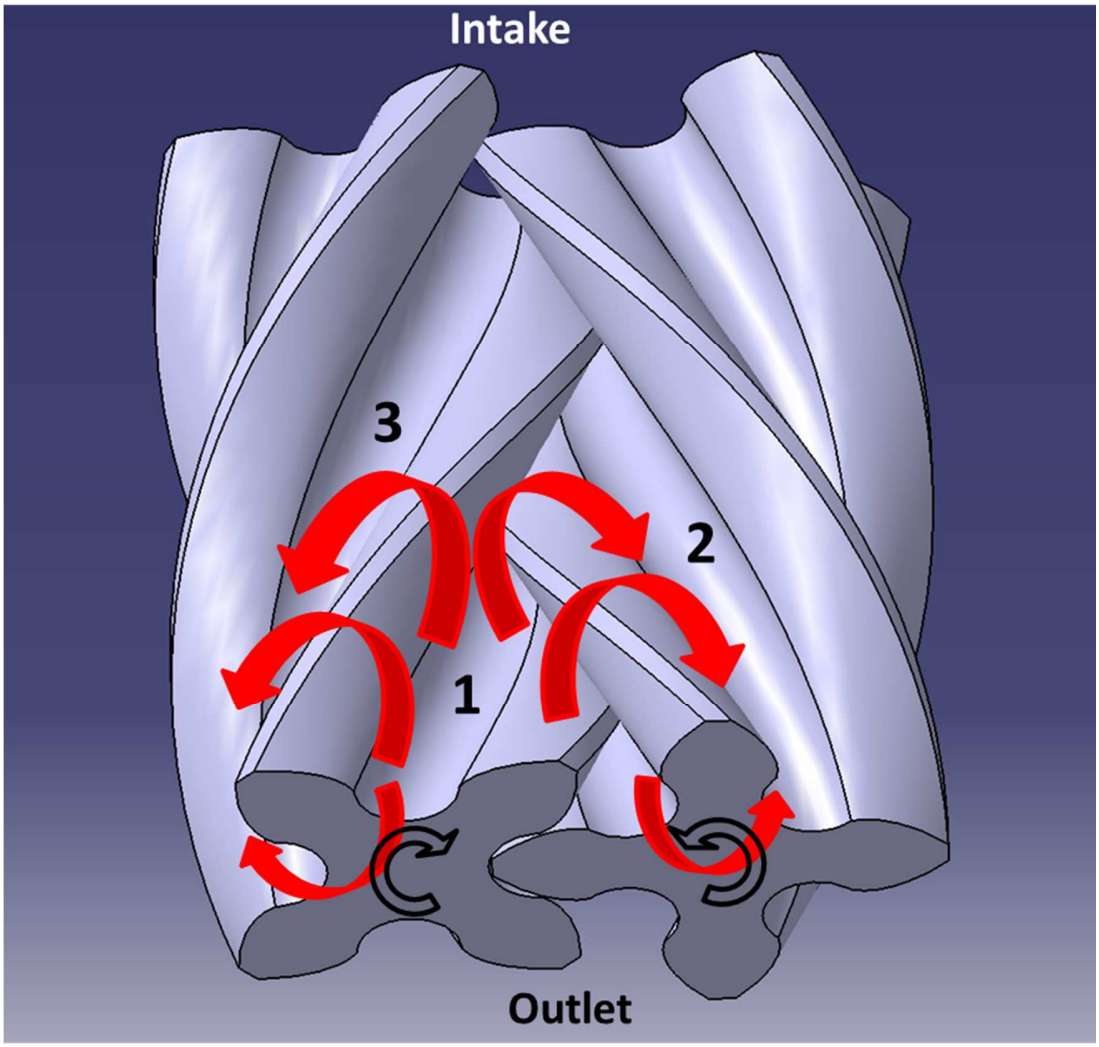

Figure 5-4: *Mass flow rate loss due to leakage between rotors and compressor casing respecting mass flow rate loss at rotors faces also (1 – inter-teeth gap opened into outlet; 2 – inter-teeth gap following gap 1 in 45 °; 3 – inter-teeth gap following gap 1 in 90°; gaps 2 and 3 are closed to outlet) (R-type supercharger) [25]*

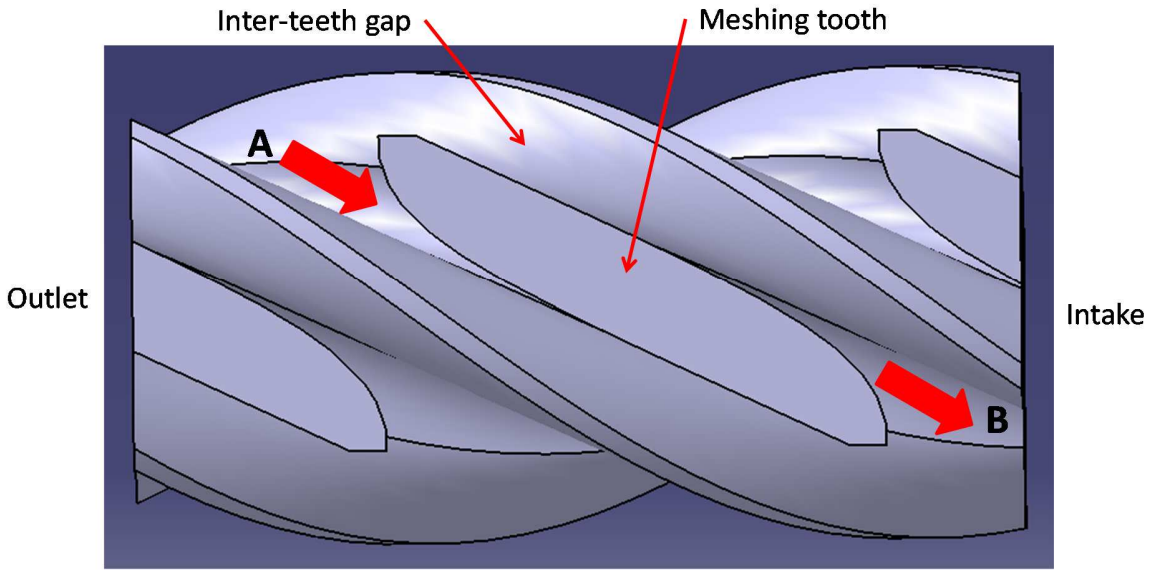

Figure 5-5: *Mass flow rate loss due to leakage between meshing teeth and gap (A – inter-teeth gap; B – inter-teeth gap following gap A in 360°) (R-type supercharger) [25]*

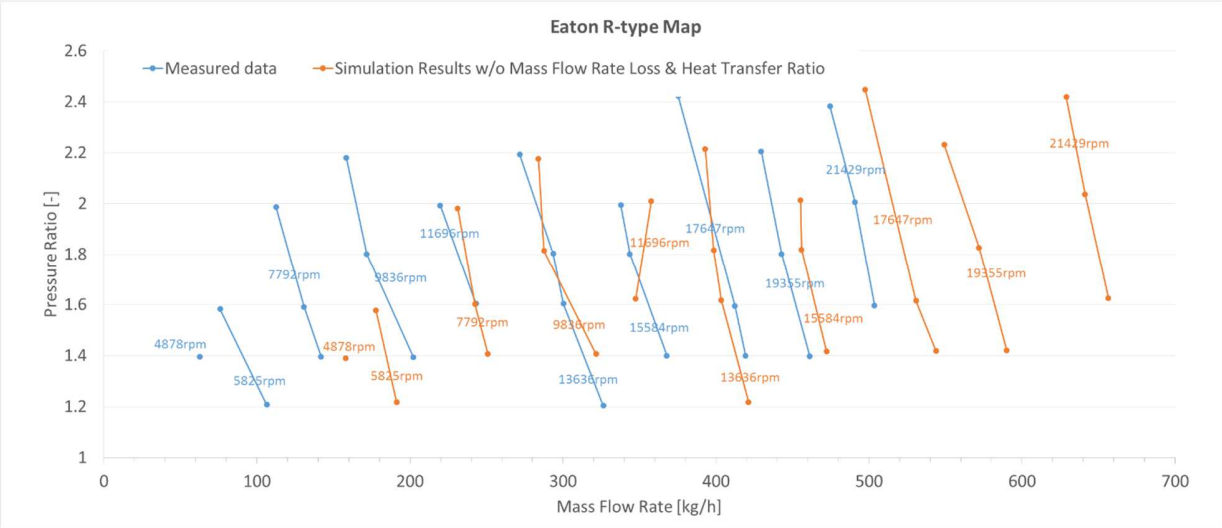

Figure 5-6: *Measured data and 1-D model results comparison – raw simulation results without taking leakages and heat transfer into account (R-type supercharger)*

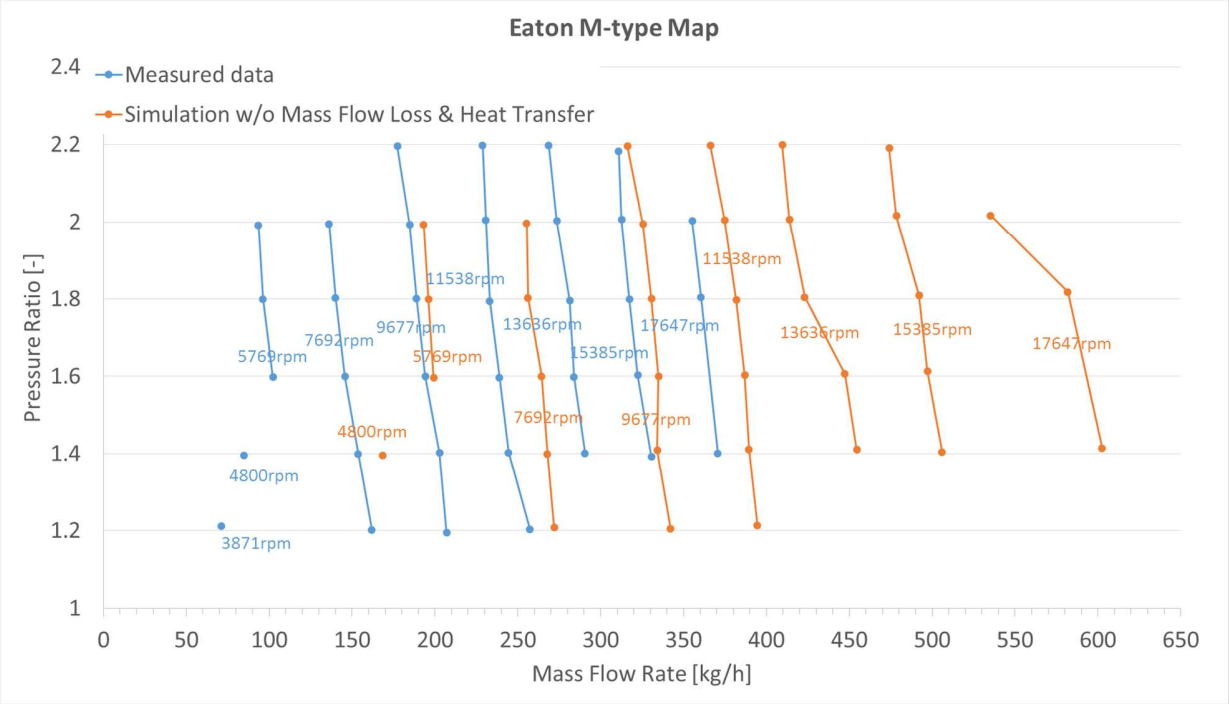

Figure 5-7: *Measured data and 1-D model results comparison – raw simulation results without taking leakages and heat transfer into account (M-type supercharger)*

Table 5-1: *1-D model convergence criteria*

Convergence Criteria				
	Supercharger Speed [rpm]	**Outlet Temperature [K]**	**Mass Flow Rate [kg/h]**	**Outlet Pressure [bar]**
Type of Steady State Criterion	cycle-to-cycle	target	cycle-to-cycle	cycle-to-cycle
Type of Steady State Tolerance	fractional	absolute	fractional	fractional
Steady State Tolerance	0.001	0.01	0.001	0.01
Consecutive Steady State Cycles	10	10	10	10

6 Supercharger Testing

6.1 Supercharger Preliminarily Testing

Initially, Roots-type supercharger (the smaller one R-type) was tested on a test bed at ČZ Strakonice, TURBO Division. The testing later continued for the bigger one R-type and M-24 superchargers at the Center of Vehicles for Sustainable Mobility located in Roztoky. Data obtained during the testing were used for the 1-D model calibration. Scheme of the used test bed is shown in ***Figure 6-1***. Following ***Figure 6-2*** presents the supercharger test bed at ČZ Strakonice, TURBO Division used for the smaller one R-type supercharger characterization.

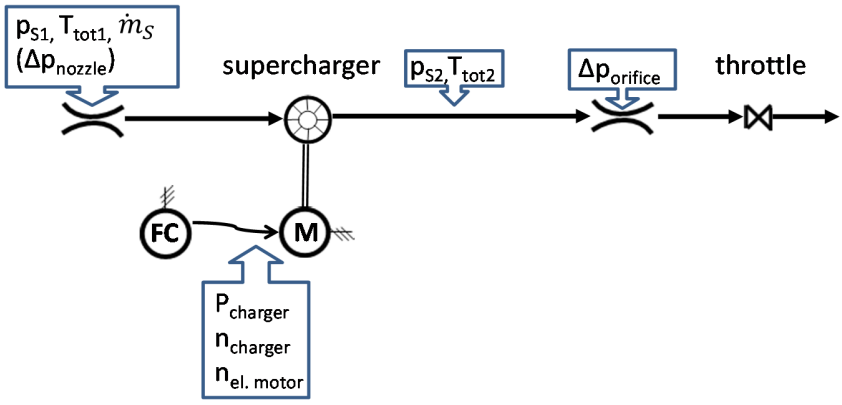

Figure 6-1: *Roots type supercharger test bed*

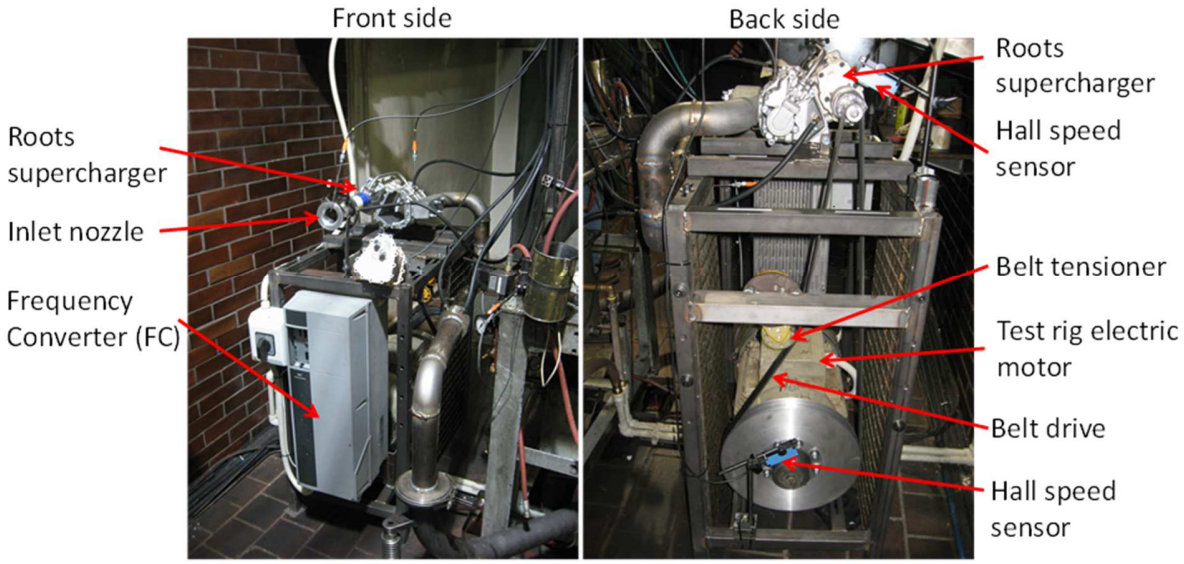

Figure 6-2: *Roots type supercharger test bed*

The supercharger testing consisted of measuring static pressures p_{S1}, p_{S2} and total temperatures T_{tot1}, T_{tot2} together with inlet mass flow rate evaluation at inlet nozzle $\dot{m}_S$. The air mass flow rate has been evaluated via standard nozzle according to DIN 1952 [30] or EN-ČSN 22 7710. The results of R250 supercharger map measurement have been used for calibration of GT-Power model in terms of mass flow rate – pressure ratio map.

6.2 Test Bed

A new test bed has been designed and built for supercharger testing using a combustion engine test cell at the Center of Vehicles for Sustainable Mobility in Roztoky. Knowledge obtained during preliminary supercharger testing at ČZ Strakonice has been used during this activity. The supercharger was driven by electric dynamometer (AVL Dyno Exact 202/12 220 kW/525 Nm), which is normally used for combustion engine testing. Its speed and pressure ratio were controlled by the operator with help of PUMA (AVL) data acquisition system (***Figure 6-4***). All the obtained values were stored by this system also. Values obtained by fast pressure sensors were analyzed by AVL Indicom software.

The supercharger testing consisted of measuring pressures and temperatures at inlet and outlet similar to testing at ČZ Strakonice. The air mass flow rate was evaluated by a calibrated flow meter (ABB Sensyflow FMT400-VTS). The supercharger test run in an open loop layout (***Figure 6-3***), where air flows to the supercharger through an approximately 2 meters long pipe with installed flow meter straight from the test cell. At outlet side air is expelled from the supercharger through a throttle to the test cell. However, the test cell was also prepared for running tests in closed loop where the expelled air from the supercharger outlet is cooled in an intercooler and delivered into the supercharger inlet (***Figure 6-4***). This test bed layout might be very useful when considering a combustion engine with two-stage boosting group using a supercharger at high pressure stage.

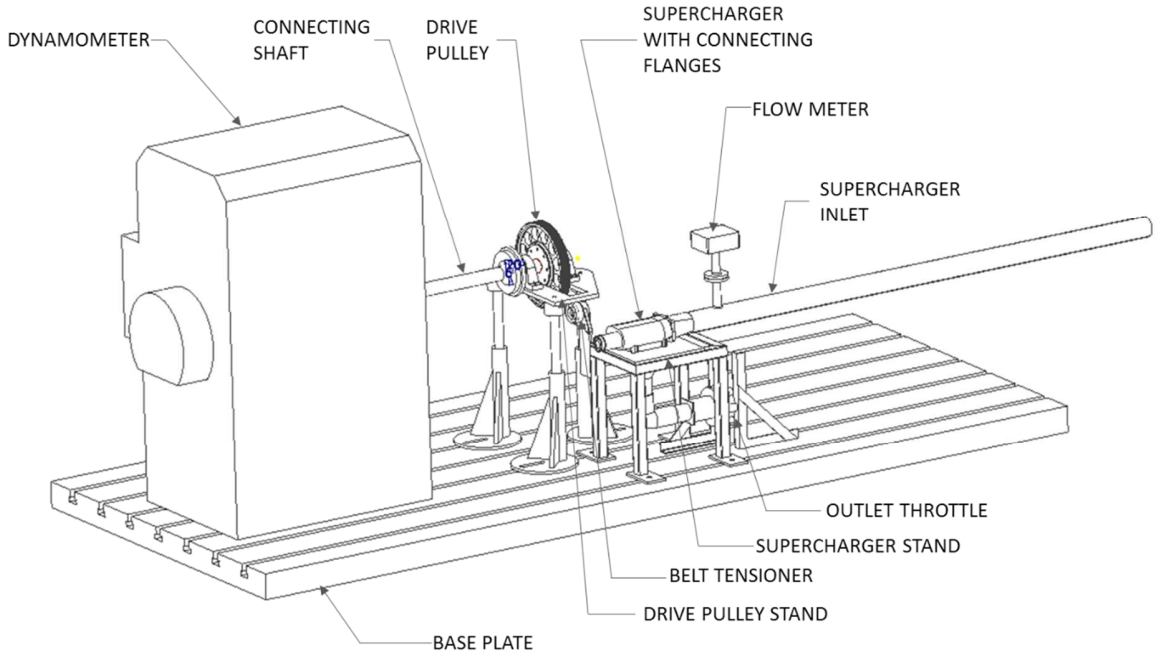

Figure 6-3: *Test bed for a supercharger testing in open-loop*

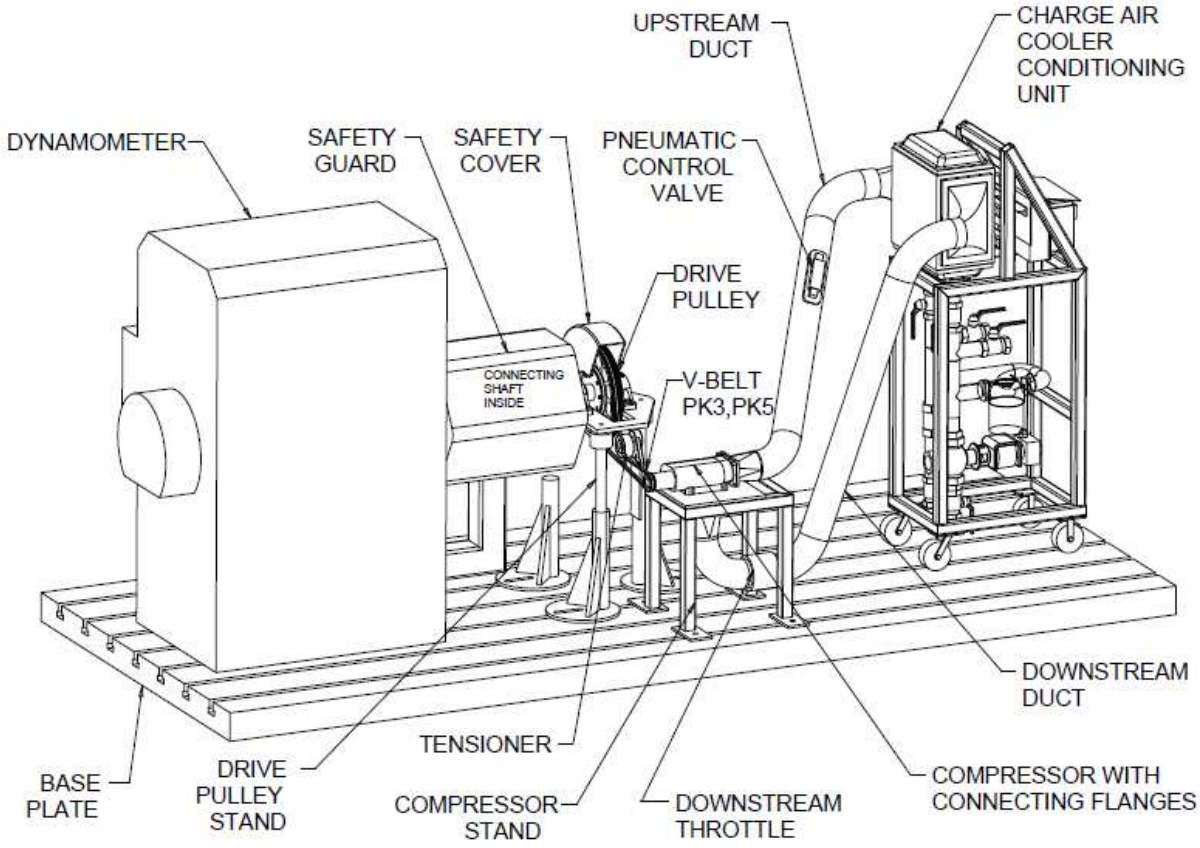

Figure 6-4: *Combustion engine test bed equipped for a supercharger testing. A layout enabling closed-loop supercharger testing is shown in this figure.*

6.3 Pressure Indication in the Supercharger Chamber

To know more about the processes in the supercharger inter-teeth gap pressure indication has been used. These data were used for detailed analysis of the supercharger in the next step of the work. Both, the bigger R-type and the M-type superchargers were characterized using test bed developed for this purpose.

Next to the measurement of static pressures p_{S1}, p_{S2}, total temperatures T_{tot1}, T_{tot2} and inlet mass flow rate a fast pressure indication in the supercharger chamber has been used to obtain pressure value during one cycle. The pressure indication at Roots-type supercharger inter-teeth gap is more

complicated unlike the case of an internal combustion engine cylinder using only one indication sensor or spark plug. Due to the fact that the supercharger chamber, in which pressure is indicated, rotates with the relevant rotor according to the machine casing pressure sensors have to be spread over the supercharger body. Values from all of the sensors have to be composed during data post-processing to get the final pressure behavior in the inter-teeth gap. It consists from different values depending on the compressor chamber position relative to the compressor housing. The post-processing of data is the key issue of this task.

Another important task is positioning of the sensors. Four fast pressure sensors were used to measure the chamber pressure at each important phase of the cycle. Important phases of the cycle are following:

- Chamber connected to the supercharger intake
- Chamber closed to intake and outlet
- Chamber opened to the outlet

In ***Figure 6-5*** is shown the placement of the pressure sensors. The supercharger housing had to be prepared appropriately for placing the fast pressure sensors. Holes had to be drilled and equipped with a M5 thread at the defined position of pressure sensors. The sensors assembly was tricky mostly due to that the supercharger housing wall thickness is about 5 mm. The pressure sensors used for this task were Kulite Semiconductor which are piezoelectric sensors with rated pressure of 10 bar and maximum pressure of 20 bar. These sensors are common in the combustion engine testing for fast pressure indication at engine intake or exhaust, for example.

Figure 6-6 shows the global view of the test bed at the test cell equipped with dynamometer, air flow meter, supercharger, throttle etc.

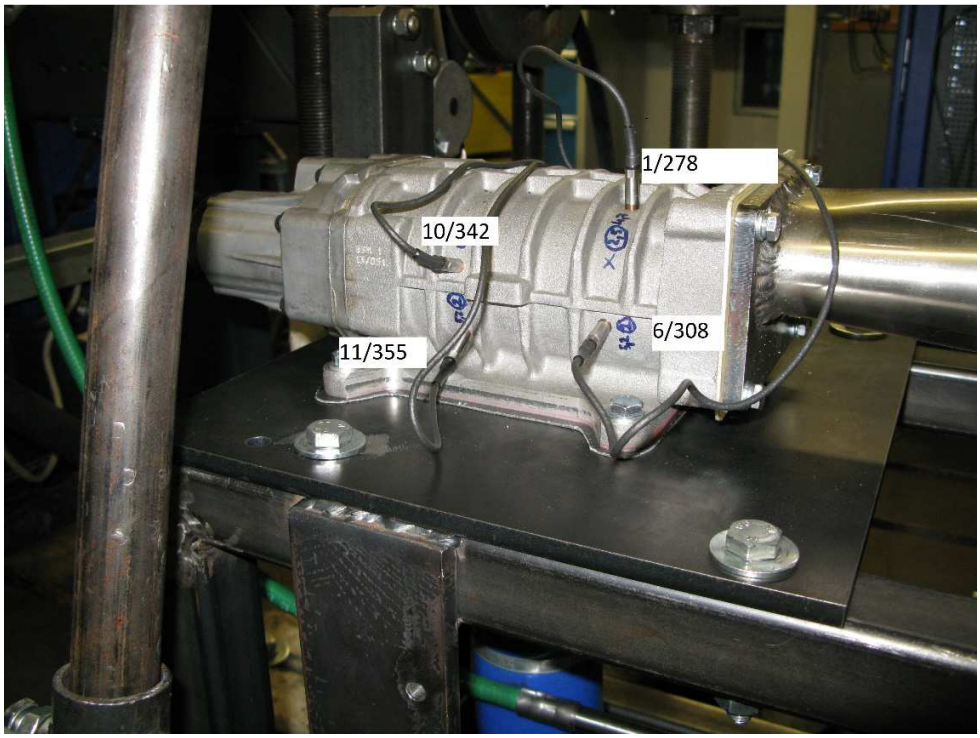

Figure 6-5: *Fast pressure sensors assembly at the supercharger housing with their names for identification of pressure signal. This placement enables measurement of pressure in the chamber at each important phase of the cycle.*

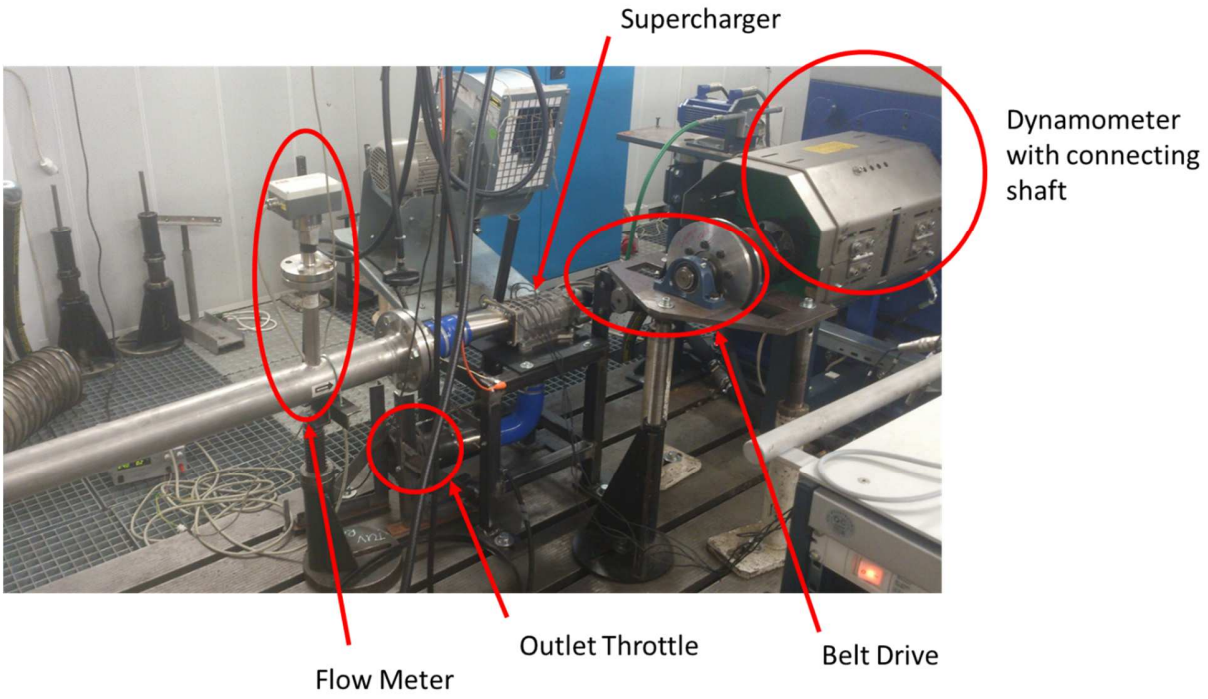

Figure 6-6: *Supercharger test bed in one of ICE test cells at the Center of Vehicles for Sustainable Mobility in Roztoky*

The plan of superchargers characterization had been prepared before the measurement started and tested operating points have been chosen and summarized in ***Table 6-1*** for R-type and M-type supercharger. The plan has been prepared with the main goal to test the supercharger inside the area of highest efficiency and at low speed, and high pressure ratios where the supercharger is mostly used when coupled with a passenger car combustion engine. The lists of both superchargers test points includes nominal speed of the dynamometer, supercharger pressure ratio and real supercharger speed during the test.

Table 6-1: *Superchargers testing plan*

Superchargers Testing Plan					
M-type Supercharger			R-type Supercharger		
Operating Point Number	Supercharger Rotor Speed	Pressure Ratio	Operating Point Number	Supercharger Pulley Speed	Pressure Ratio
[-]	[rpm]	[-]	[-]	[rpm]	[-]
1	4000	1.2	1	5000	1.4
2	5000	1.4	2	6000	1.2
3	6000	1.6	3	6000	1.6
4	6000	1.8	4	8000	1.4
5	6000	2	5	8000	1.6
6	8000	2	6	8000	2
7	8000	1.8	7	10000	1.4
8	8000	1.6	8	10000	1.8
9	8000	1.4	9	10000	2.2
10	8000	1.2	10	12000	1.6
11	10000	1.2	11	12000	2
12	10000	1.4	12	14000	1.2
13	10000	1.6	13	14000	1.6
14	10000	1.8	14	14000	1.8
15	10000	2	15	14000	2.2
16	10000	2.2	16	16000	1.4
17	12000	2.2	17	16000	1.8
18	12000	2	18	16000	2
19	12000	1.8	19	18000	1.4
20	12000	1.6	20	18000	1.6
21	12000	1.4	21	18000	2.4
22	12000	1.2	22	20000	1.4
23	14000	1.4	23	20000	1.8
24	14000	1.6	24	20000	2.2
25	14000	1.8	25	22000	1.6
26	14000	2	26	22000	2
27	14000	2.2	27	22000	2.4
28	16000	2.2			
29	16000	2			
30	16000	1.8			
31	16000	1.6			
32	16000	1.4			
33	18000	1.4			
34	18000	1.8			
35	18000	2			

6.4 Pressure Indication Results

Raw pressure values of 9 cycles obtained during supercharger test are shown in following ***Figure 6-7*** for R-type supercharger and in ***Figure 6-8*** for 7 cycles of the M-type supercharger at the same operating point. Data are shown in that format there as obtained from AVL Indicom and displayed using AVL Concerto software. The x axis represented by a time line has to be transformed to degrees of supercharger rotors position for further use in 1-D model calibration. Pressure value called **1/278** is measured when the inter-teeth gap is opened to inlet, **10/342** and **6/308** are measured when the gap is connected to inlet and outlet through connection areas (inlet and outlet ports closed) and finally **11/355** is obtained when the gap is connected to outlet through outlet port. The closer is the chamber to the connection with exhaust the higher is the pressure peak even if the outlet port is closed (**10/342** and **6/308**). This is caused by connection with outlet through connection areas via previous gaps and due to internal leakages in the supercharger caused by clearances between rotors or rotors and housing. Finally, after connecting the chamber to the exhaust an abrupt compression occurs up to the pressure in the exhaust (**11/355**), followed by pressure oscillations. The data have been evaluated this way for each operating point and were compared with 1-D model results.

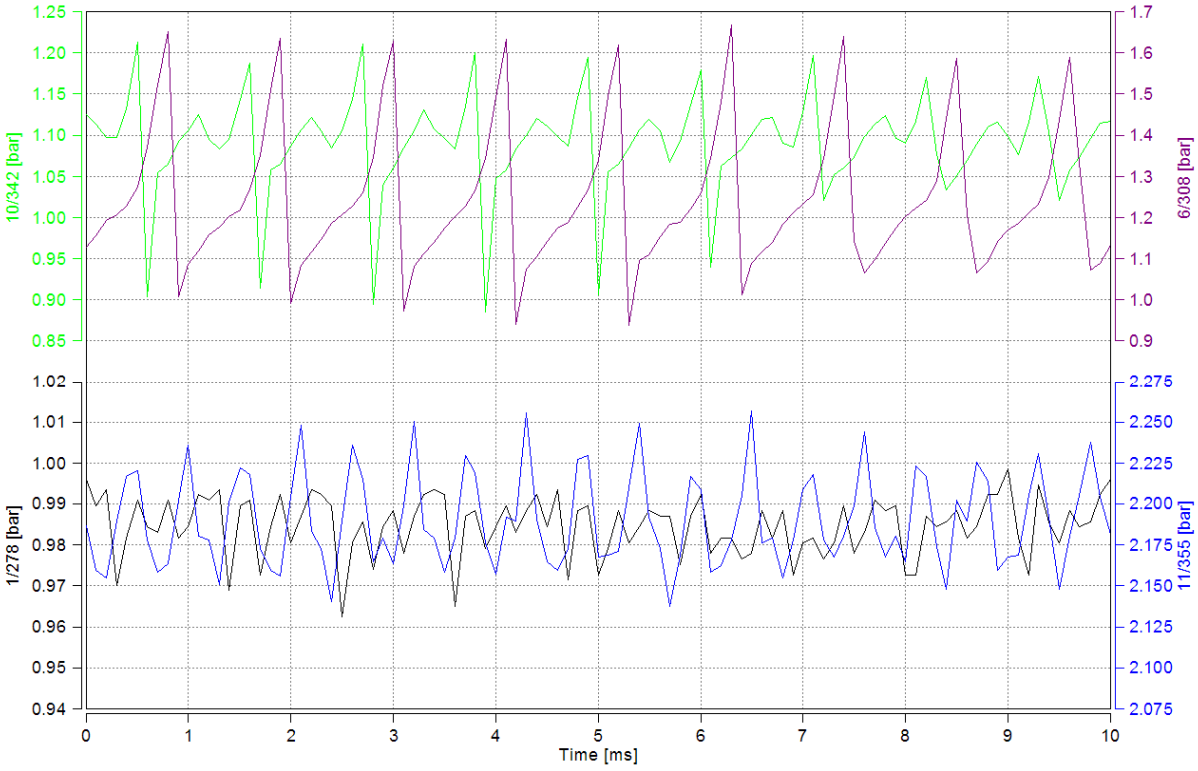

Figure 6-7: *Pressure values obtained during inter-teeth gap pressure indication for 14000 rpm and pressure ratio of 2.2 (R-type supercharger)*

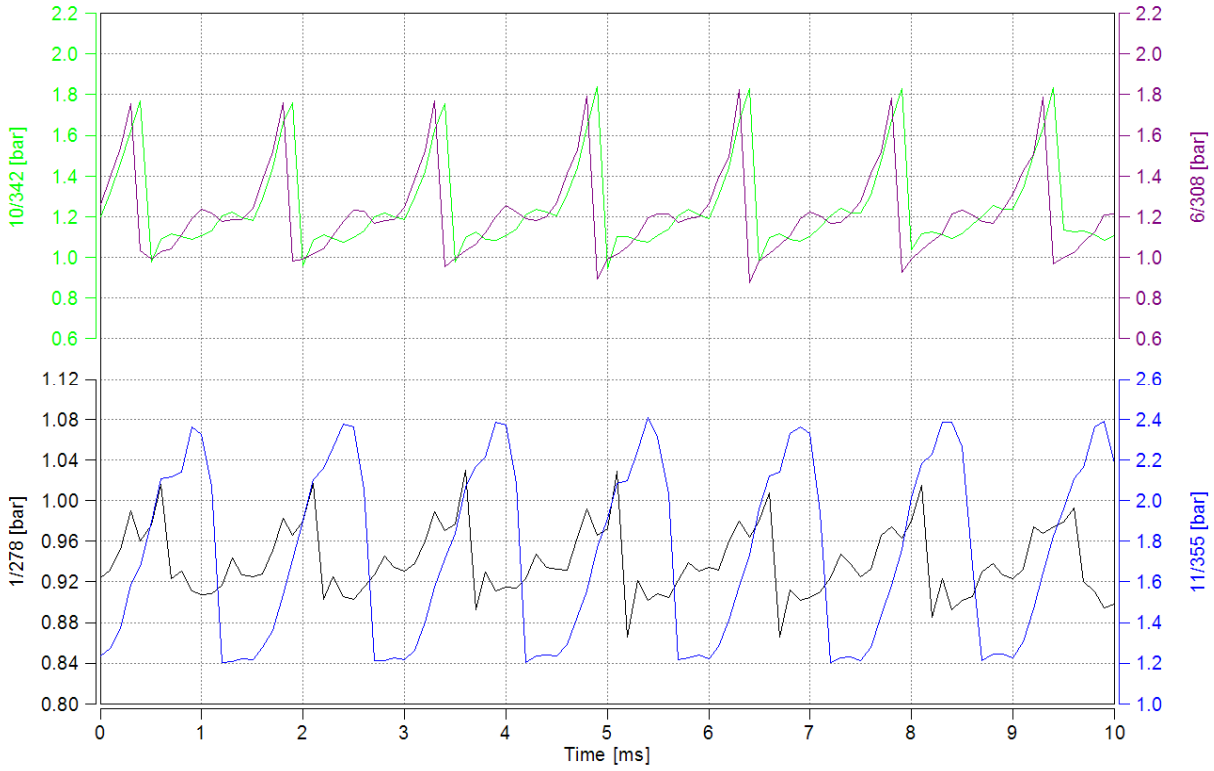

Figure 6-8: *Pressure values obtained during inter-teeth gap pressure indication for 14000 rpm and pressure ratio of 2.2 (M-type supercharger)*

6.5 Evaluation of the Results

As shown in ***Figure 6-7*** and ***Figure 6-8*****,** raw pressure values obtained during inter-teeth gap pressure indication are four separate chains of values, which have to be cut, connected appropriately and seated to an x axis represented by degrees of supercharger rotor position. How to do that is shown in ***Figure 6-9*** - ***Figure 6-12***. The position of measured data from each sensor in inter-teeth gap pressure is given by the position of each sensor at the supercharger housing.

Evaluation of the results is demonstrated at R-type supercharger at the operating point 14000 rpm/2.2 pressure ratio.

The approach is following:

1. The raw pressure signal from each sensor has to be cut to get the part corresponding to only one cycle (***Figure 6-9***).
2. The time base has to be transferred to degrees in the next step (***Figure 6-10***). This transfer is defined by the following equation:

$$\boldsymbol{\alpha = \frac{360 \cdot t \cdot n}{60} = 6 \cdot t \cdot n}, \tag{6.1}$$

   where $\boldsymbol{\alpha}$ is the rotor position in *degrees*, $\boldsymbol{t}$ is time of the pressure value in *seconds* and $\boldsymbol{n}$ is the speed of the supercharger in *rpm.*
3. After that, pressure values from each sensor are positioned appropriately according to the sensor position at the supercharger housing (***Figure 6-11***).
4. Finally, the positioned data are connected (***Figure 6-12***).

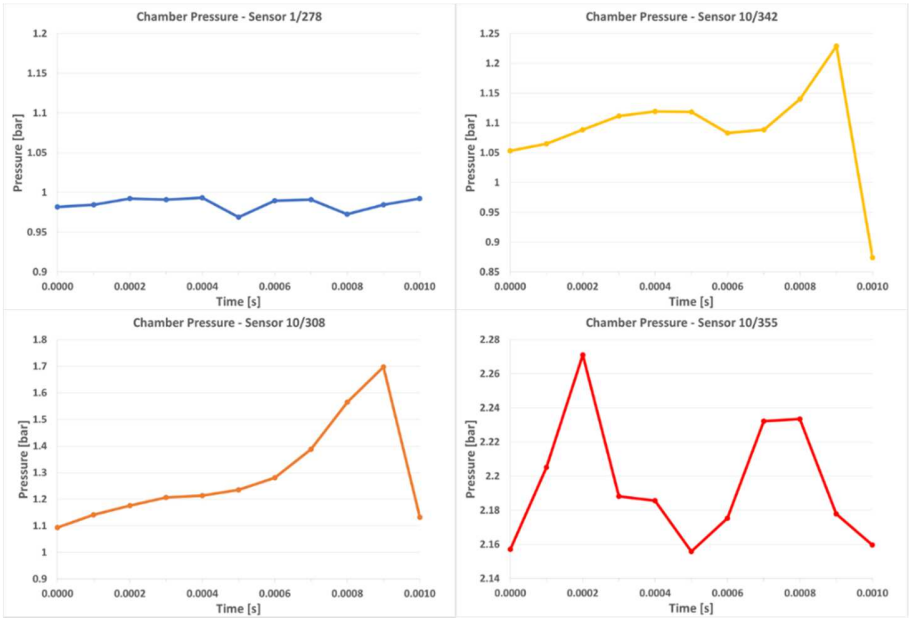

Figure 6-9: *Pressure values from each sensor corresponding to one cycle (at time base at this stage) (R-type supercharger)*

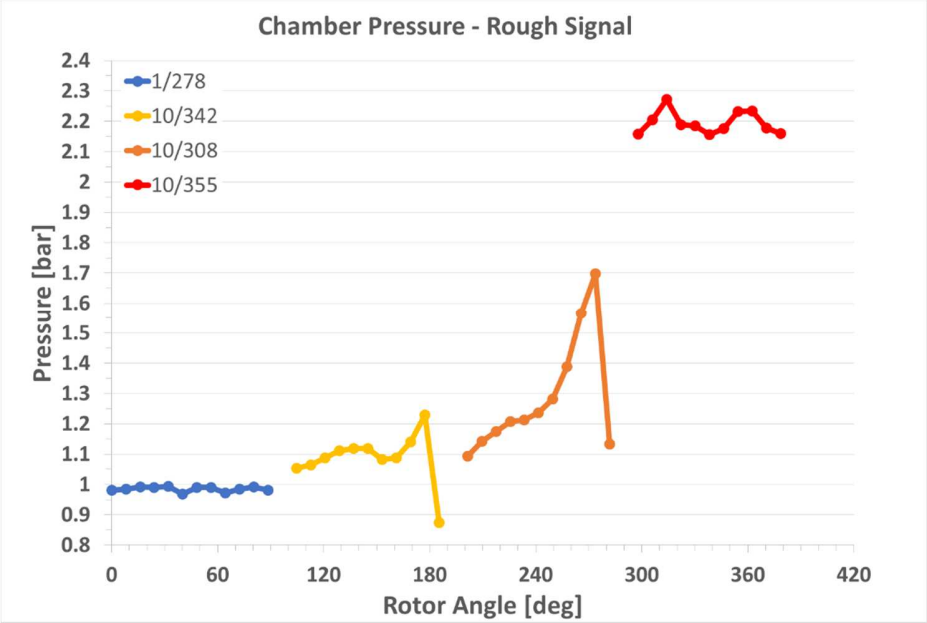

Figure 6-10: *Pressure data from each sensor put on the degrees base (R-type supercharger)*

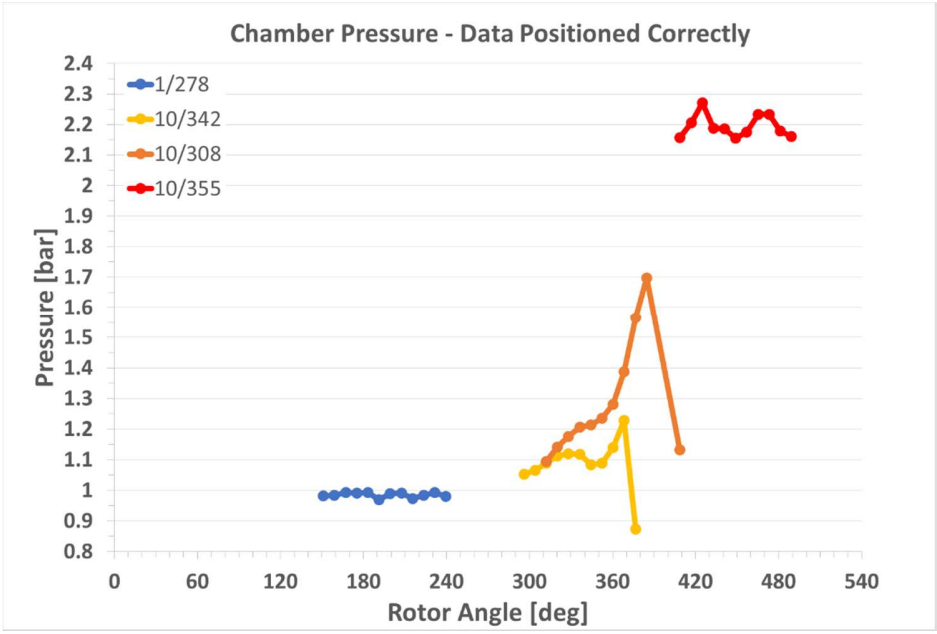

Figure 6-11: *Pressure data corresponding to relevant pressure sensor position (R-type supercharger)*

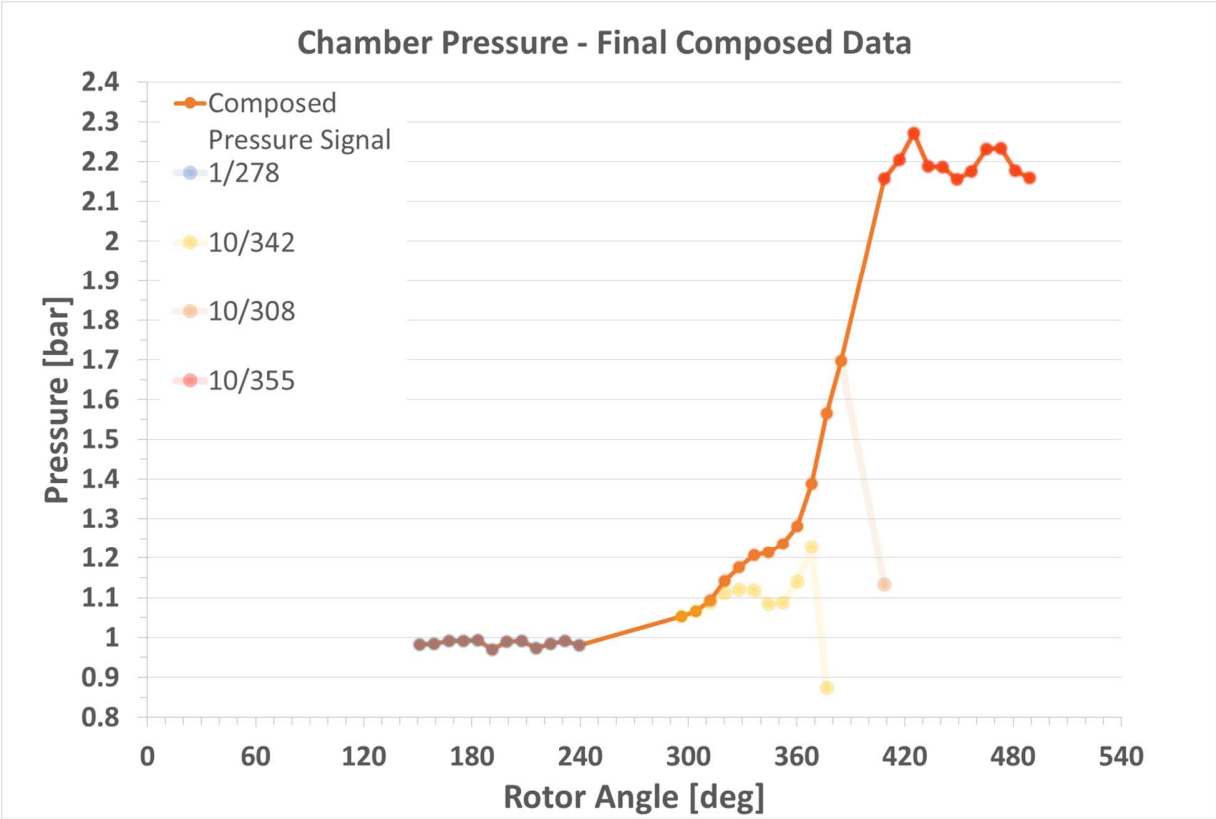

Figure 6-12: *Final pressure data (orange curve) measured in supercharger inter-teeth gap using four pressure sensors placed around the supercharger casing (R-type supercharger)*

As is obvious from ***Figure 6-11*** and ***Figure 6-12*****,** the pressure data obtained using sensor **10/342** and **10/308** overlap each other. This is caused by their position at the supercharger casing when they sense pressure in the inter-teeth gap at the same time but from different position – **10/342** near the supercharger inlet and **10/308** near the outlet. That is why only two first values from **10/342** sensor data are used for each operating point and the rest is defined by pressure obtained from **10/308**. Interesting is also different behavior of pressure from these two sensors between approximately 320 deg and 360 deg. The reason, why pressure decrease occurs in pressure signal of the **10/342** sensor, is unknown at this time. It might be caused by some reflected pressure wave in the inter-teeth gap when filling by backflow from supercharger outlet and **10/342** register it more sensitively because of its position farer from the high pressure source – connection with inter-teeth gap already opened into supercharger outlet. But this is only hypothesis, which should be

investigated in detail in future work. Next to that, data from both sensors finishes with relatively low values of pressure (around 370 deg for **10/342** and around 410 deg for **10/308**). They were probably sensed in time when rotor tooth passes around the pressure sensor and blinded it. Thus these values have not been considered also.

This evaluation has been used for all R-type supercharger test points and all results are shown in **Appendix A**.

The same data evaluation approach has been used for values obtained during M-type supercharger testing. As is obvious from ***Figure 6-13***, overlap of data obtained from different sensors is much higher than in the case of R-type supercharger. This is caused by the supercharger casing design and thus quite tricky placement of the sensors. Next to that, significant difference in pressure values are obvious between 240 deg and 310 deg. This is not clear yet, but it might have a consequence in pressure wave dynamic in the supercharger chamber, probably. The obtained pressure differs according to the sensor position on the supercharger casing. Evaluated pressure behavior for tested points for M-type supercharger are presented in **Appendix B**.

The composed measured data were compared to simulation results obtained from 1-D model in the next step.

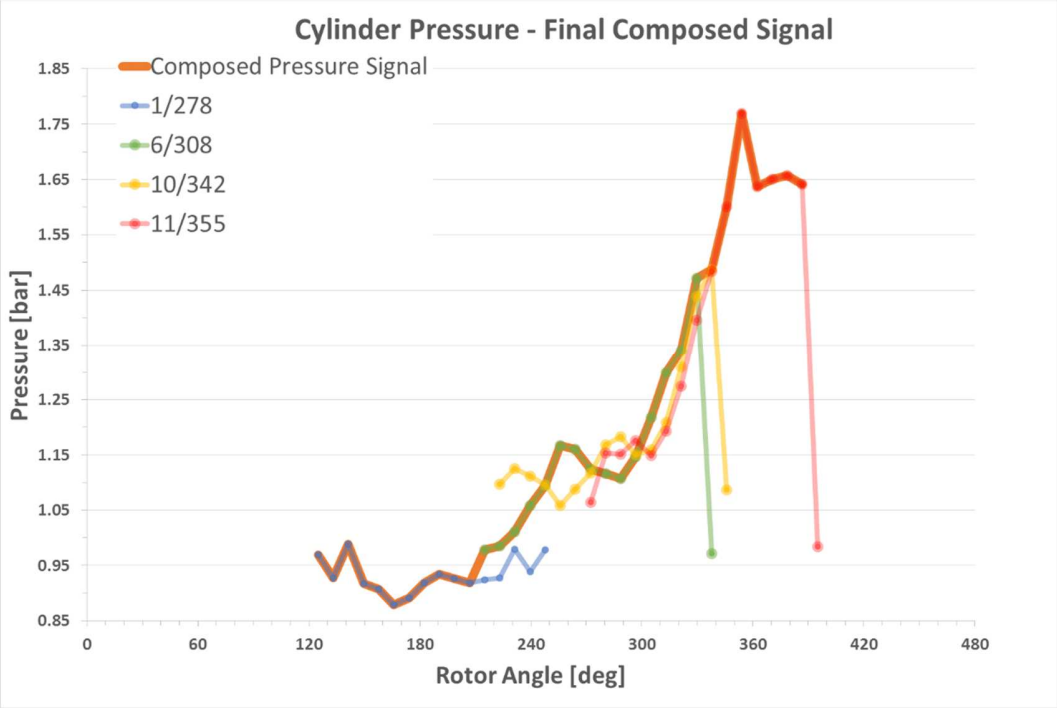

Figure 6-13: *Final pressure data (orange curve) measured in supercharger inter-teeth gap using four pressure sensors placed around the supercharger casing (M-type supercharger)*

7 1-D Model Calibration

Based on supercharger testing results, the 1-D model in GT-Power has been calibrated for both supercharger types. The calibration was made to fit measured mass flow rate and isentropic efficiency for each test point shown in supercharger map. As described in **Chapter 5** there are five calibration parameters to be considered during the calibration process:

1. Clearance Ratio
2. Leakage Area
3. Leakage Area Discharge Coefficient
4. Supercharger Casing Wall Heat Transfer Coefficient
5. Supercharger Wall Temperature

7.1 Clearance Ratio Sensitivity Study

Sensitivity study of R-type supercharger mass flow rate to clearance ratio has been made. As mentioned above GT-Power is a simulation environment developed primarily for simulations of machines, which use crankshaft mechanism, combustion engines, piston compressors, pumps etc. thus a transformation is needed to be made when a simulation of other type of machine is considered. Despite the fact, there is no internal compression in Roots-type supercharger a clearance ratio has to be defined when substituting supercharger's inter-teeth gap and meshing tooth by a cylinder and piston typical for combustion engines. The clearance ratio has been varied during the study from 3 up to 15. The mass flow rate has been evaluated when changing clearance ratio at different supercharger operating points and is shown in ***Figure 7-1***. As is obvious from this figure, mass flow rate is much more sensitive to the value of clearance ratio with increasing supercharger speed and pressure ratio. The mass flow rate does not depend on clearance ratio from its value of 8 at 8000rpm and pressure ratio of 1.4. Increasing of clearance ratio from the value of 10 does not affect mass flow rate for 14000rpm – pressure ratio of 1.8 and 18000rpm –2.4. Finally, change of clearance ratio 12 for higher one has no significant impact on mass flow rate at 22000rpm and pressure ratio of 2.4. That is why 12 has been chosen as the value of clearance ratio for further simulations for all points shown in supercharger map.

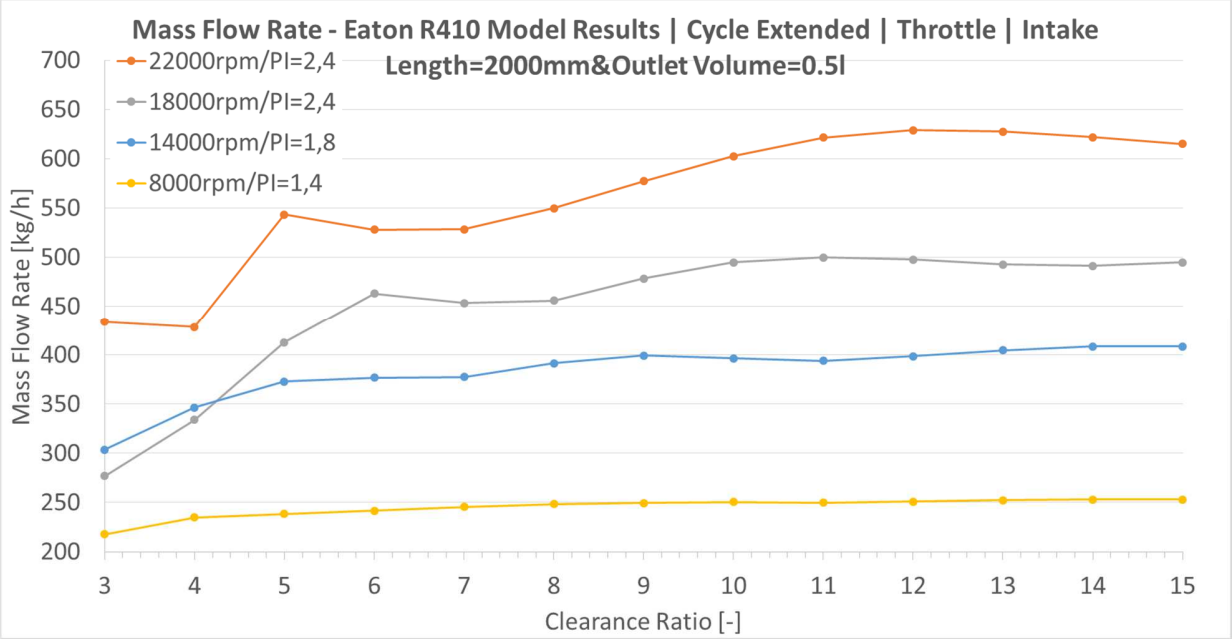

Figure 7-1: *Clearance ratio sensitivity study results*

7.2 Mass Flow Rate and Isentropic Efficiency Calibration

After appropriate clearance ratio has been chosen, mass flow rate and isentropic efficiency had to be calibrated at each point of supercharger map according to measured values. Operating points considered during the model calibration are shown in ***Table 7-1***. The table includes real supercharger speed during test, *equivalent speed* used in the model due to the cycle length transformation (610 deg -> 720 deg) and time of one cycle in the test.

Table 7-1: *R-type supercharger operating points used for 1-D model calibration*

Operating Point Number	Supercharger Nominal Speed	Pressure Ratio	Supercharger speed	*Equivalent Speed*	Time of one rotor revolution
[-]	[rpm]	[-]	[rpm]	[rpm]	[ms]
1	5000	1.4	4878	5758	12.3
2	6000	1.2	5825	6876	10.3
3	6000	1.6	5882	6943	10.2
4	8000	1.4	7792	9197	7.7
5	8000	1.6	7792	9197	7.7
6	8000	2	7692	9079	7.8
7	10000	1.4	9836	11610	6.1
8	10000	1.8	9836	11610	6.1
9	10000	2.2	9724	11478	6.17
10	12000	1.6	11696	13805	5.13
11	12000	2	11673	13778	5.14
12	14000	1.2	13636	16095	4.4
13	14000	1.6	13453	15879	4.46
14	14000	1.8	13483	15915	4.45
15	14000	2.2	13423	15843	4.47
16	16000	1.4	15584	18395	3.85
17	16000	1.8	15385	18159	3.9
18	16000	2	15464	18252	3.88
19	18000	1.4	17647	20829	3.4
20	18000	1.6	17391	20527	3.45
21	18000	2.4	17291	20409	3.47
22	20000	1.4	19355	22845	3.1
23	20000	1.8	19355	22845	3.1
24	20000	2.2	19355	22845	3.1
25	22000	1.6	21429	25293	2.8
26	22000	2	21277	25113	2.82
27	22000	2.4	21201	25025	2.83

Mass flow rate results yielded by the supercharger model are calibrated to measured data using leakages as mentioned above. Leakage area is in the 1-D model defined using a poppet valves with defined lift and optimized diameter. Since the lash between meshing rotors or between rotor and supercharger casing is the same at real supercharger, a mean value of the valve diameter was chosen to be constant for all supercharger characteristics points (***Figure 7-2***) after preliminary calculation. Changes in clearance area size due to temperature extension of each supercharger part are included in a discharge coefficient. The discharge coefficient considers also different speeds of the

supercharger components at different operating points and thereby different flow velocities through this slots. The effective area of clearances at each operating point is defined by flow area given by geometrical dimensions at cold stayed and by the discharge coefficient (***Figure 7-3***). Dividing the effective area of leakages between meshing rotors by the length of contact curve a virtual lash is obtained, which corresponds to the discharge coefficient equal to 1. The same calculation is performed also for leakages between rotors and supercharger casing (***Figure 7-4***). The size of both lashes seems to be reasonable. Corresponding discharge coefficients are plotted in ***Figure 7-5***.

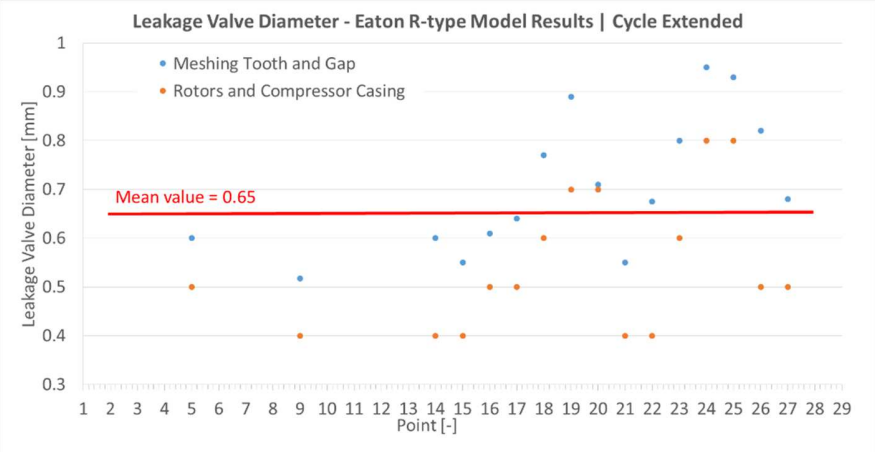

Figure 7-2: *Preliminary calculation of diameter for valve simulating leakage area in the rotors mesh or between rotor and supercharger casing at constant lift and the mean value of diameter used for further calculations | Simulation points numbered according to* ***Table 7-1***

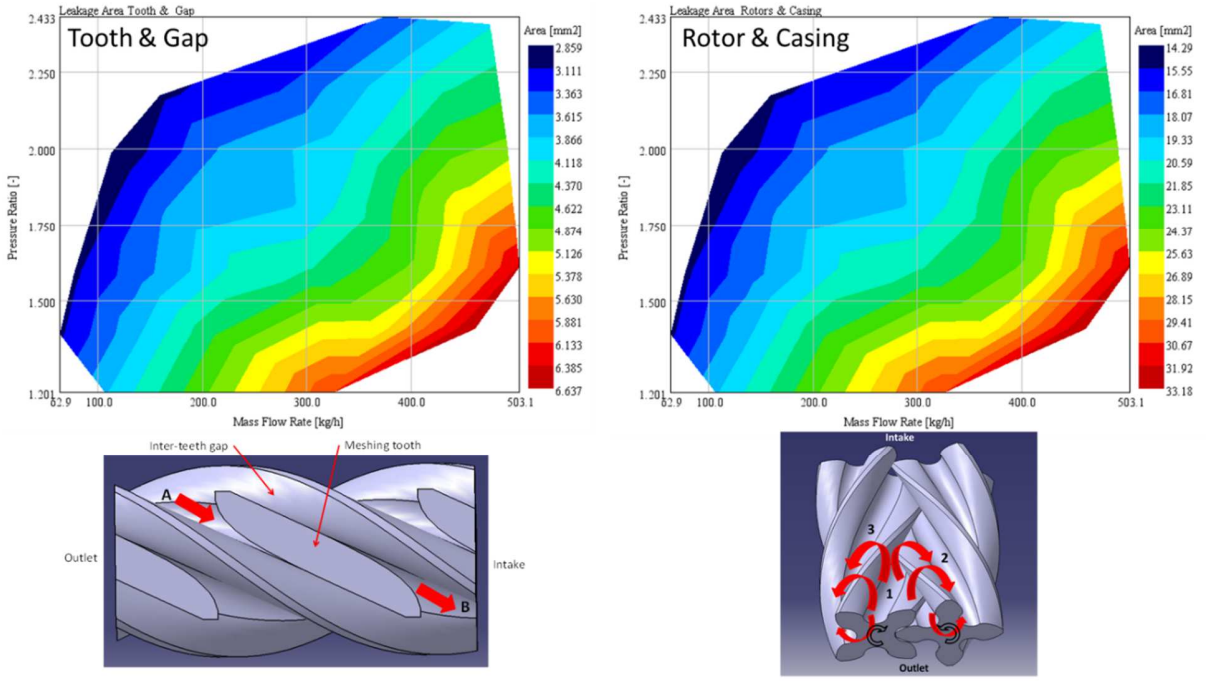

Figure 7-3: *Effective area of leakages at R-type supercharger at the whole supercharger map calculated for fixed leakage valve diameter and lift - only discharge coefficient calibrated | Leakage area between meshing tooth and gap at the left side with the scheme of leakage process below, leakage area between rotors and supercharger casing at the right with the scheme of leakage process below*

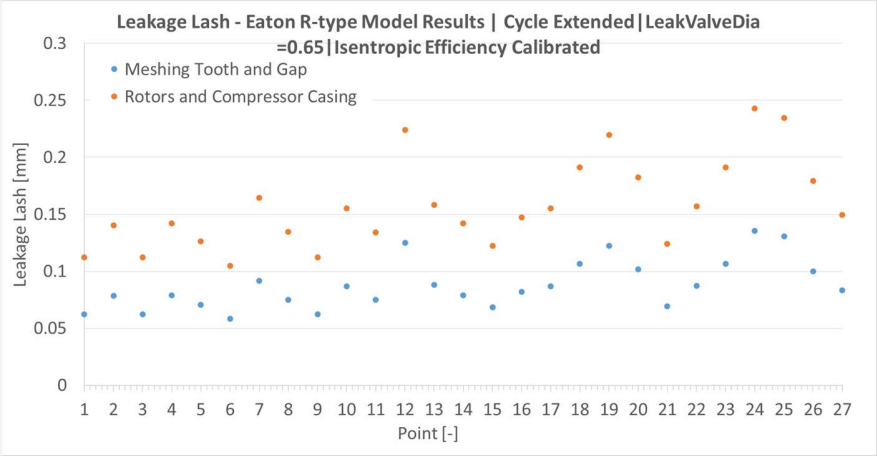

Figure 7-4: *Virtual size of lashes between meshing rotors (blue points) and between rotors and supercharger casing (orange points) originating in 1-D simulation results | Simulation points numbered according to* ***Table 7-1***

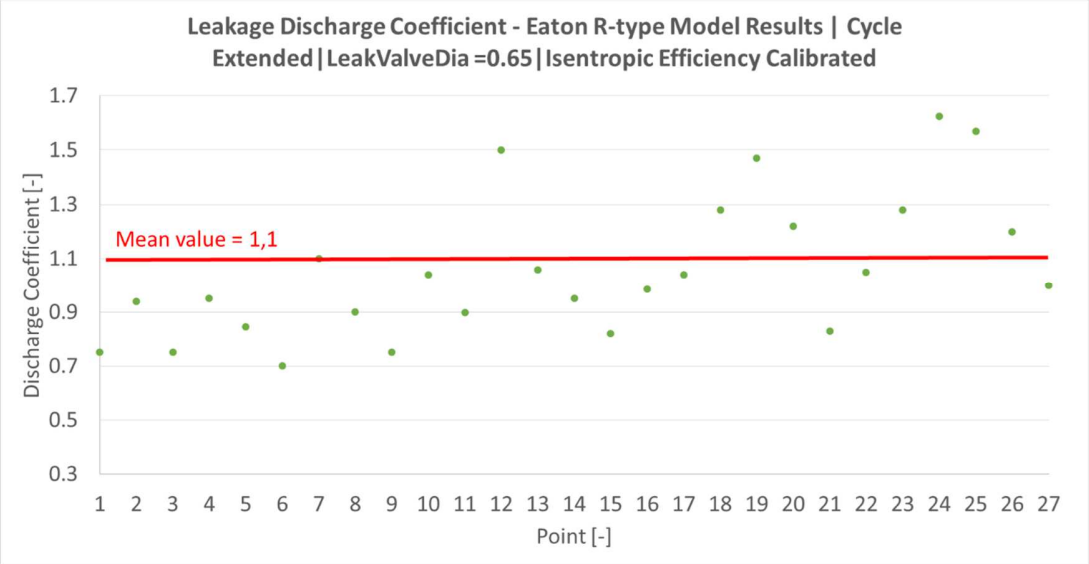

Figure 7-5: *Discharge coefficient values corresponding to effective leakage areas plotted in* ***Figure 7-3*** *| Mean value chosen for sensitivity study | Simulation points numbered according to* ***Table 7-1***

Next to that, supercharger inter-teeth gap wall heat transfer coefficient together with the inter-teeth gap wall temperature are used to calibrate supercharger's isentropic efficiency at the same time. Finally, there are four parameters to be optimized to get measured values of mass flow rate and isentropic efficiency actually. That is why an effort for reduction of optimization parameters number is justified. Thus constant flow area (valve diameter and lift) of leakages has been chosen for all operating points and only the discharge coefficient varied. Reasonable values have been chosen in case of heat transfer coefficient for the low pressure phase of the supercharger working cycle (inlet opened) at each operating point. These values have been multiplied by two for the phase of the cycle when backflow from supercharger outlet occurs and thus gas in inter-teeth gap is compressed (***Figure 7-6***). This assumption when multiplying the heat transfer coefficient by the factor of two has no real background in measurement but it is based on experience with combustion engine heat transfer and should be verified in future work.

Selecting appropriate values of leakages flow area (constant value of valve diameter and lift) and heat transfer coefficient only leakages discharge coefficient and inter-teeth gap wall temperature remain as parameters to be optimized at each supercharger operating point.

Comparison of supercharger outlet temperature obtained during testing and yielded by calibrated model are shown in ***Figure 7-7***. Small difference between measured and simulation results respects only the accuracy of the calibration process. Values of chamber wall temperature from the calibrated 1-D model are plotted in the same figure. Only simulation results are available for this quantity at this time and should be verified in the future. Surprisingly, wall temperature results higher than outlet temperature at operating point number 12 (14000rpm – PR=1.2). This is caused probably by relatively high heat capacity of supercharger rotors and casing together with fast change of operating points during tests – from 12000rpm/PR=2.0 to 12000rpm/PR=1.6 and to 14000rpm/PR=1.2 finally. Correlation chart of measured and simulated outlet temperatures is shown in ***Figure 7-8*** for easier comparison of measured data and simulated results.

Finally, comparison of measured and simulated isentropic efficiency is plotted in ***Figure 7-9*** where good agreement of both values is obvious.

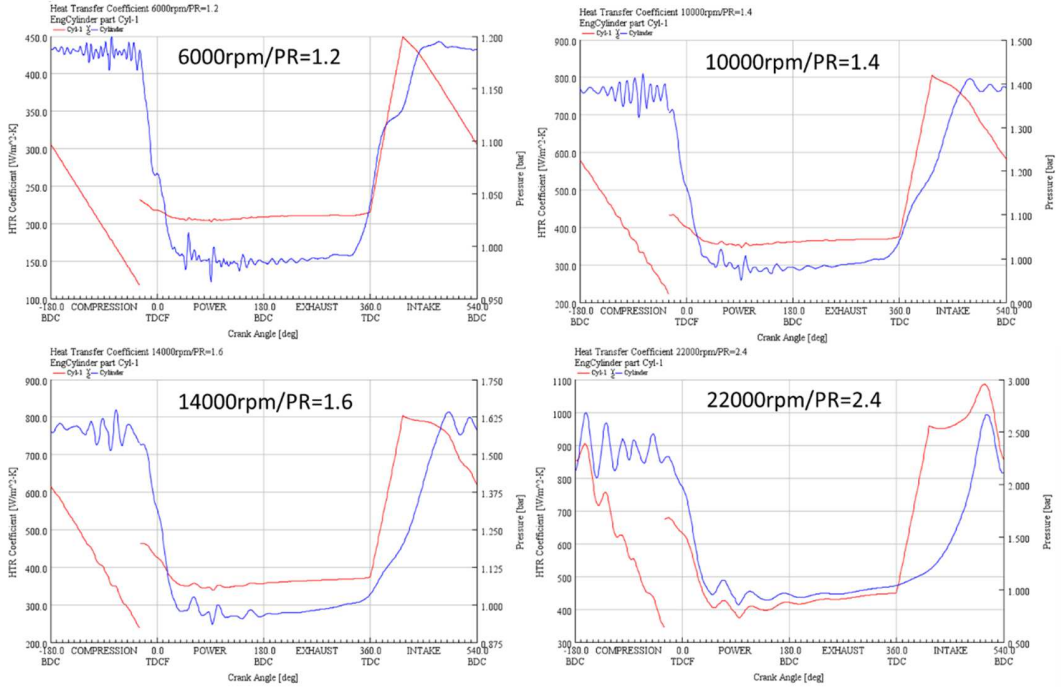

Figure 7-6: *Heat transfer coefficient values (red) together with chamber pressure (blue) for different R-type supercharger operating points.*

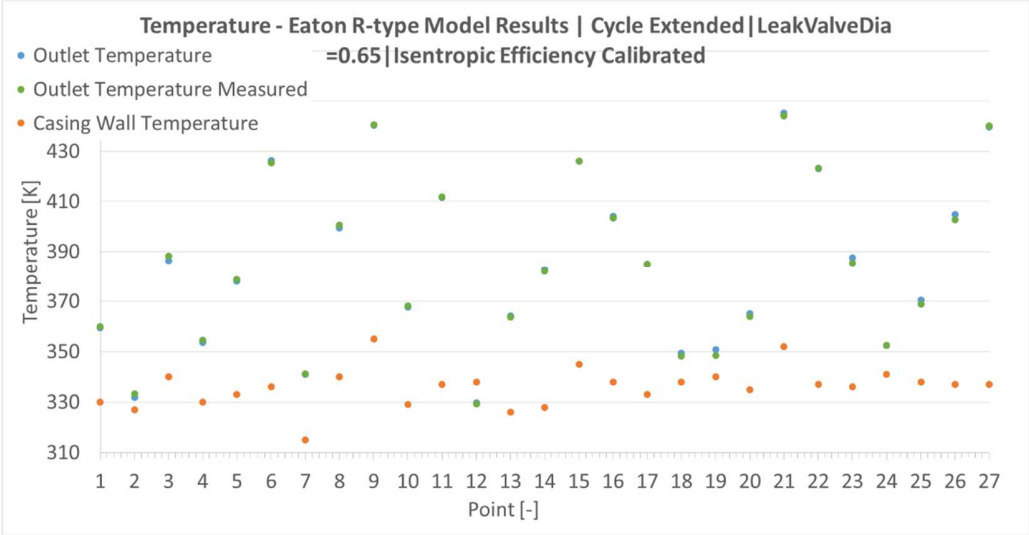

Figure 7-7: *Supercharger outlet temperature (blue dots) compared to measured values (green dots) and to inter-teeth gap wall temperature (orange dots - only simulation results available) after 1-D model calibration | Simulation points numbered according to* ***Table 7-1***

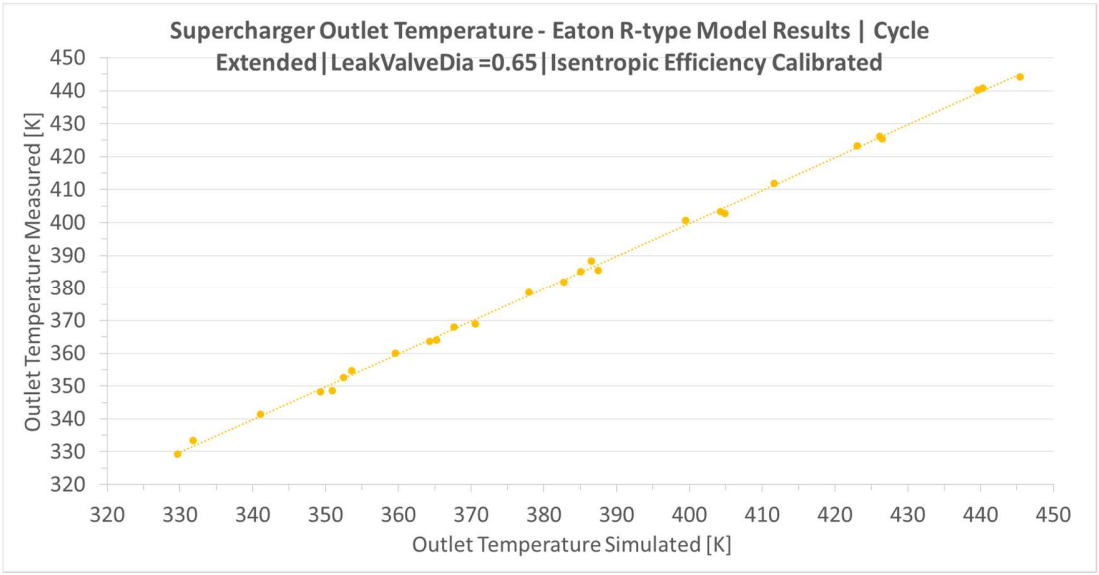

Figure 7-8: *Correlation chart of supercharger outlet temperature results - measured versus simulation results*

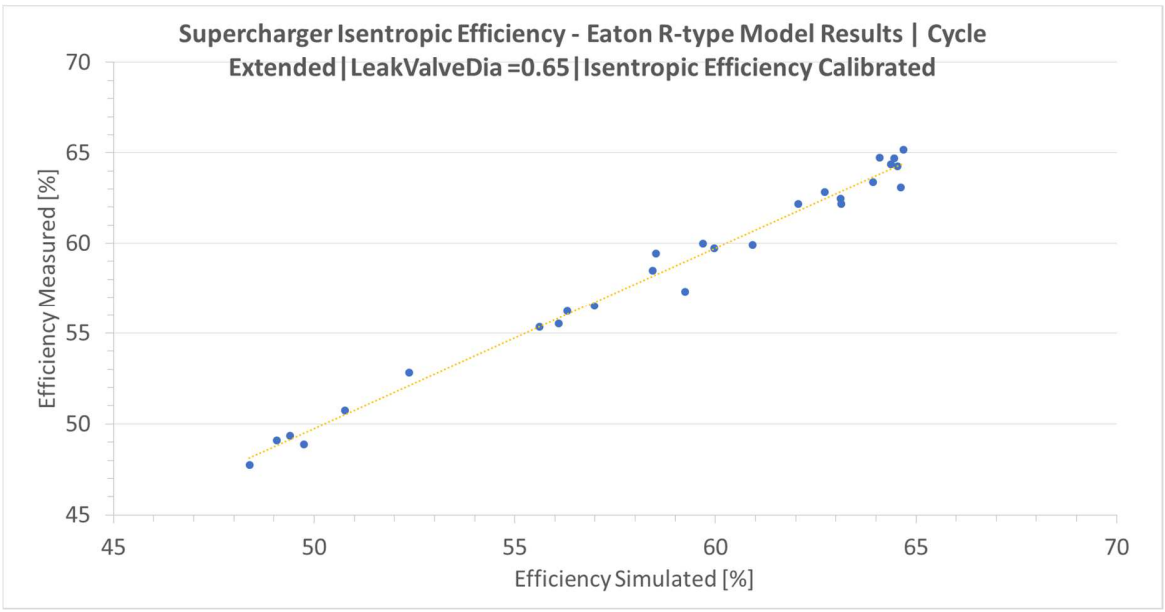

Figure 7-9: *Comparison of measured and simulated values of R-type supercharger isentropic efficiency*

The same approach has been applied for M-type supercharger model calibration. Since this activity should only demonstrate the capability of the 1-D model to work with different supercharger designs it has been only 9 operating points from measured characteristic calibrated for the M-type supercharger (***Table 7-2***).

Table 7-2: *M-type supercharger operating points used for 1-D model calibration*

Operating Point Number	**Supercharger Nominal Speed**	**Pressure Ratio**	**Compressor speed**	***Equivalent Speed***	**Time of one rotor revolution**
[-]	**[rpm]**	**[-]**	**[rpm]**	**[rpm]**	**[ms]**
1	10000	1.2	9677	12903	6.2
2	10000	1.8	9677	12903	6.2
3	10000	2.2	9524	12698	6.3
4	14000	1.4	13636	18182	4.4
5	14000	1.6	13636	18182	4.4
6	14000	2.2	13333	17778	4.5
7	18000	1.4	17647	23529	3.4
8	18000	1.8	17647	23529	3.4
9	18000	2	17143	22857	3.5

After preliminary simulations, the mean value of valves diameter simulating leakages in the supercharger was set to 1.5mm, the lift remain at the same value like at R-type supercharger. The size of virtual lashes after the calibration of M-type model to measured mass flow rate and isentropic efficiency is shown in ***Figure 7-10***. In ***Figure 7-11*** are presented values of discharge coefficient of leakage orifices. Looking in this figure it seems, that the size of the valves simulating leakages in the M-type supercharger model were chosen too big thus the discharge coefficient results in values lower than 1 for the most of considered cases. Looking in ***Figure 7-12*** it's obvious that the outlet temperatures were calibrated successfully and supercharger chamber wall temperatures feature reasonable values. The measured and simulated outlet temperatures are compared later in correlation chart in ***Figure 7-13*** also. Good agreement of measured and simulated values of isentropic efficiency is obvious from the comparison presented in ***Figure 7-14***.

Finally, not only R-type also M-type supercharger model calibration was successful and measured data were easily achieved by the calibrated model. Next to that, all the calibration parameters features reasonable values.

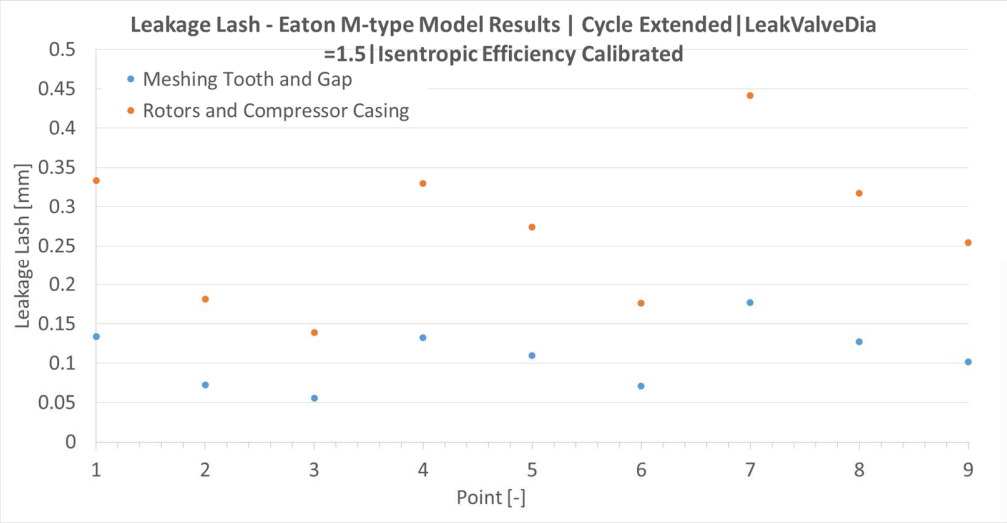

Figure 7-10: *Size of virtual lashes between supercharger components after the mass flow rate and isentropic efficiency calibration | Simulation points numbered according to* ***Table 7-2*** *(M-type supercharger)*

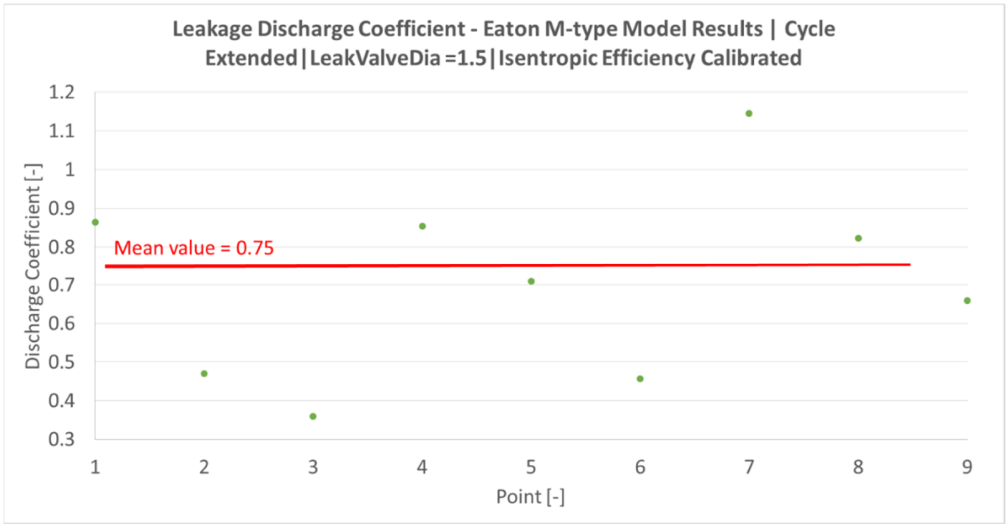

Figure 7-11: *Discharge coefficient of leakage orifices with its mean value | Simulation points numbered according to* ***Table 7-2*** *(M-type supercharger)*

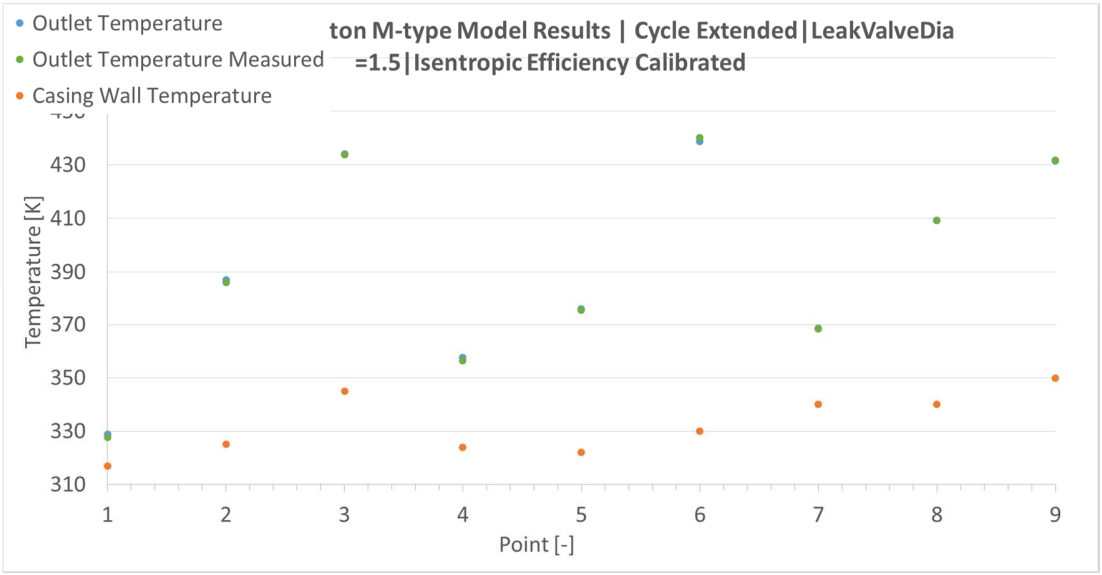

Figure 7-12: *Supercharger outlet temperature (blue dots) compared to measured values (green dots) and to inter-teeth gap wall temperature (orange dots - only simulation results available) after 1-D model calibration | Simulation points numbered according to* ***Table 7-2*** *(M-type supercharger)*

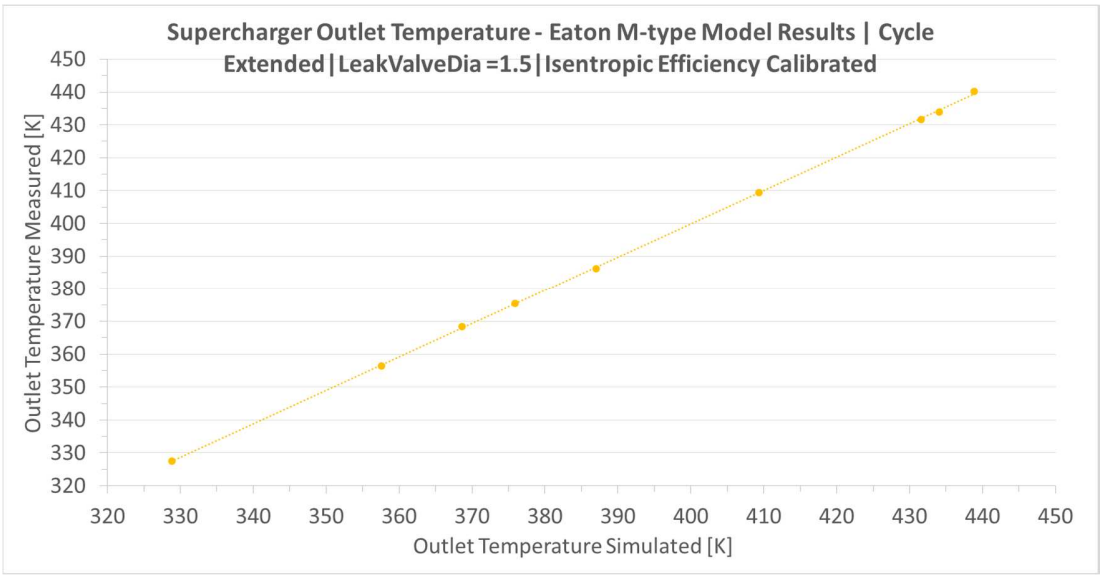

Figure 7-13: *Correlation chart of supercharger outlet temperature data - measured versus simulation values (M-type supercharger)*

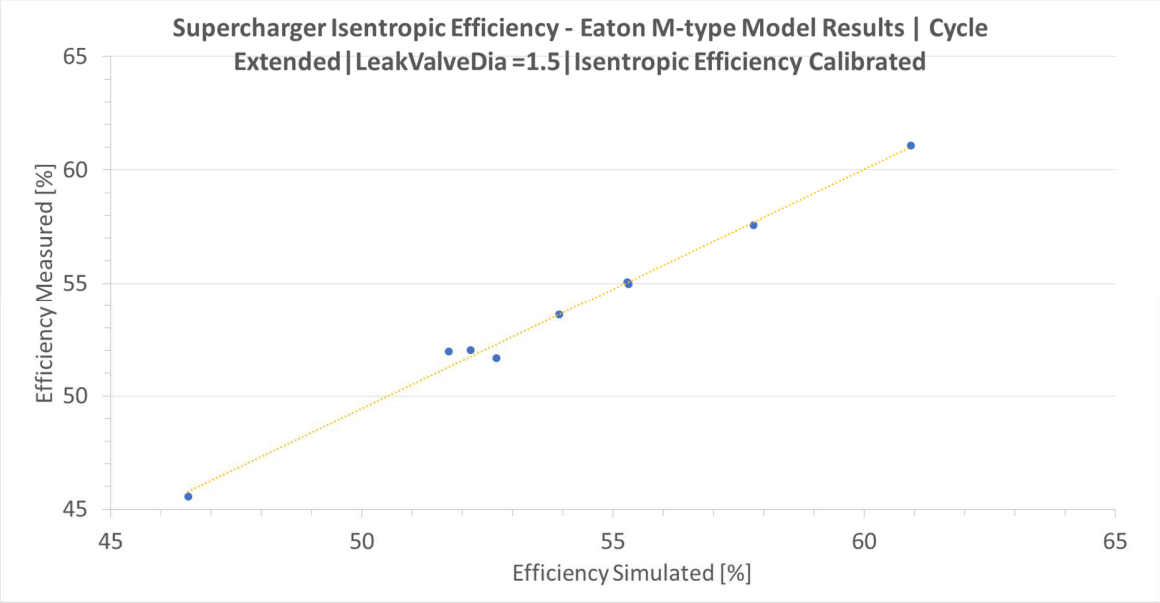

Figure 7-14: *Isentropic efficiency measured and simulated data comparison (M-type supercharger)*

7.3 Impact of Constant Leakage Discharge Coefficient on Model Accuracy

Having values of discharge coefficient for all of the supercharger operating points and the calibrated model, there is a question: "How big would be the difference in mass flow rate and isentropic efficiency when using only one value of this parameter?" This is very interesting when using the 1-D model of supercharger for a prediction of parameters of some unknown supercharger type without measured data. A mean value of the discharge coefficient has been selected for this study for R-type supercharger based on data in ***Figure 7-5***, and all the supercharger operating points were re-simulated using this value. Comparison of results of this study, with results of fully optimized supercharger model for each operating point, are plotted in ***Figure 7-15***. Looking at ***Figure 7-16***, the mass flow rate deviation seems to be reasonably low (lower than 12%) in the region of high mass flow rates (all blue shades). At the lowest mass flows the deviation increases up to 80%, which is unacceptable and thus the value of the discharge coefficient should be lowered to 0,8 or 0,9 for this region. Similar situation occurs when looking at comparison of isentropic efficiency (***Figure 7-17*** and ***Figure 7-18***). The difference is low for high mass flow rates and pressure ratios (lower than 10% relatively) unlike low mass flow rates region where the difference

grows up to 46%. That is why heat transfer ratio should be increased or wall temperature should be lowered for low mass flow rates compared to values used in fully calibrated model.

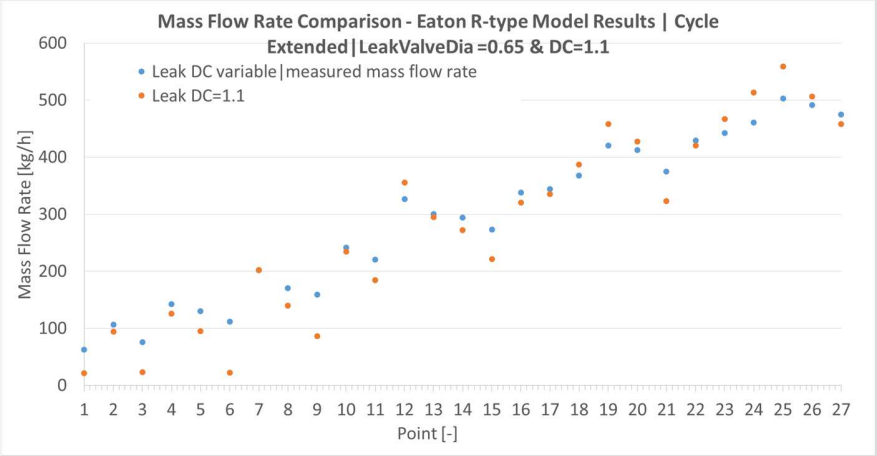

Figure 7-15: *Comparison of mass flow rate results when using calibrated leakage discharge coefficient for each operating point and when using its mean value | Simulation points numbered according to* ***Table 7-1*** *(R-type supercharger)*

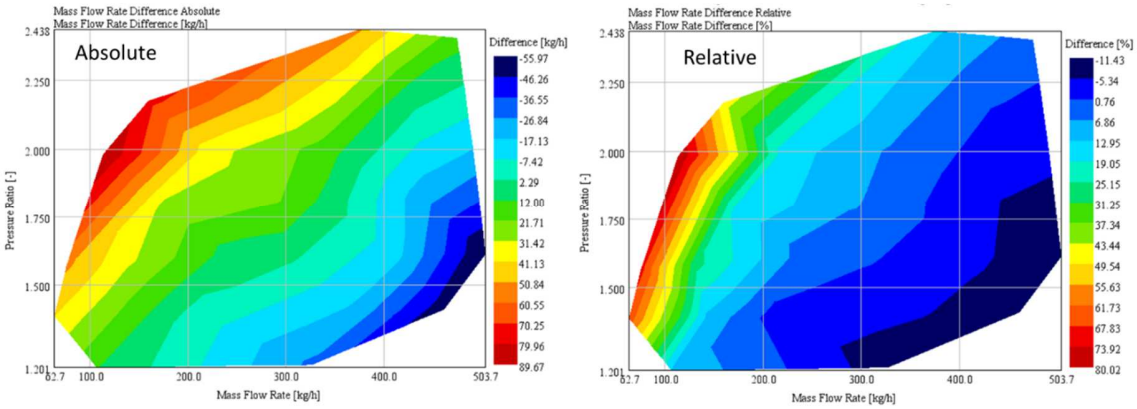

Figure 7-16: *Mass flow rate difference evaluated for the case when using the mean value of leakage discharge coefficient | Absolute difference on the left - relative on the right (R-type supercharger)*

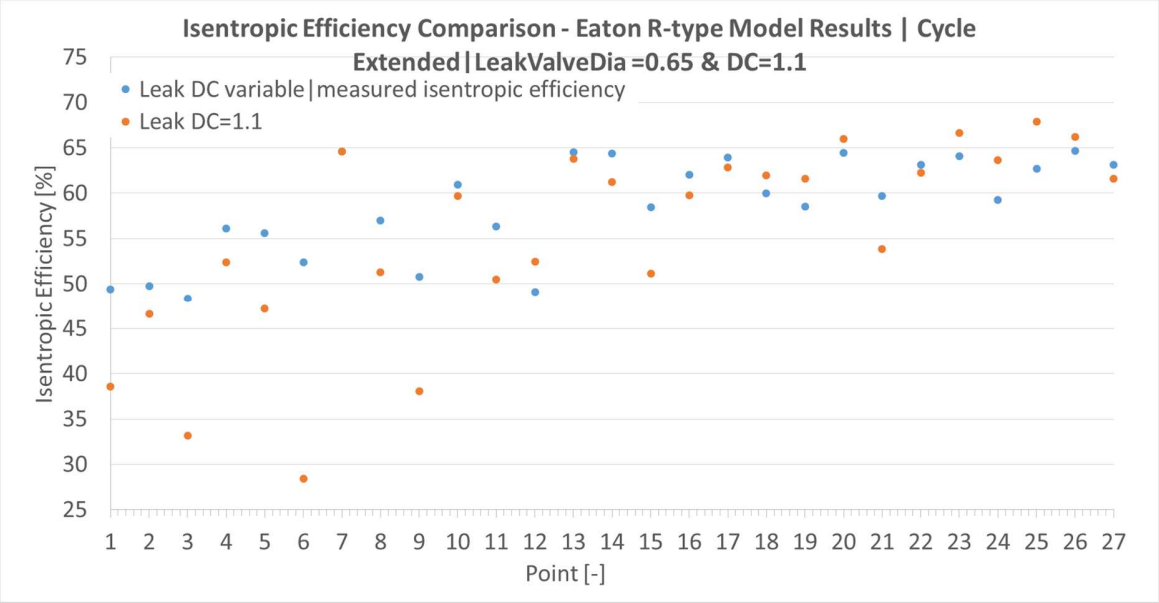

Figure 7-17: *Isentropic efficiency comparison when using calibrated leakage discharge coefficient for each operating point and when using its mean value | Simulation points numbered according to* ***Table 7-1*** *(R-type supercharger)*

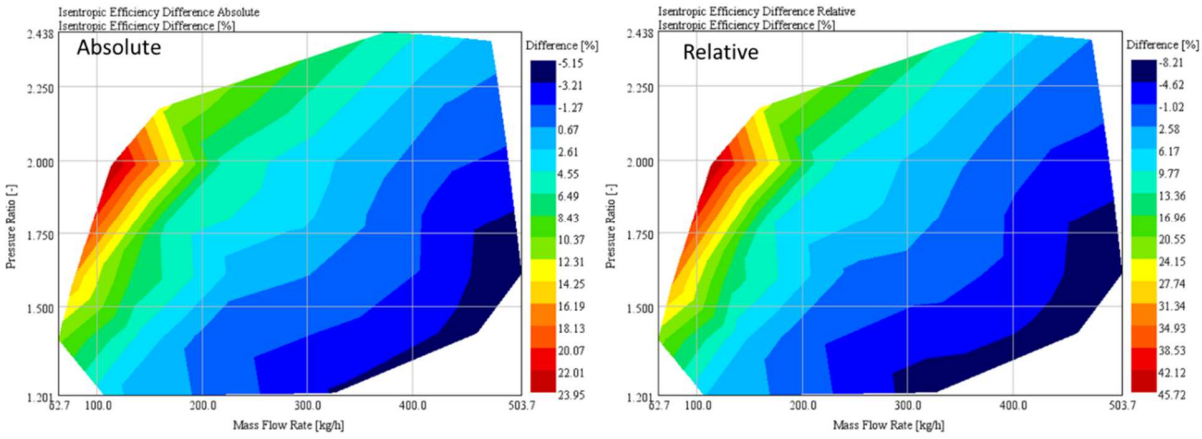

Figure 7-18: *Isentropic efficiency difference evaluated for the case when using the mean value of leakage discharge coefficient | Absolute difference on the left - relative on the right (R-type supercharger)*

This study has been simulated also for M-type supercharger. The leakages discharge coefficient was selected equal to 0.75 based on ***Figure 7-11***. Comparison of results of this study and results of fully optimized supercharger model, are plotted in ***Figure 7-19*** - ***Figure 7-22***. Unfortunately,

point 3 does not achieve even reduced mass flow rate. As is obvious from ***Figure 7-19***. That is why this points has been put aside from the evaluation of mass flow rate and isentropic efficiency difference prediction (***Figure 7-20*** and ***Figure 7-22***). Unrealistic values of mass flow rate and isentropic efficiency achieved at this point would disable the comparison of results for the rest of points. As shown in ***Figure 7-20***, the prediction of mass flow rate with the constant value of leakage discharge coefficient would feature reasonably low deviation - about 20% in the region from dark blue up to yellow shades. For lower mass flow rates and high pressure ratios, the discharge coefficient should be reduced. Considering isentropic efficiency difference (***Figure 7-22***), the deviation is up to 11% relatively in the same region of mass flow rate – pressure ratio map (dark blue – yellow shades). For lower mass flow rates and high pressure ratios the deviation in isentropic efficiency is up to 23%. As in the case of R-type supercharger, heat transfer ratio should be increased or wall temperature should be lowered for low mass flow rates compared to values used in fully calibrated model. Moreover, the study might be influenced by low number of considered operating points in the case of M-type supercharger.

The most important conclusion from this study is that the model features comparable difference in mass flow rate or isentropic efficiency despite on rotor geometry.

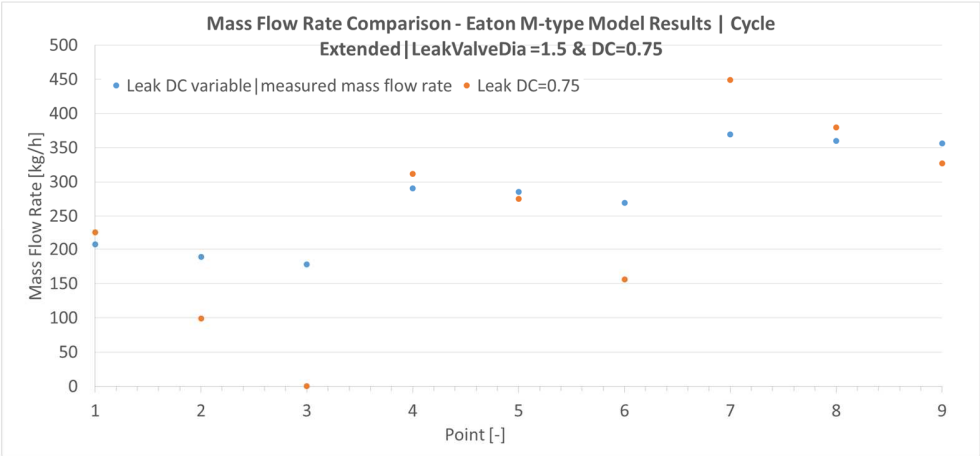

Figure 7-19: *Comparison of mass flow rate results when using calibrated leakage discharge coefficient for each operating point and when using its mean value | Simulation points numbered according to* ***Table 7-2*** *(M-type supercharger)*

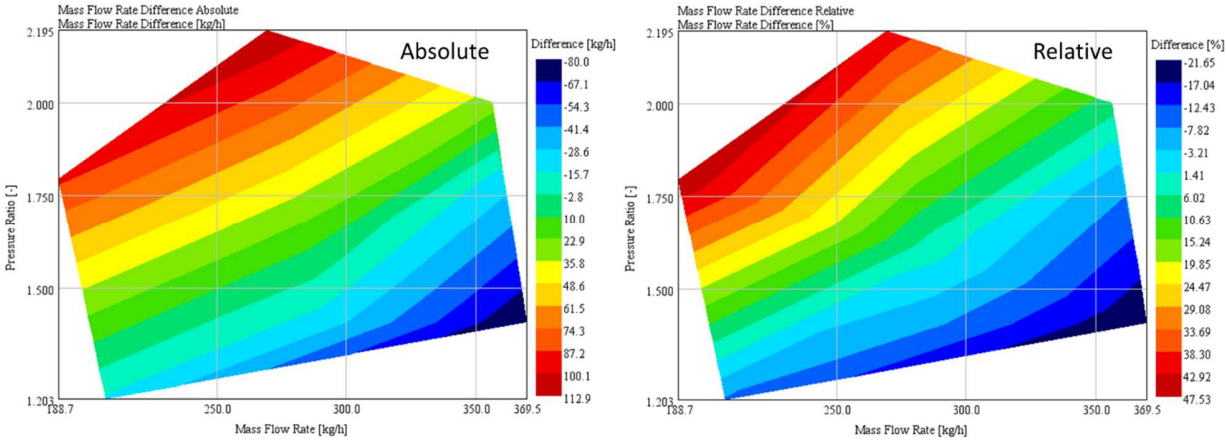

Figure 7-20: *Mass flow rate difference evaluated for the case when using the mean value of leakage discharge coefficient | Absolute difference on the left - relative on the right (M-type supercharger)*

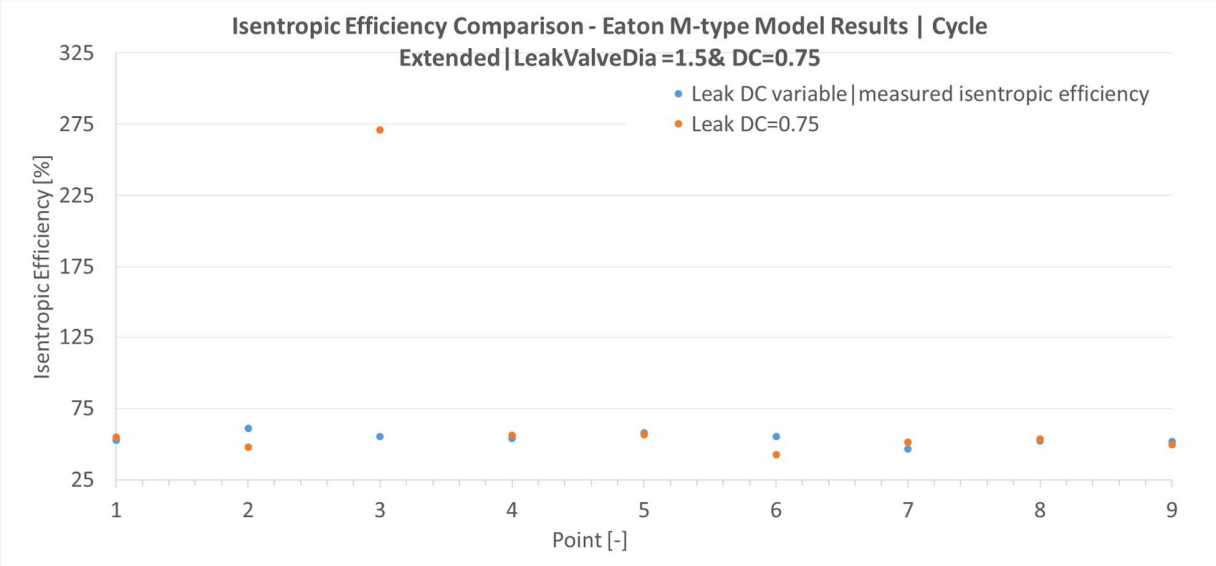

Figure 7-21: *Isentropic efficiency comparison when using calibrated leakage discharge coefficient for each operating point and when using its mean value | Simulation points numbered according to* ***Table 7-2*** *(M-type supercharger)*

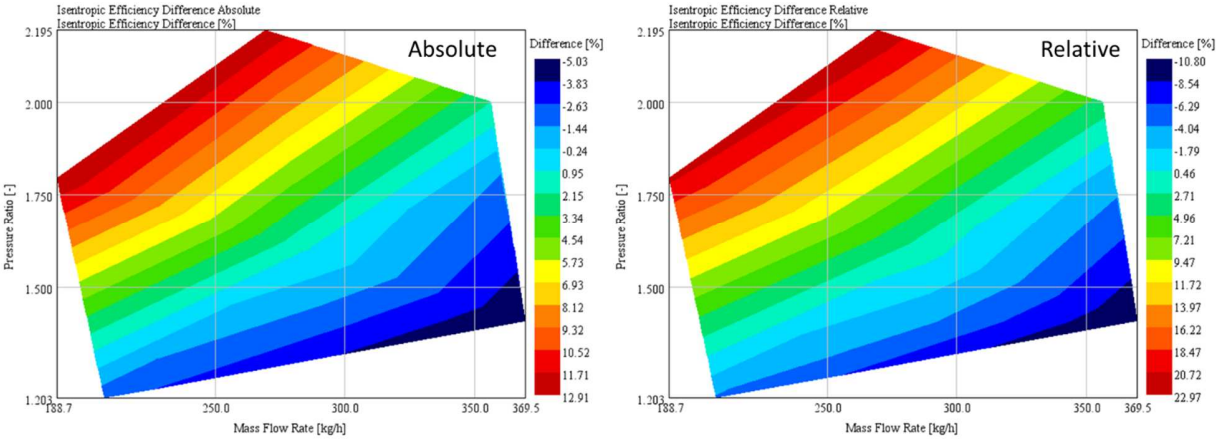

Figure 7-22: *Isentropic efficiency difference evaluated for the case when using the mean value of leakage discharge coefficient | Absolute difference on the left - relative on the right (M-type supercharger)*

8 Results

Measured data and results, yielded by fully calibrated 1-D model, are compared in this chapter. As is obvious from ***Figure 8-1*****,** the model can be accurately calibrated to measured data considering mass flow rate – pressure ratio map. In ***Figure 8-2*** is shown a good agreement between measured and simulation results considering isentropic efficiency. Next to that, dimensions of clearances (virtual lashes) results in reasonable values comparing to the real supercharger. Inter-teeth gap wall temperature calibrated to measured temperature at supercharger outlet and to reasonable heat transfer coefficient estimation yielded realistic values also.

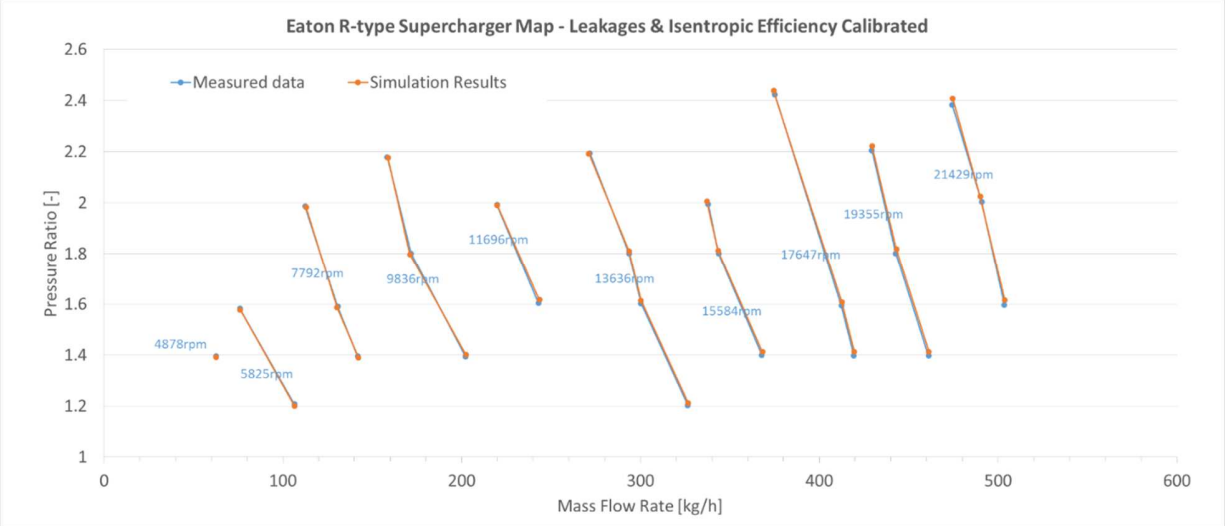

Figure 8-1: *Supercharger map yielded by the fully calibrated 1-D model compared to the measured map (blue dots)*

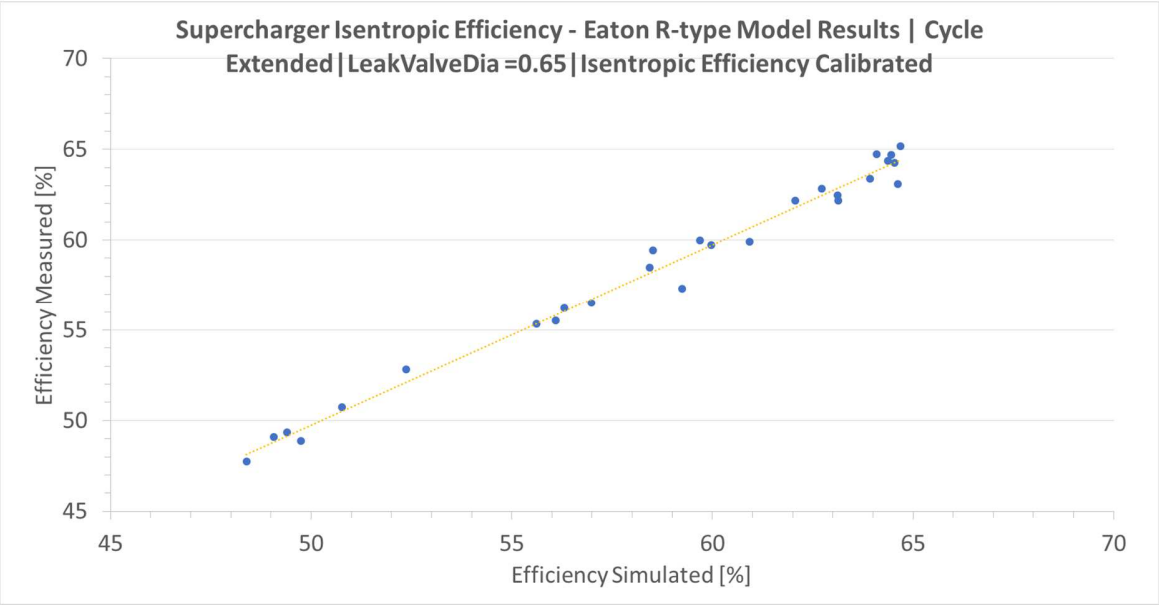

Figure 8-2: *Comparison of measured and simulated values of R-type supercharger isentropic efficiency*

Comparison of measured and simulated results of M-type supercharger feature very good agreement (***Figure 8-3*** and ***Figure 8-4***), as well. Number of operating points considered in the case of M-type supercharger was limited. The model demonstrates capability to work very well for the superchargers of different design.

Moreover, inter-teeth gap pressure behavior obtained during supercharger test agrees very well with the simulation results. In ***Figure 8-5*** inter-teeth gap pressure is compared for 14000rpm and pressure ratio equal to 2.2 – the same operating point already presented in chapter 6.5. Comparisons for all other supercharger operating points are in **Appendix A**.

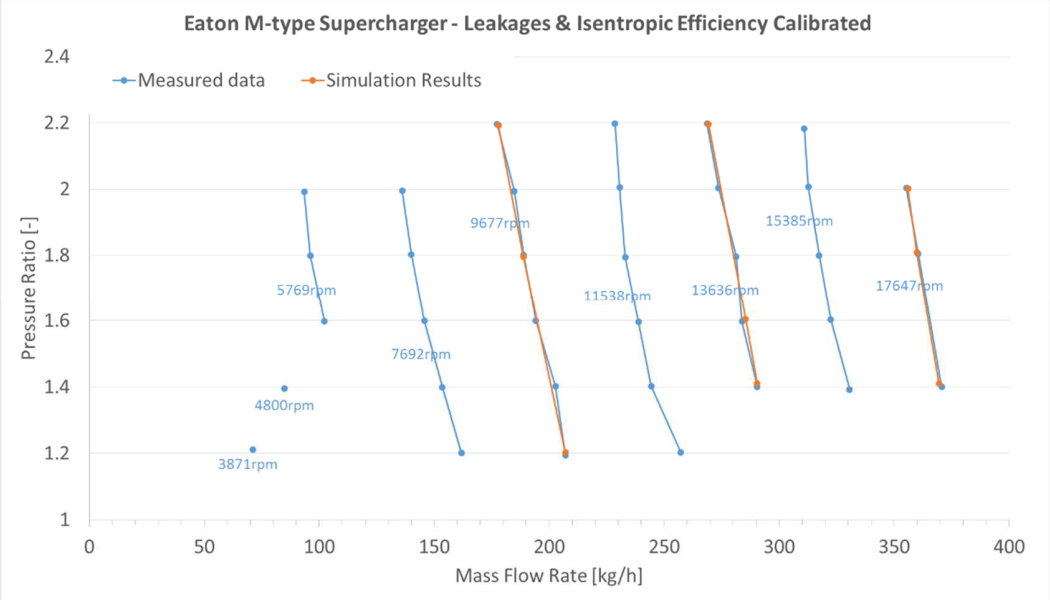

Figure 8-3: *M-type supercharger data yielded by the fully calibrated 1-D model compared to the measured map*

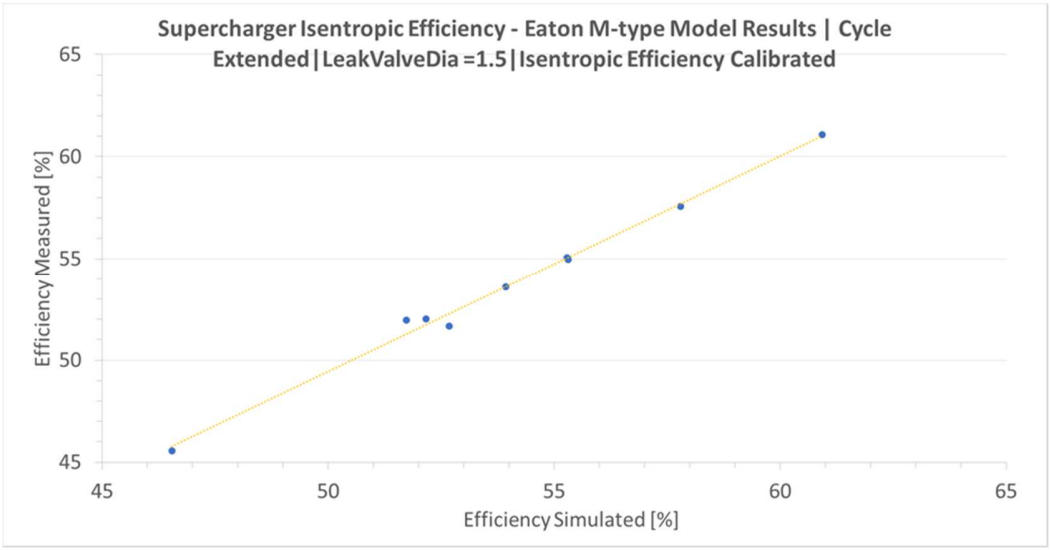

Figure 8-4: *Comparison of measured and simulated values of M-type supercharger isentropic efficiency*

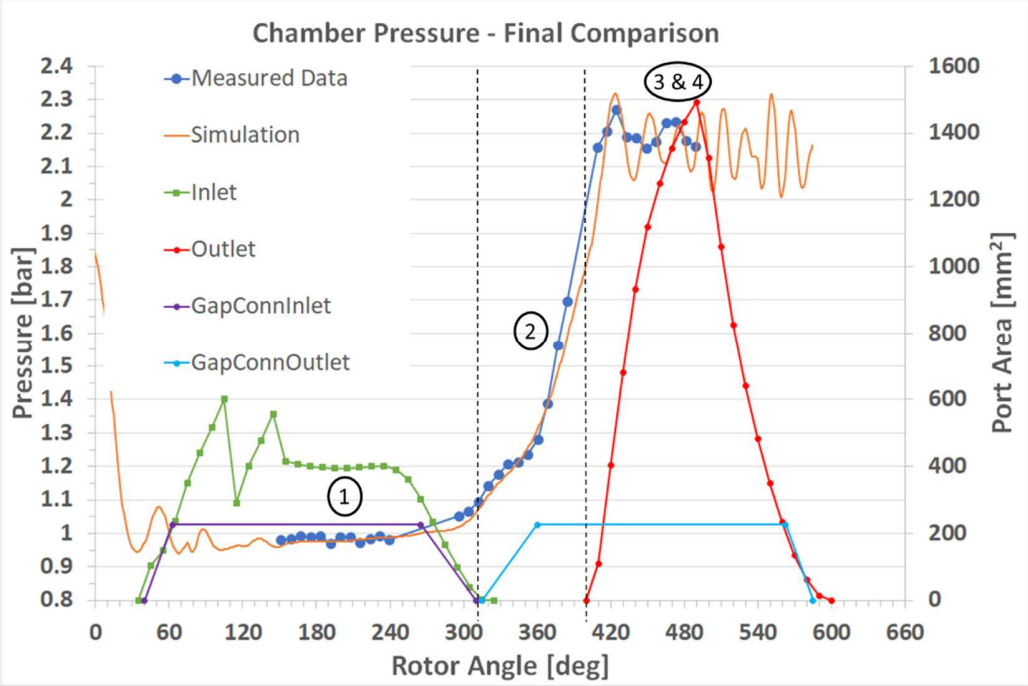

Figure 8-5: *Comparison of measured inter-teeth gap pressure and simulation results for the R-type supercharger at 14000rpm & pressure ratio of 2.2. Inlet and outlet port areas are shown in this figure for better understanding.*

Inter-teeth gap pressure, obtained from supercharger simulation, respects all the phenomena occurring in the supercharger chamber during one cycle (numbers in black circles in ***Figure 8-5*** corresponds to description of phases below):

1. Air delivery into the inter-teeth gap increasing its volume
2. Connection to supercharger outlet via small area given by rotors design
3. Chamber opening to outlet through the main outlet port
4. Pressure fluctuations when chamber opened to supercharger outlet

Similar diagram for M-type supercharger is shown in ***Figure 8-6***. The working process is slightly different from the R-type supercharger influenced by different timing of ports and by use of two small outlet ports. The description of the process is following:

1. Air delivery into the inter-teeth gap increasing its volume

2. Air delivery in closed inter-teeth gap along supercharger casing. Air compressed only by leakage flow through clearances
3. Connection to supercharger outlet via two small outlet ports and via small area given by rotors design
4. Pressure fluctuations when chamber opened to supercharger outlet

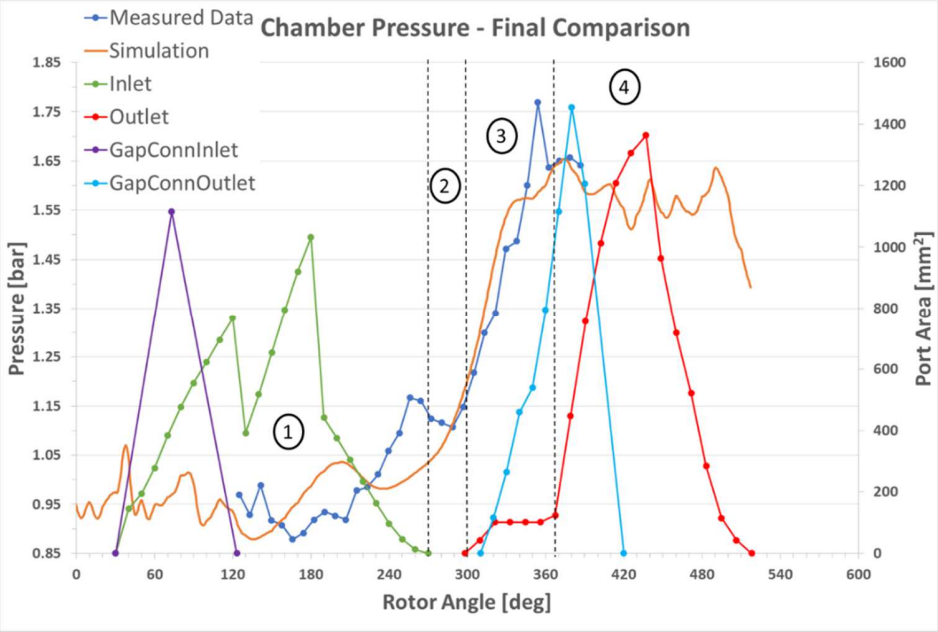

Figure 8-6: *Comparison of measured inter-teeth gap pressure and simulation results for the M-type supercharger at 14000rpm & pressure ratio of 1.6. Inlet and outlet port areas are shown in this figure for better understanding.*

Therefore, the model reflects the reality quite well. Moreover, the use of generally calibrated 1-D model for a prediction of mass flow rate and isentropic efficiency is possible even for not yet calibrated Roots-type supercharger. The leakage discharge coefficient should be reduced, chamber wall temperature should be lowered or heat transfer coefficient should be increased for low mass flow rates compared to values used in fully calibrated model. Then results with reasonable accuracy will be obtained.

9 Frequency Analysis of Supercharger Outlet Pressure

The backflow during outlet opening and closing causes pressure fluctuations, dependent on the dynamic system of volumes and connecting pipes (***Figure 8-5***). Well-known howling of the Roots-type supercharger during its operation is a result. Should the Roots-type supercharger be used, the reduction of NVH by suitable muffler is needed. The use of large mufflers at outlet complicates supercharger application.

The developed 1-D model offers a tool for reduction of experiment & simulation time during the design of a combustion engine inlet plenum. A great benefit of the 1-D model is a reduction of simulation time compared to the complex simulation in 3-D CFD. It yields useful input data for noise frequency analysis. Based on this analysis, an appropriate muffler (e.g., Helmholtz resonator) may be designed.

Simulation results of the R-type supercharger were analyzed using Fast Fourier Transformation built-in to GT-Power. This tool can analyze input signal – inter-teeth gap pressure in this case – substitute the original signal by a signal composed from goniometric functions sin x and cos x, and yields amplitudes for each harmonic component. This approach was used to analyze inter-teeth gap pressure at following operating points - ***Table 9-1***.

Table 9-1: *R-type supercharger operating points used for FFT*

Supercharger Speed	[rpm]	6000	8000	10000	12000	14000	16000	18000	20000	22000	22000
Pressure Ratio	[-]	1.6	1.6	1.8	1.6	1.6	1.8	1.6	1.8	1.6	2.4

Looking at ***Figure 9-1 - Figure 9-3***, several important conclusions might be stated:

1. Significant harmonic components are the same for all operating points, independent on supercharger speed or mass flow rate.
2. Amplitudes are slightly increasing with increased speeds.
3. Amplitudes are significantly increasing with increasing pressure ratio. This statement is demonstrated in ***Figure 9-3*****,** where amplitudes are plotted for different pressure ratios at 14000rpm of supercharger speed.

Results of harmonic analysis of the M-type supercharger are in line with this conclusions (***Figure 9-4*** - ***Figure 9-7***)

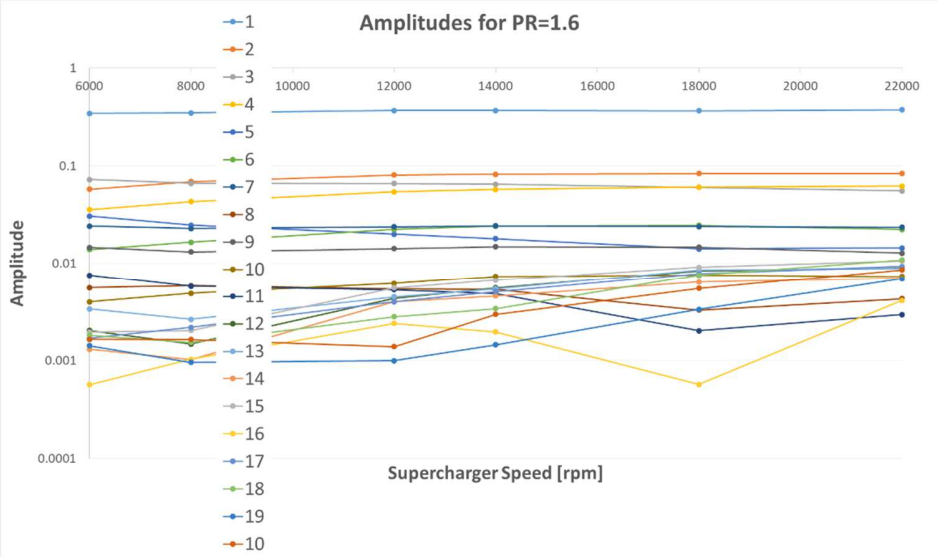

Figure 9-1: *Chart depicting significant harmonic components at pressure ratio = 1.6 and their amplitudes for different supercharger speeds (R-type supercharger)*

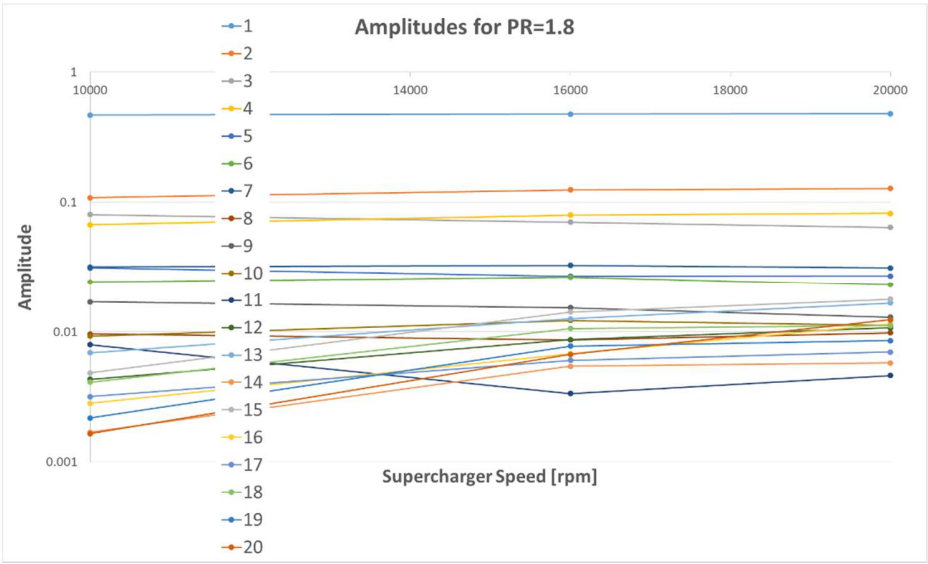

Figure 9-2: *Chart depicting significant harmonic components at pressure ratio = 1.8 and their amplitudes for different supercharger speeds (R-type supercharger)*

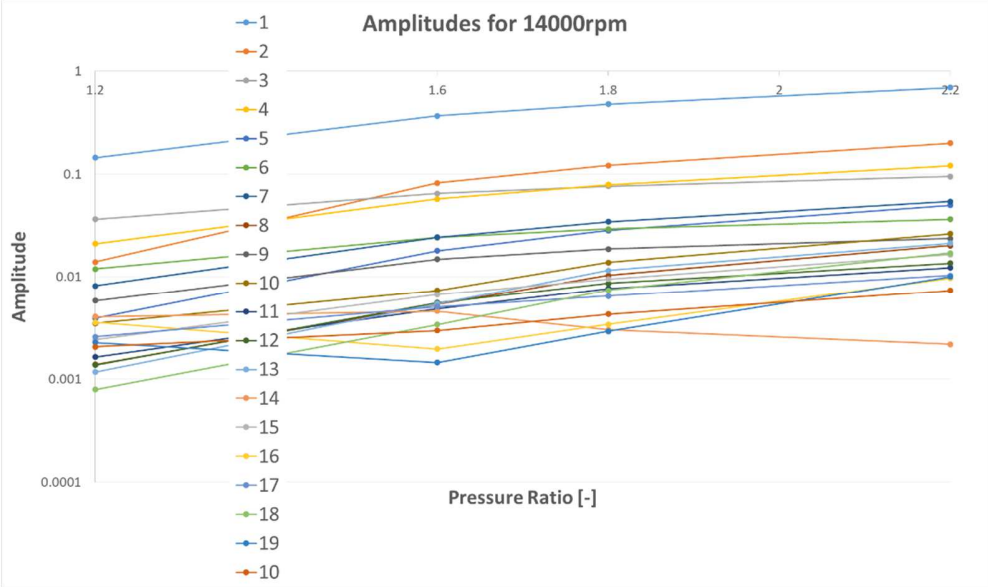

Figure 9-3: *Amplitudes dependency on supercharger pressure ratio at 14000rpm (R-type supercharger)*

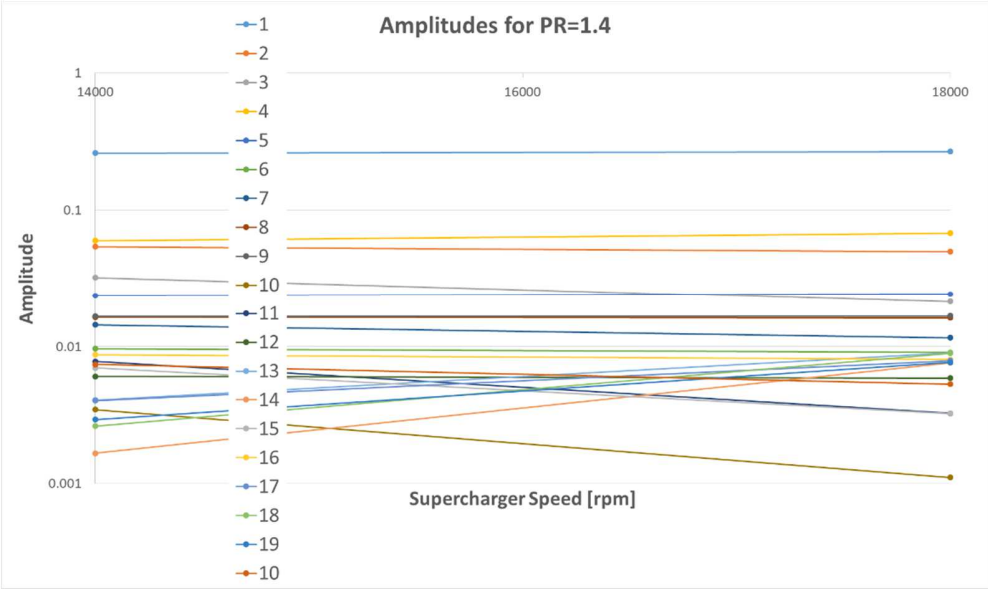

Figure 9-4: *Amplitudes of significant harmonic components at pressure ratio = 1.4 (M-type supercharger)*

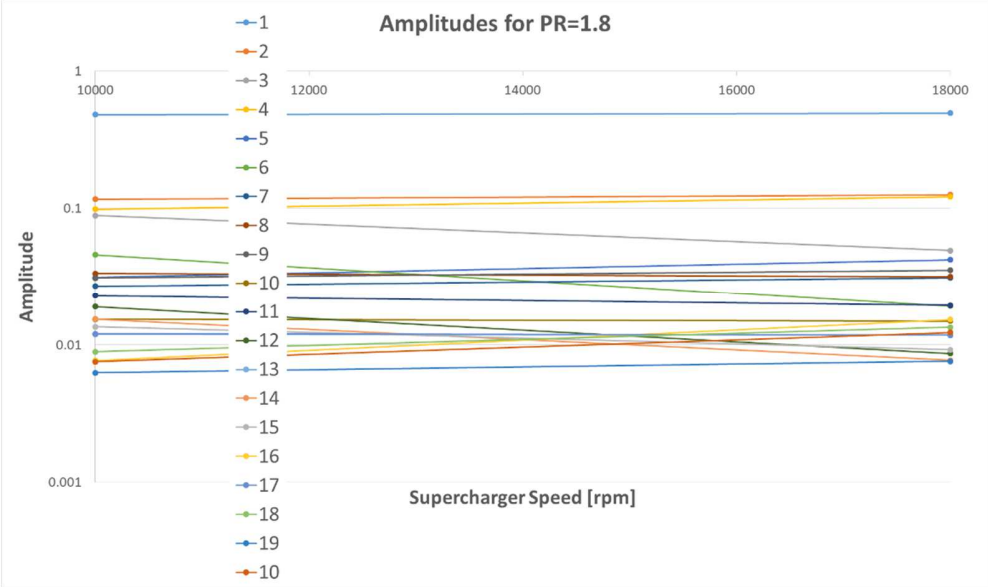

Figure 9-5: *Amplitudes of significant harmonic components at pressure ratio = 1.8 (M-type supercharger)*

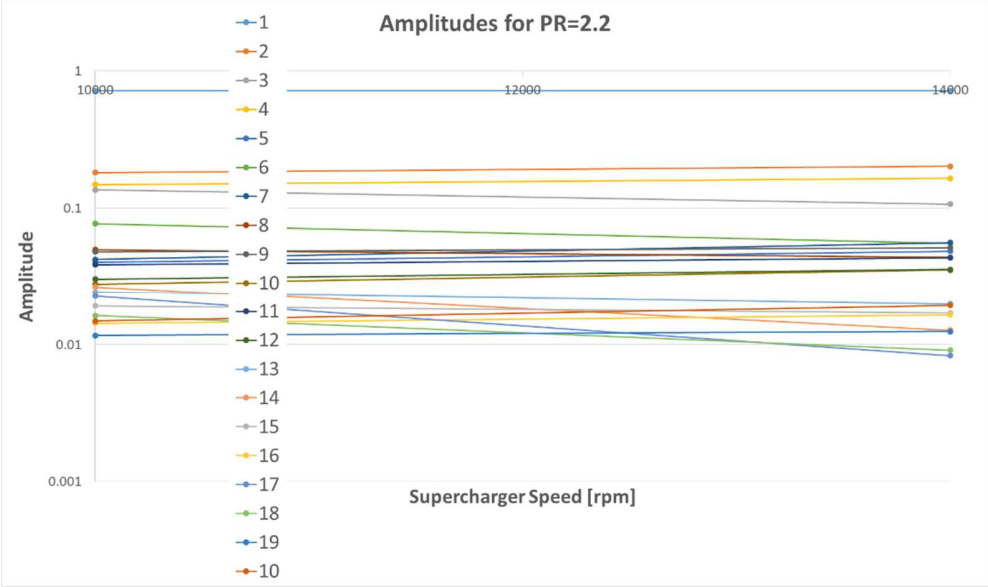

Figure 9-6: *Amplitudes of significant harmonic components at pressure ratio = 2.2 (M-type supercharger)*

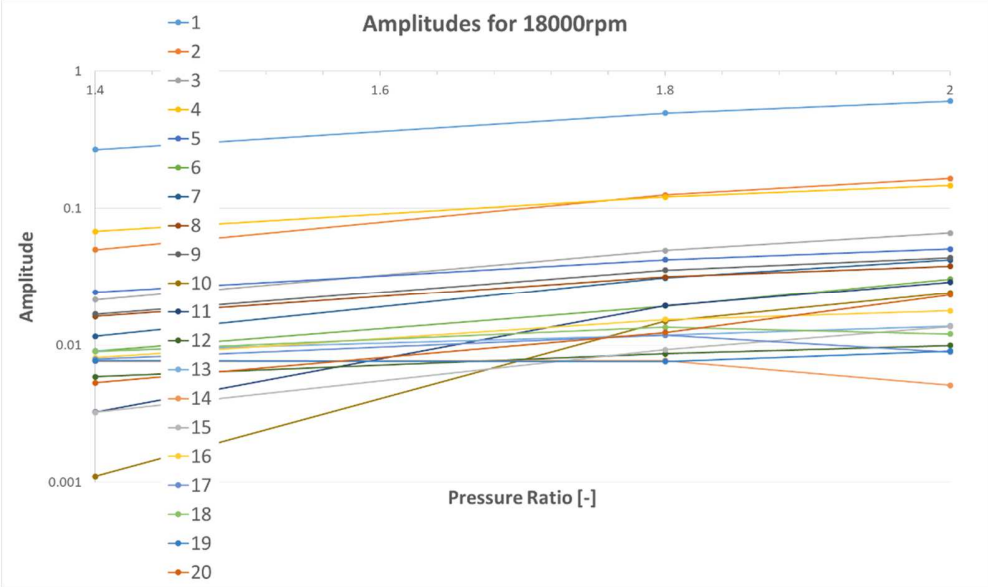

Figure 9-7: *Amplitudes dependency on supercharger pressure ratio at 18000rpm (M-type supercharger)*

10 Conclusions and Outlook

This thesis has presented a methodology, validation and practical use of the newly developed Roots supercharger model in 1-D simulation thermodynamic tool. The dimensions of 1-D model modules are based on 3-D supercharger geometry, obtained from a standard 3-D CAD system. The validation of the model has been performed for two different types of Roots-type superchargers - R-type and M-type – at different operating conditions. The results have been subjected to global analysis and generalized. The practical application has shown the model is capable to predict substantial parameters of low frequency pressure pulsations, which might be used as input data for noise abatement measures (e.g., Helmholtz resonator design). The model may be used also for predicting unknown parameters of a supercharger under development with reasonable accuracy. Moreover, all 1-D model predictions are achieved with significantly lower computational effort than in the case of 3-D complex CFD calculations.

10.1 Fulfilling Objectives: The Contribution of the Thesis

The 1-D mathematical model of Roots-type supercharger has been developed, using a global analysis of the device geometry including 3-D CAD model, port timing, leakages and clearances analysis. The analysis has been done for Eaton R- and M-type superchargers, partially applied in [2] and [13]. The 1-D model in GT-Power using virtual cylinders and valves was built. The 1-D model has been successfully calibrated by data received from superchargers testing at different operating conditions and published in [25]. The calibration parameters feature reasonable values corresponding to the real supercharger design and the physics of phenomena inside the supercharger. The analysis of isentropic efficiency including pressure indication in each working chamber of a supercharger has been done to get a better idea about the real processes in studied device. The calibration of isentropic efficiency has been done by fixing cylinder heat transfer coefficient and inter-teeth gap wall temperature. The model can deliver low-frequency pressure pulsations information [29] as a boundary condition for noise prediction and reduction. It yields good perspective of using the calibrated 1-D model for NVH analysis and optimization.

10.2 Outlook for Future Work

The supercharger model calibration will be refined by application to more supercharger types and by using more measured values, e.g., of inter-teeth gap wall temperatures. That will bring additional knowledge about yet unexplained calibration parameters behavior. Enhanced pressure indication using more pressure sensors along the rotor will yield better knowledge about physical processes occurring in inter-teeth gap at different operating conditions. Pressure waves along an inter-teeth chamber can be detected using sensors of high eigen-frequency. It might explain the difference in pressure values obtained in one inter-teeth gap by two sensors placed at different positions.

The 1-D model will be connected easily to an engine model in commercial code environment. It will make possible analyzing the supercharger – turbocharger – combustion engine interactions at steady and unsteady engine operation, which is important for the ICE powertrain vehicle applications.

Bibliography

[1] Martinez – Botas, R., Pesiridis, A., Ming Yang, Y.: *Overview of boosting options for future downsized engines*. Technological Sciences, Science China, 2011, doi:10.1007/s11431-010-4272-1.

[2] Brynych, P. - Macek, J. - Pohořelský, L.: *Air System Proposal and Testing for a Downsized Two-Stroke Diesel Engine*. In Proceedings of the FISITA 2012 World Automotive Congress. Peking: SAE-China; FISITA (Eds.), 2012, vol. 1, p. 289-314. ISBN 978-3-642-33841-0.

[3] Chlumský, V.: *Rotační kompresory a vývěvy (Rotational Compressors and Exhausters, in Czech)*. SNTL Prague 1966.

[4] Huang, P. X.: *Pulsation Generation and Control of Roots Supercharger: A Shock Tube Mechanism*. SAE Technical Paper 2013-01-1887, 2013, doi: 10.4271/2013-01-1887.

[5] http://www.jagweb.com/aj6eng/supercharging_article.php

[6] Takabe, S., Ikeya, N., Miyagi, Y.: *Second Generation Lysholm Compressor*. SAE Technical Paper 980774, 1998.

[7] Takabe, S., Hatamura, K., Kanesaka, H., Kurata, H., Iguchi, Y., Matsubara, H.: *Development of the high Performance Lysholm Compressor for Automotive Use*. SAE Technical Paper 940843, 1994.

[8] Miyagi, Y., Takabe, S., Miyashita, K., Ikaya, N.: *Experimental Study of New Lysholm Supercharger with a Simple Unloading System*. SAE Technical Paper 960952, 1998.

[9] http://kennebell.net/tech/supercharger-tech/twin-screw-vs-roots/

[10] http://www.mercedes-benz.de/content/germany/mpc/mpc_germany_website/de/home_mpc/passengercars/home/world/mythos/gallery_of_legends.flash.html#1923

[11] http://www.volkspage.net/technik/ssp/ssp/SSP_359.pdf

[12] http://www.volkswagen.co.uk/technology/petrol/tsi

[13] Pohořelský, L., Brynych, P., Macek, J., Vallaude, P.-Y., Ricaud, J.-C., Obernesser, P., Tribotté, P.: *Air System Conception for a Downsized Two-Stroke Diesel Engine*. SAE Paper 2012-01-0831.

[14] Chadwell Ch., Alger A., Roberts Ch., Arnold S.: *Boosting Simulation of High Efficiency Alternative Combustion Mode Engines*. SAE Paper2011-01-0360.

[15] https://www.sae.org/news/2017/09/ice-breaker

[16] Eiser, A., Fitzen, M., Heiduk, T., Mendle, J., Zahlmann, S., Bäumel, F.: *3.0l TFSI The New Top-of-the-Range V6-Engine from Audi*. MTZ 09/2009 Volume 70.

[17] Wetzel, P.: *Downspeeding a Light Duty Diesel Passenger Car with a Combined Supercharger and Turbocharger Boosting System to Improve Vehicle Drive Cycle Fuel Economy.* SAE Technical Paper 2013-01-0932, 2013, doi: 10.4271/2013-01-0932.

[18] https://s21.q4cdn.com/257785122/files/doc_downloads/UQM-echarging-brochure_web1.pdf

[19] Yu, W., Sichuan, X., Ni, H.: *Air Compressor for Fuel Cell Vehicles: An Systematic Review*. SAE Technical Paper 2015-01-1172, 2015, doi.: 10.4271/2015-01-1172.

[20] Knutsson, M., Kjellson, E., Glover, R., and Boden, H.: *In-Duct Acoustic Source Data for Roots Blowers*. SAE Technical Paper 2017-01-1792, 2017, doi:10.4271/2017-01-1792.

[21] Patil, V., Sara, R., Milind, T., and Glover, R.: *Improved Techniques in Intake Acoustic System Modeling of a Supercharged Engine.* SAE Technical Paper 2017-01-1790, 2017, doi:10.4271/2017-01-1790.

[22] Li H., Tu J., Subic A., Abu-Hijleh B.: *The Leakage Analysis in a Twin-Screw Supercharger by Using an Integrated CAD/CFD Three-Dimensional Model.* In: LIU G., TAN V., HAN X. (eds): Computational Methods. Springer, Dordrecht, 2006.

[23] Froehlich, M., Stewart, N.: *TVS V-Series Supercharger Development for Single and Compound Boosted Engines*. SAE Technical Paper 2013-01-0919, 2013, doi: 10.4271/2013-01-0919.

[24] Pradhan, S. and Jeemon, P. K.: *Modeling and Validation of a Roots-type Supercharger Using GT-SUITE.* SAE Technical Paper 2018-01-0164, 2018, doi:10.4271/2018-01-0164.

[25] Brynych, P., Macek, J., Vitek, O., and Cervenka, L.: *1-D Model of Roots Type Supercharger.* SAE Technical Paper 2013-01-0927, 2013, doi:10.4271/2013-01-0927.

[26] Pohorelsky L., Zak Z., Vitek O., Macek J.: *Study of Pressure Wave Supercharger Potential using a 1-D and a 0-D Approach*. SAE Paper 2011-01-1143.

[27] Macek J., Vítek O., Burič J. and Doleček V.: *Comparison of Lumped and Unsteady 1-D Models for Simulation of a Radial Turbine*. SAE Int. J. Engines Vol. 2(1) 173-188, 2009, ISSN 1946-396. SAE Paper 2009-01-0303.

[28] Šejvl, M.: *Theorie a výpočty ozubených kol (Theory and Calculations of Gears)*, 1st Volume (in Czech). SNTL Prague 1957.

[29] Brynych, P., Macek, J., Tribotte, P., De Paola, G. et al.: *System Optimization for a 2-Stroke Diesel Engine with a Turbo Super Configuration Supporting Fuel Economy Improvement of Next Generation Engines*. SAE Technical Paper 2014-32-0011, 2014, doi:10.4271/2014-32-0011.

[30] DIN 1952, *VDI-Durchfluß. Meßregeln*, 1943.

[31] Macek, J., Pohořelský, L., Brynych, P., *Supercharger and Turbocharger Tests at CZ a.s. Strakonice*. Internal report, ČVUT Praha 2010.

[32] Gamma Technologies, Inc. *GT-POWER Users' Manual version 7.1*, 2011.

[33] Gamma Technologies, Inc. *GT-SUITE Flow Theory Manual 7.1*, 2011.

[34] Burenius, R.: Using 1D Simulations to Optimize a Supercharger for a Twin Charged DI Gasoline Engine. GT-Power Conference, 2015.

Appendix A

Measured data and simulation results obtained from calibrated 1-D model are compared for each operating point of R-type supercharger map in this **Appendix A**.

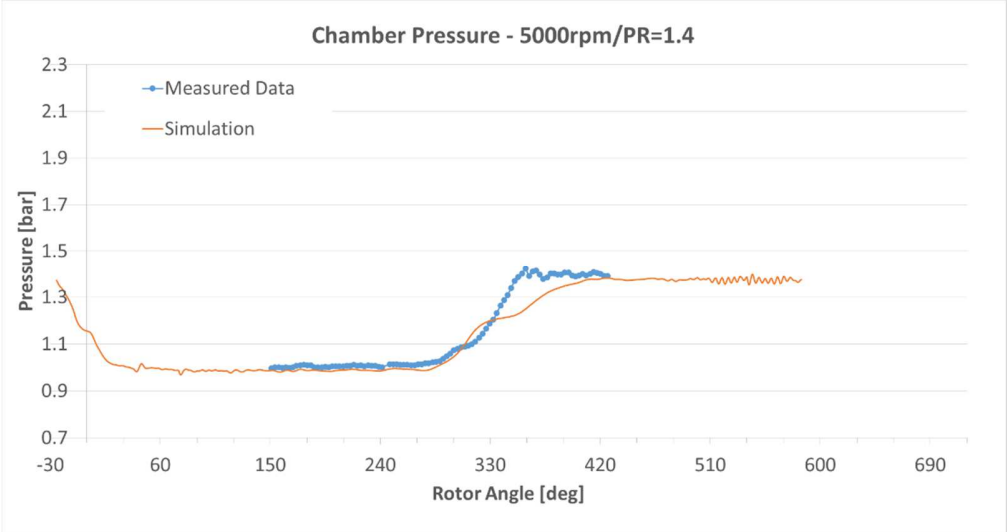

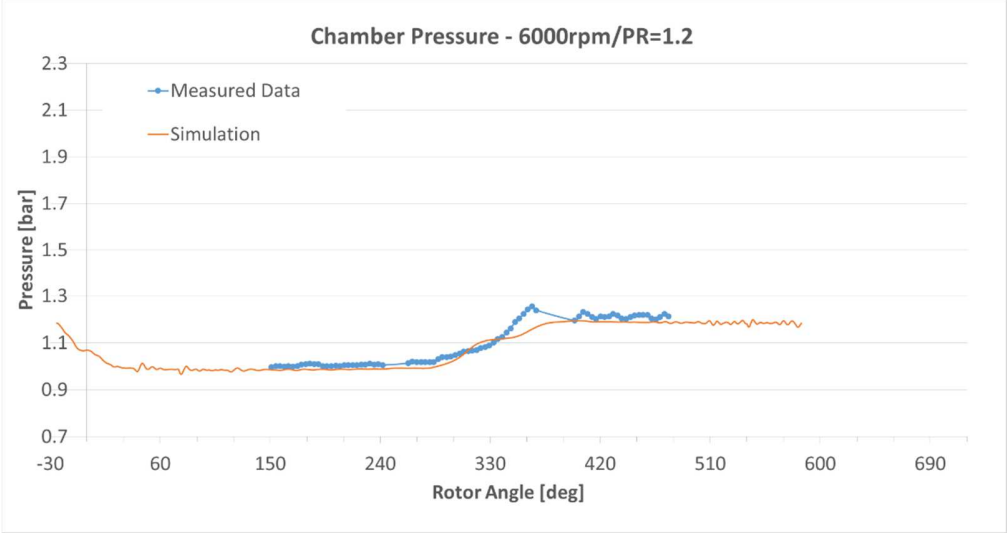

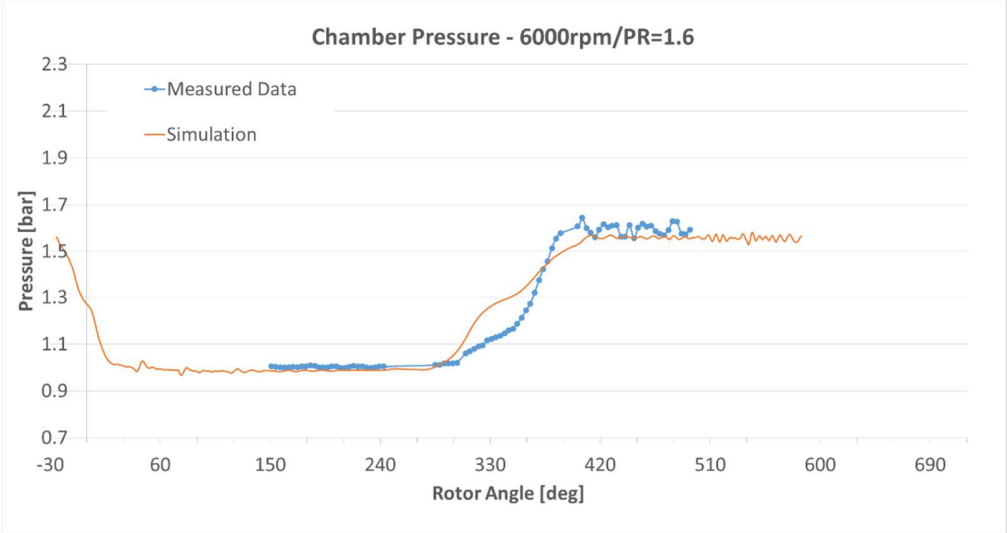
Chamber Pressure - 6000rpm/PR=1.6
Measured Data
Simulation
Pressure [bar]
2.3
2.1
1.9
1.7
1.5
1.3
1.1
0.9
0.7
-30
60
150
240
330
420
510
600
690
Rotor Angle [deg]

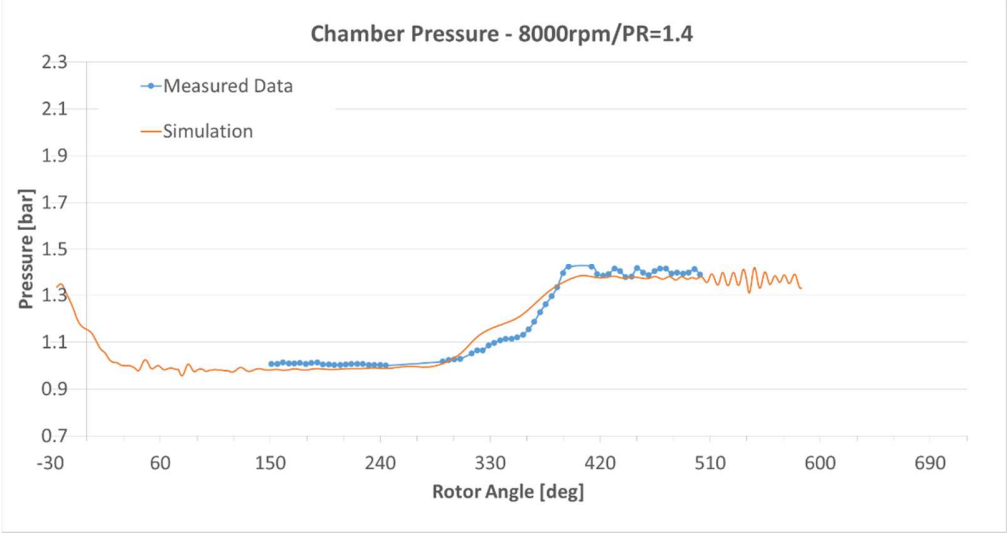
Chamber Pressure - 8000rpm/PR=1.4
Measured Data
Simulation
Pressure [bar]
2.3
2.1
1.9
1.7
1.5
1.3
1.1
0.9
0.7
-30
60
150
240
330
420
510
600
690
Rotor Angle [deg]

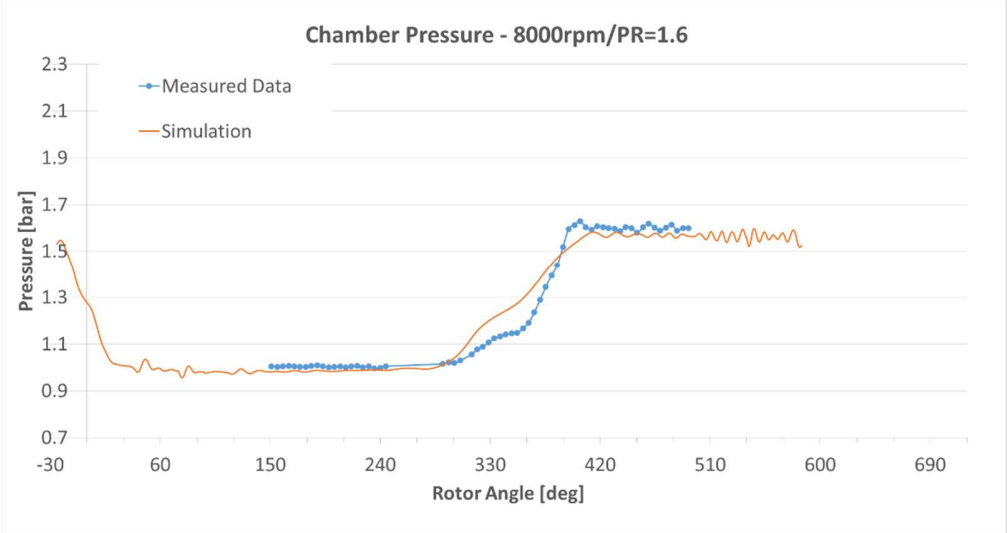
Chamber Pressure - 8000rpm/PR=1.6
Measured Data
Simulation
Pressure [bar]
2.3
2.1
1.9
1.7
1.5
1.3
1.1
0.9
0.7
-30
60
150
240
330
420
510
600
690
Rotor Angle [deg]

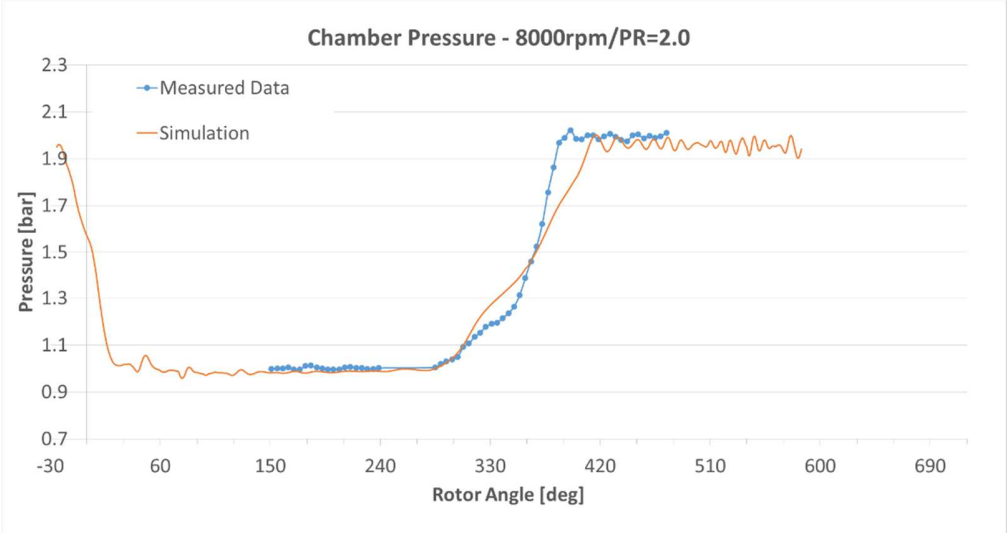
Chamber Pressure - 8000rpm/PR=2.0
Measured Data
Simulation
Pressure [bar]
2.3
2.1
1.9
1.7
1.5
1.3
1.1
0.9
0.7
-30
60
150
240
330
420
510
600
690
Rotor Angle [deg]

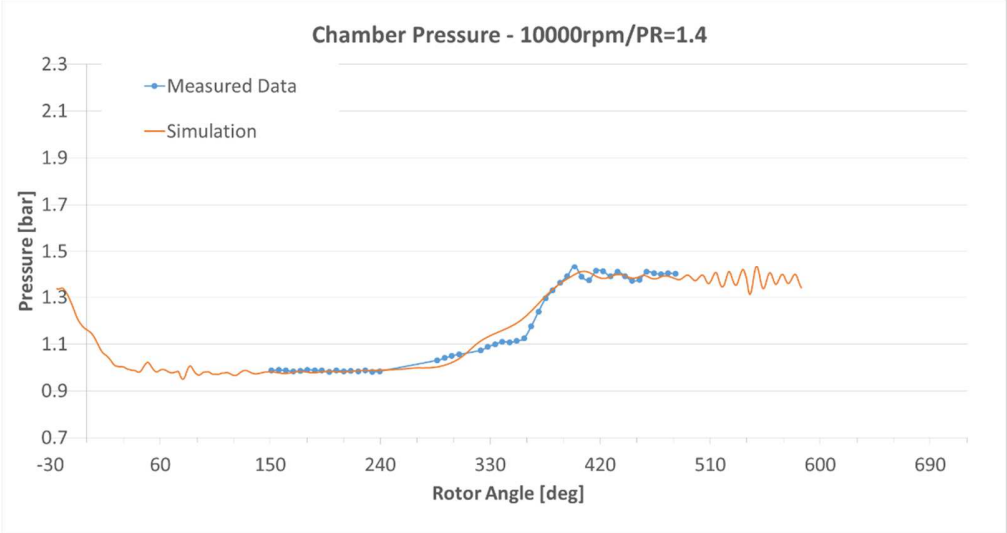
Chamber Pressure - 10000rpm/PR=1.4
Measured Data
Simulation
Pressure [bar]
2.3
2.1
1.9
1.7
1.5
1.3
1.1
0.9
0.7
-30
60
150
240
330
420
510
600
690
Rotor Angle [deg]

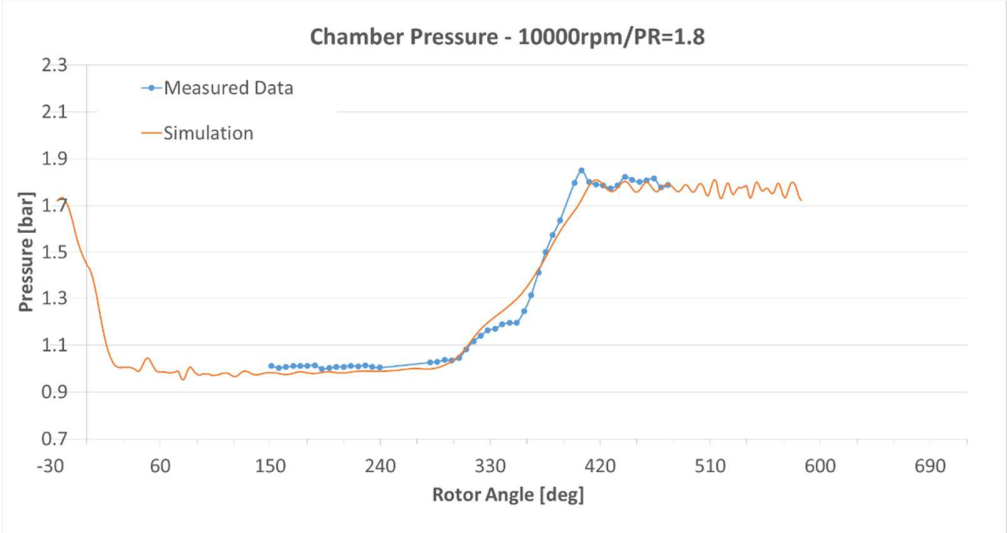
Chamber Pressure - 10000rpm/PR=1.8
Measured Data
Simulation
Pressure [bar]
2.3
2.1
1.9
1.7
1.5
1.3
1.1
0.9
0.7
-30
60
150
240
330
420
510
600
690
Rotor Angle [deg]

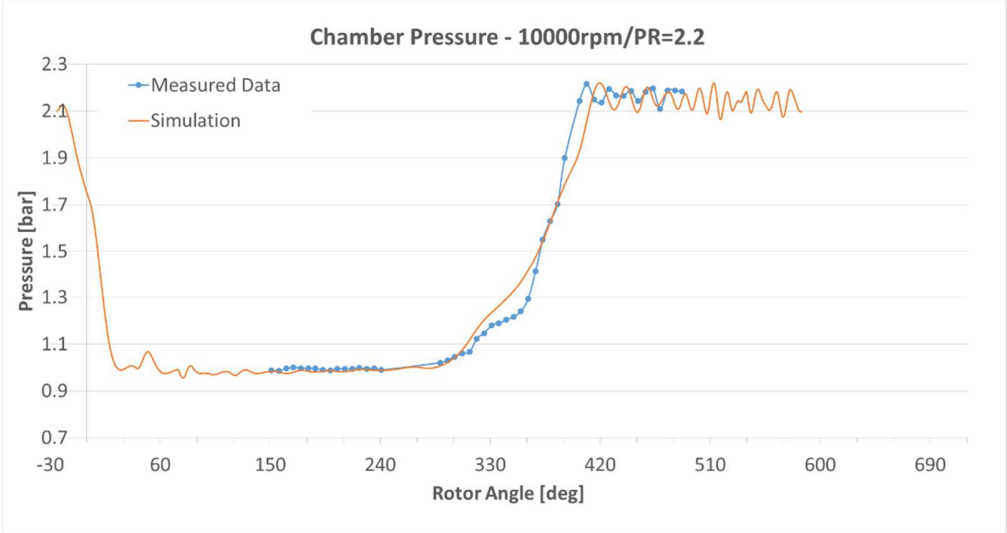
Chamber Pressure - 10000rpm/PR=2.2
Measured Data
Simulation
Pressure [bar]
2.3
2.1
1.9
1.7
1.5
1.3
1.1
0.9
0.7
-30
60
150
240
330
420
510
600
690
Rotor Angle [deg]

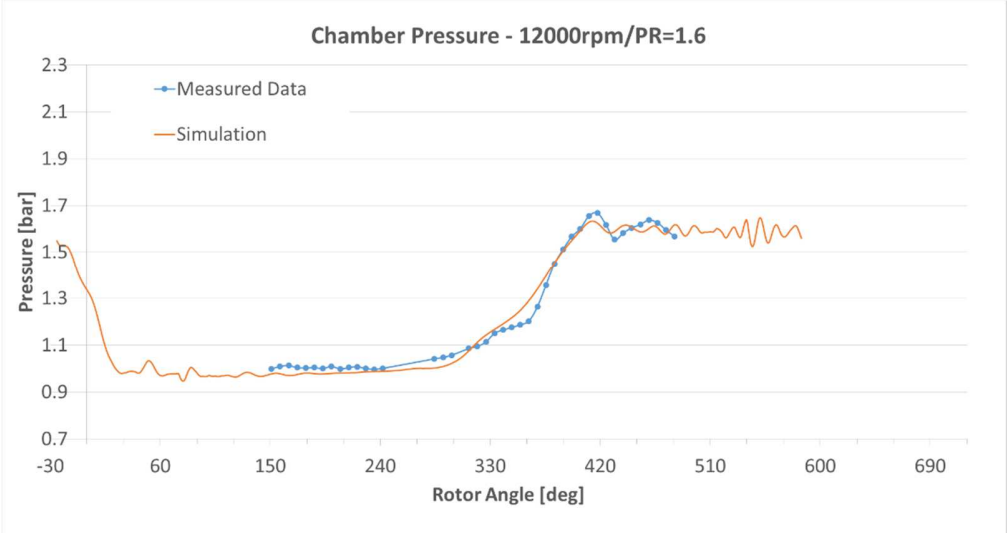
Chamber Pressure - 12000rpm/PR=1.6
Measured Data
Simulation
Pressure [bar]
2.3
2.1
1.9
1.7
1.5
1.3
1.1
0.9
0.7
-30
60
150
240
330
420
510
600
690
Rotor Angle [deg]

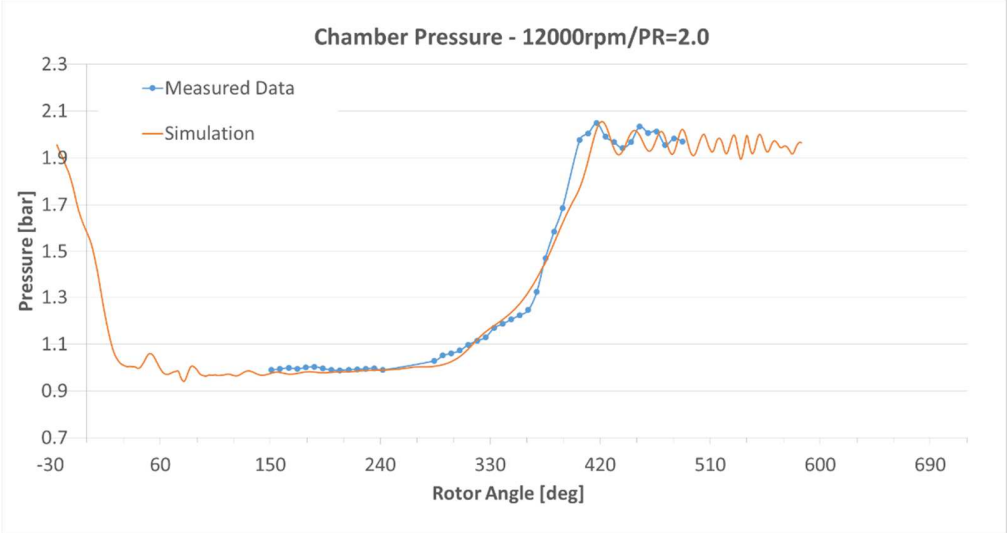
Chamber Pressure - 12000rpm/PR=2.0
Measured Data
Simulation
Pressure [bar]
2.3
2.1
1.9
1.7
1.5
1.3
1.1
0.9
0.7
-30
60
150
240
330
420
510
600
690
Rotor Angle [deg]

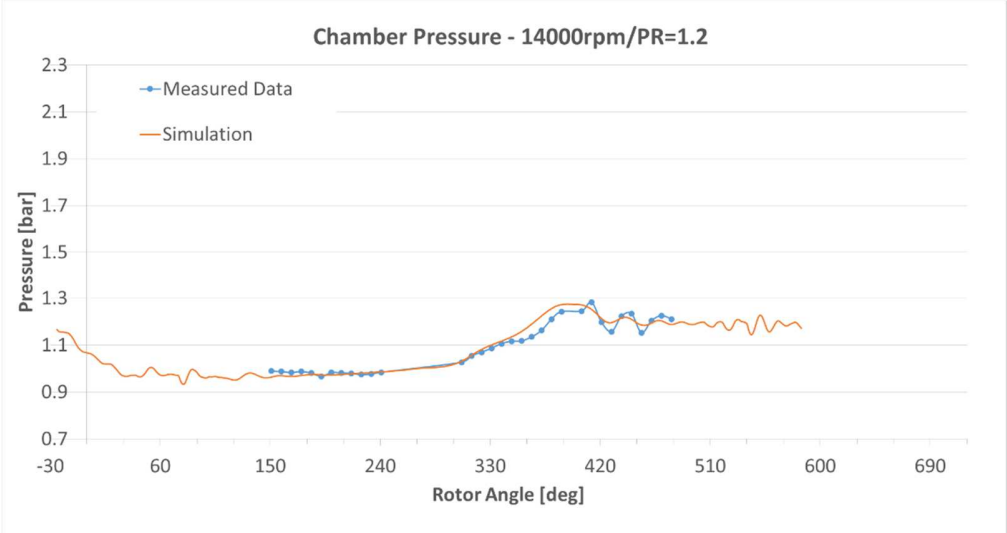
Chamber Pressure - 14000rpm/PR=1.2
Measured Data
Simulation
Pressure [bar]
2.3
2.1
1.9
1.7
1.5
1.3
1.1
0.9
0.7
-30
60
150
240
330
420
510
600
690
Rotor Angle [deg]

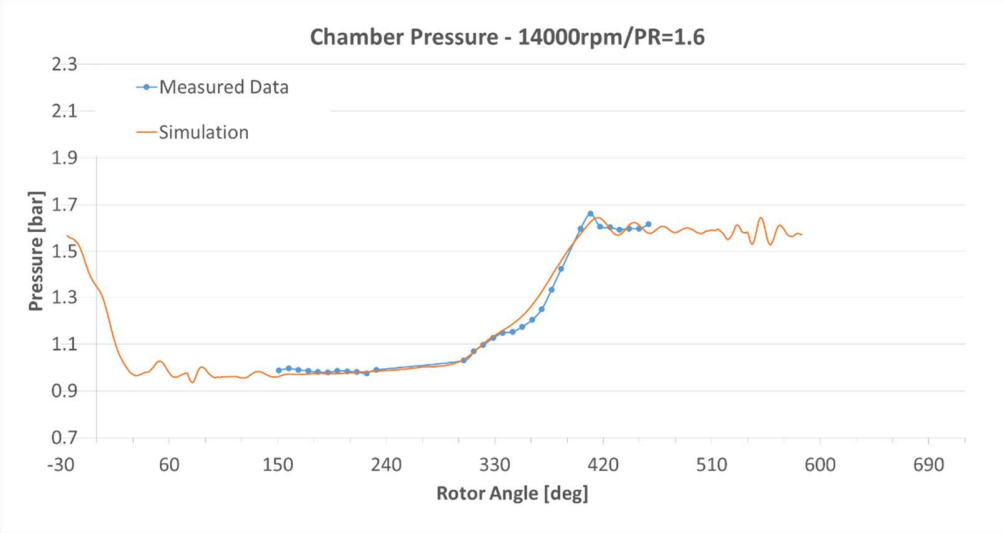
Chamber Pressure - 14000rpm/PR=1.6
Measured Data
Simulation
Pressure [bar]
2.3
2.1
1.9
1.7
1.5
1.3
1.1
0.9
0.7
-30
60
150
240
330
420
510
600
690
Rotor Angle [deg]

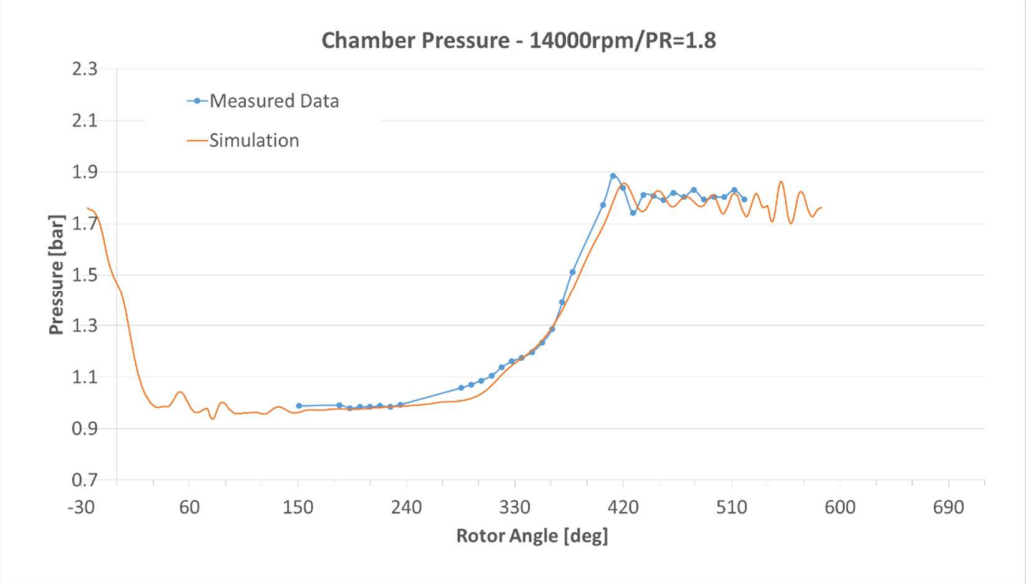
Chamber Pressure - 14000rpm/PR=1.8
Measured Data
Simulation
Pressure [bar]
2.3
2.1
1.9
1.7
1.5
1.3
1.1
0.9
0.7
-30
60
150
240
330
420
510
600
690
Rotor Angle [deg]

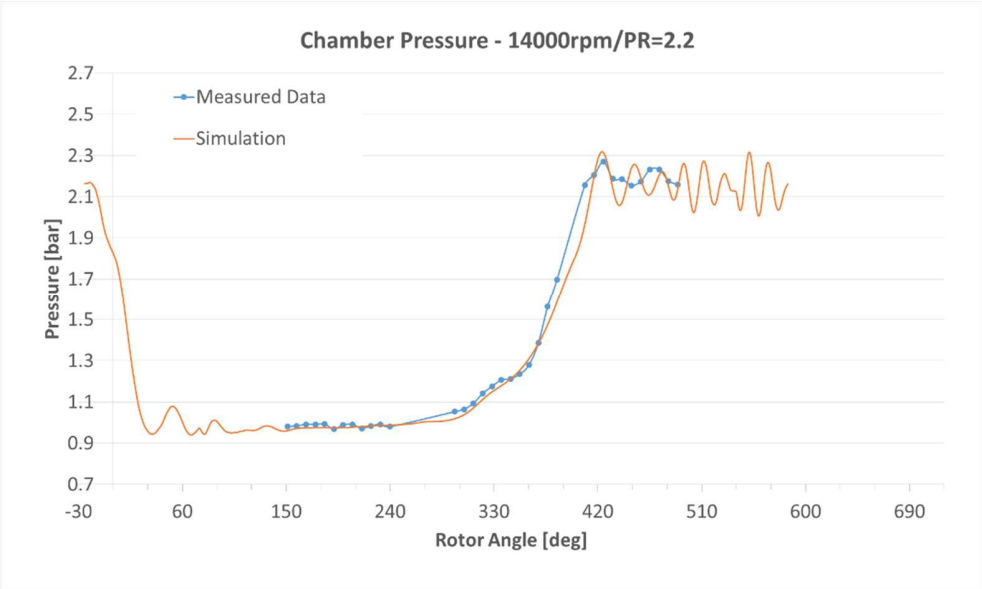
Chamber Pressure - 14000rpm/PR=2.2
Measured Data
Simulation
Pressure [bar]
2.7
2.5
2.3
2.1
1.9
1.7
1.5
1.3
1.1
0.9
0.7
-30
60
150
240
330
420
510
600
690
Rotor Angle [deg]

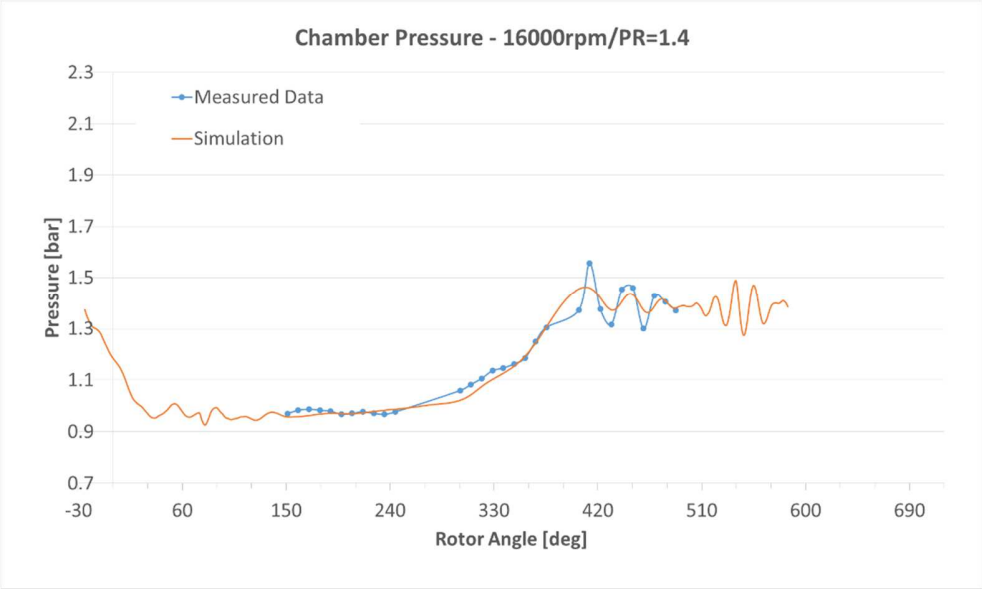
Chamber Pressure - 16000rpm/PR=1.4
Measured Data
Simulation
Pressure [bar]
2.3
2.1
1.9
1.7
1.5
1.3
1.1
0.9
0.7
-30
60
150
240
330
420
510
600
690
Rotor Angle [deg]

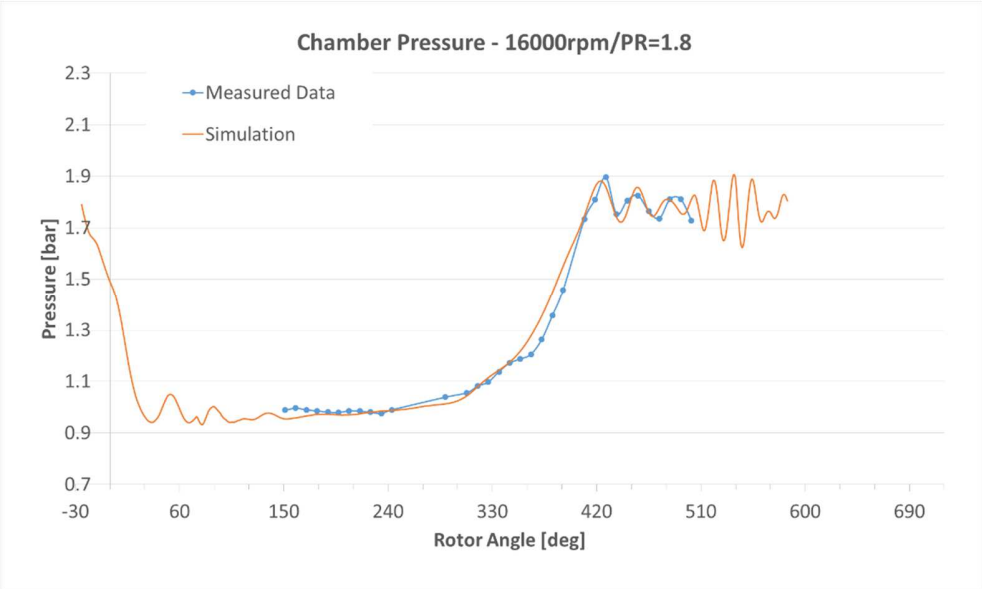
Chamber Pressure - 16000rpm/PR=1.8
Measured Data
Simulation
Pressure [bar]
2.3
2.1
1.9
1.7
1.5
1.3
1.1
0.9
0.7
-30
60
150
240
330
420
510
600
690
Rotor Angle [deg]

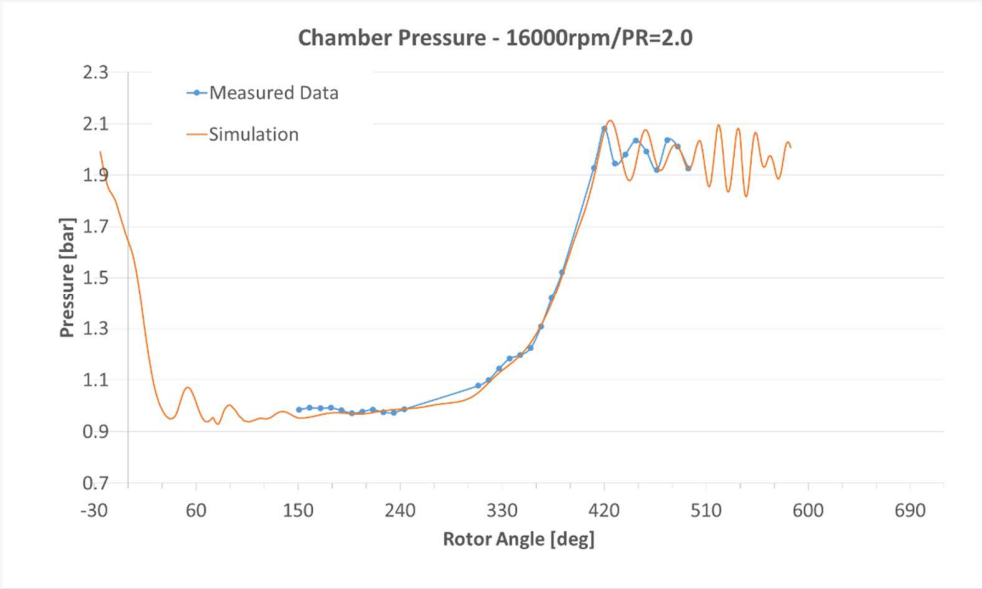
Chamber Pressure - 16000rpm/PR=2.0
Measured Data
Simulation
Pressure [bar]
2.3
2.1
1.9
1.7
1.5
1.3
1.1
0.9
0.7
-30
60
150
240
330
420
510
600
690
Rotor Angle [deg]

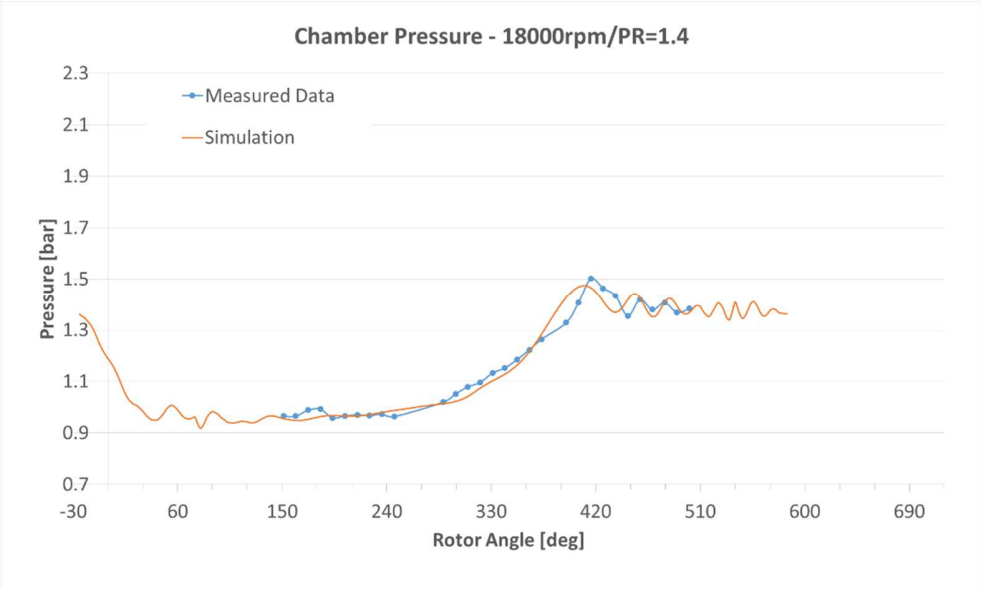
Chamber Pressure - 18000rpm/PR=1.4
Measured Data
Simulation
Pressure [bar]
2.3
2.1
1.9
1.7
1.5
1.3
1.1
0.9
0.7
-30
60
150
240
330
420
510
600
690
Rotor Angle [deg]

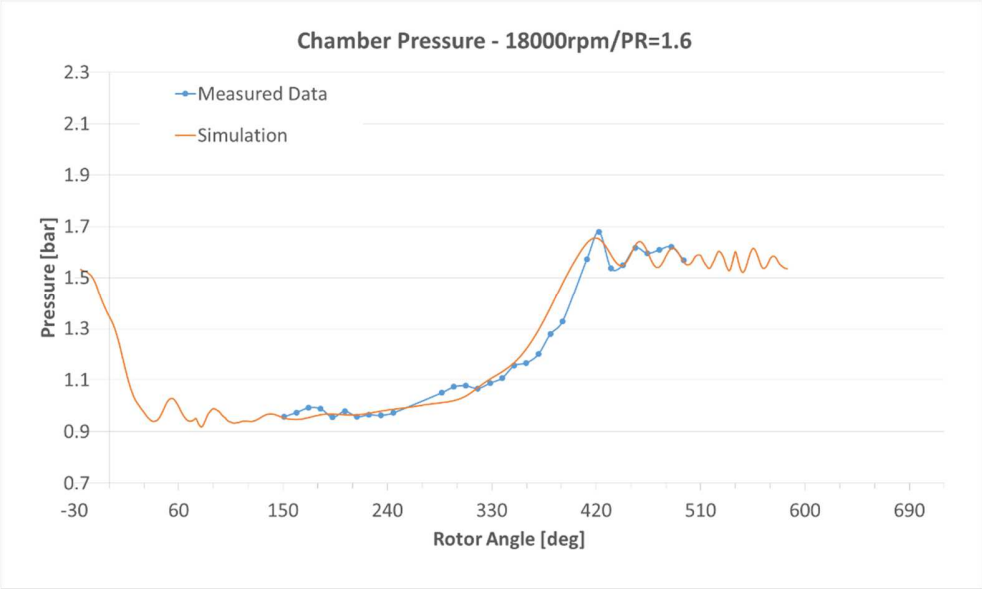
Chamber Pressure - 18000rpm/PR=1.6
Measured Data
Simulation
Pressure [bar]
2.3
2.1
1.9
1.7
1.5
1.3
1.1
0.9
0.7
-30
60
150
240
330
420
510
600
690
Rotor Angle [deg]

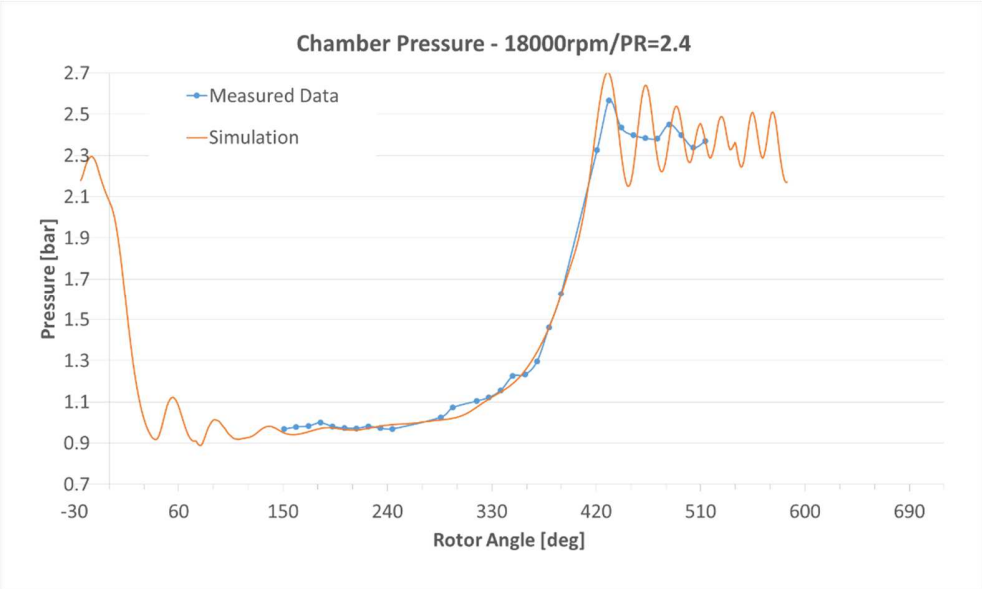
Chamber Pressure - 18000rpm/PR=2.4
Measured Data
Simulation
Pressure [bar]
2.7
2.5
2.3
2.1
1.9
1.7
1.5
1.3
1.1
0.9
0.7
-30
60
150
240
330
420
510
600
690
Rotor Angle [deg]

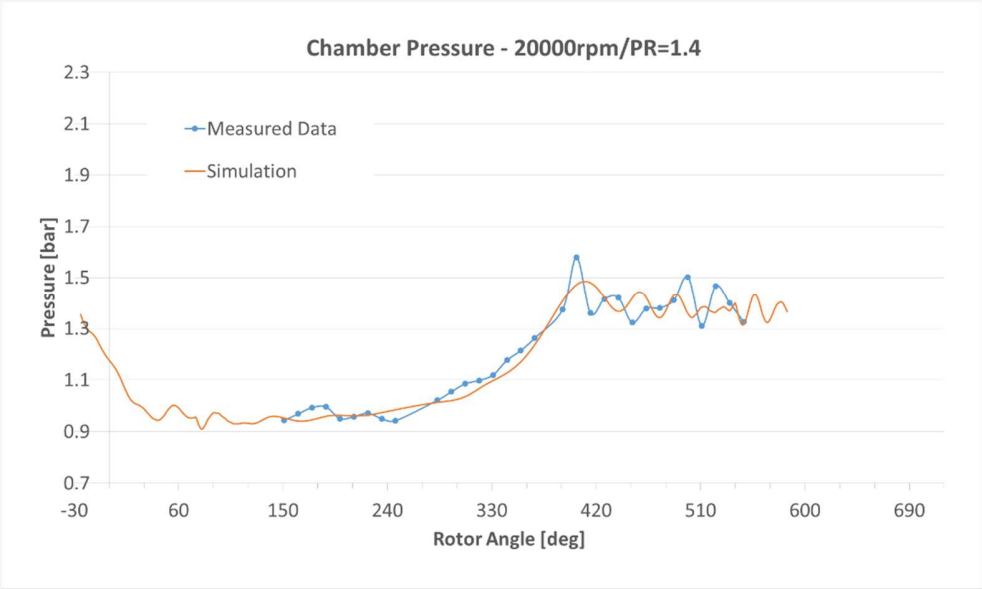
Chamber Pressure - 20000rpm/PR=1.4
Measured Data
Simulation
Pressure [bar]
2.3
2.1
1.9
1.7
1.5
1.3
1.1
0.9
0.7
-30
60
150
240
330
420
510
600
690
Rotor Angle [deg]

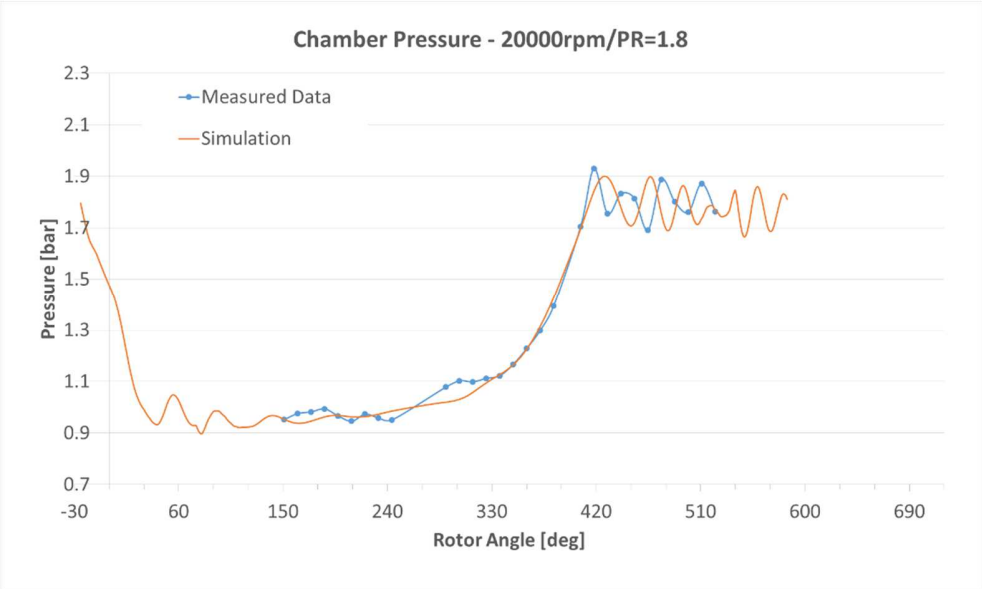
Chamber Pressure - 20000rpm/PR=1.8
Measured Data
Simulation
Pressure [bar]
2.3
2.1
1.9
1.7
1.5
1.3
1.1
0.9
0.7
-30
60
150
240
330
420
510
600
690
Rotor Angle [deg]

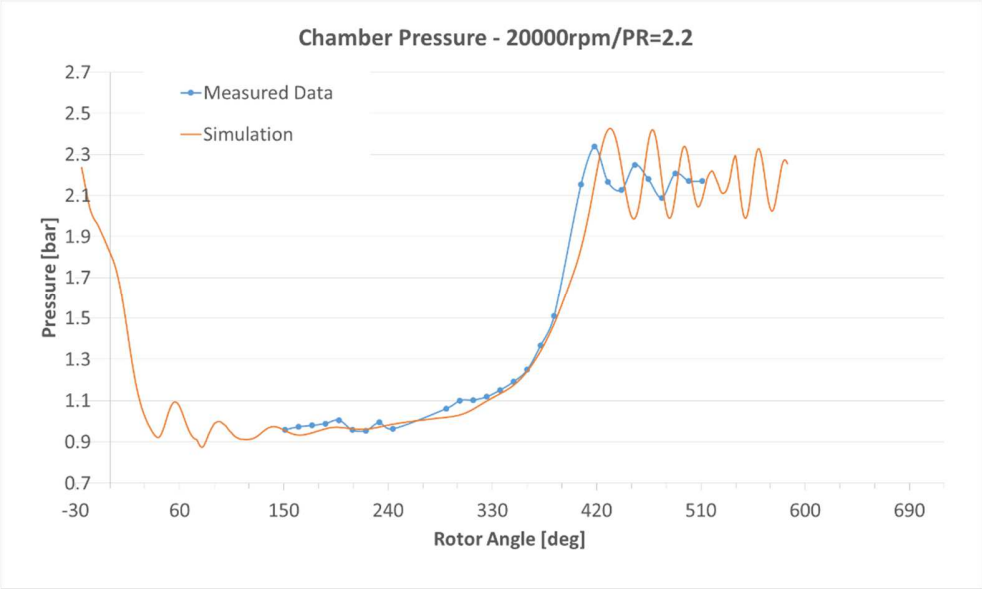
Chamber Pressure - 20000rpm/PR=2.2
Measured Data
Simulation
Pressure [bar]
2.7
2.5
2.3
2.1
1.9
1.7
1.5
1.3
1.1
0.9
0.7
-30
60
150
240
330
420
510
600
690
Rotor Angle [deg]

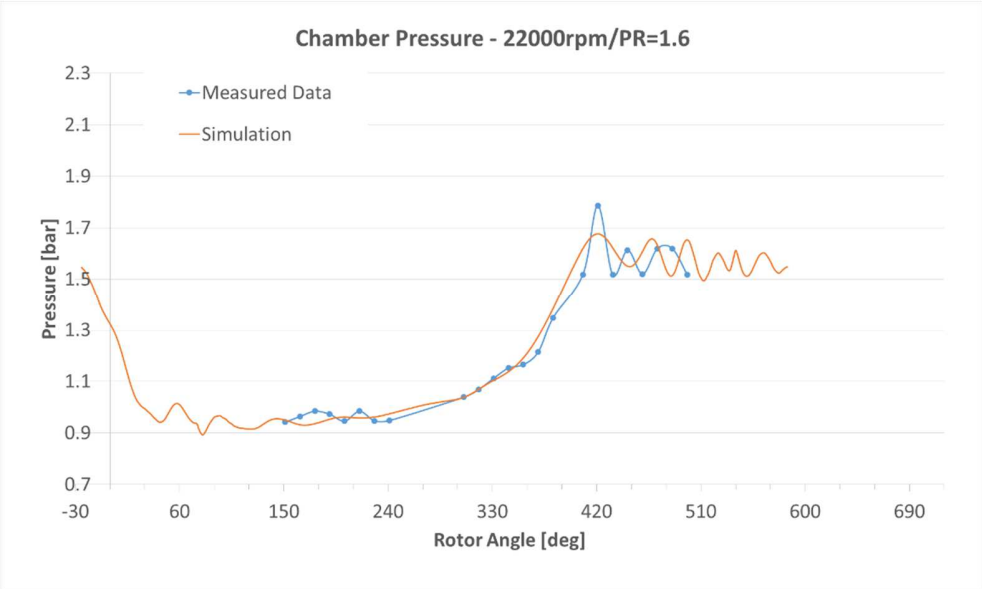
Chamber Pressure - 22000rpm/PR=1.6
Measured Data
Simulation
Pressure [bar]
2.3
2.1
1.9
1.7
1.5
1.3
1.1
0.9
0.7
-30
60
150
240
330
420
510
600
690
Rotor Angle [deg]

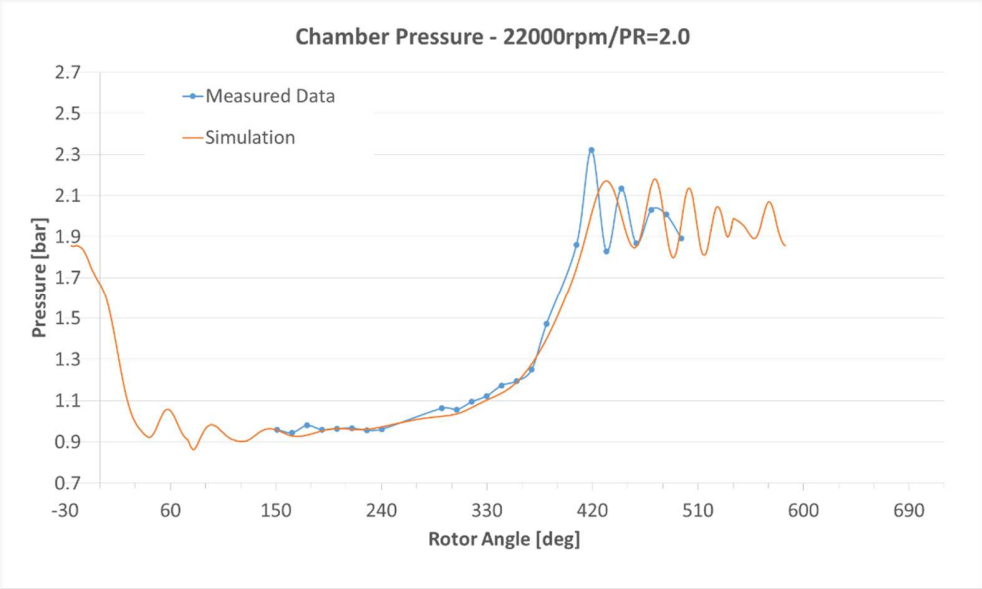
Chamber Pressure - 22000rpm/PR=2.0
Measured Data
Simulation
Pressure [bar]
2.7
2.5
2.3
2.1
1.9
1.7
1.5
1.3
1.1
0.9
0.7
-30
60
150
240
330
420
510
600
690
Rotor Angle [deg]

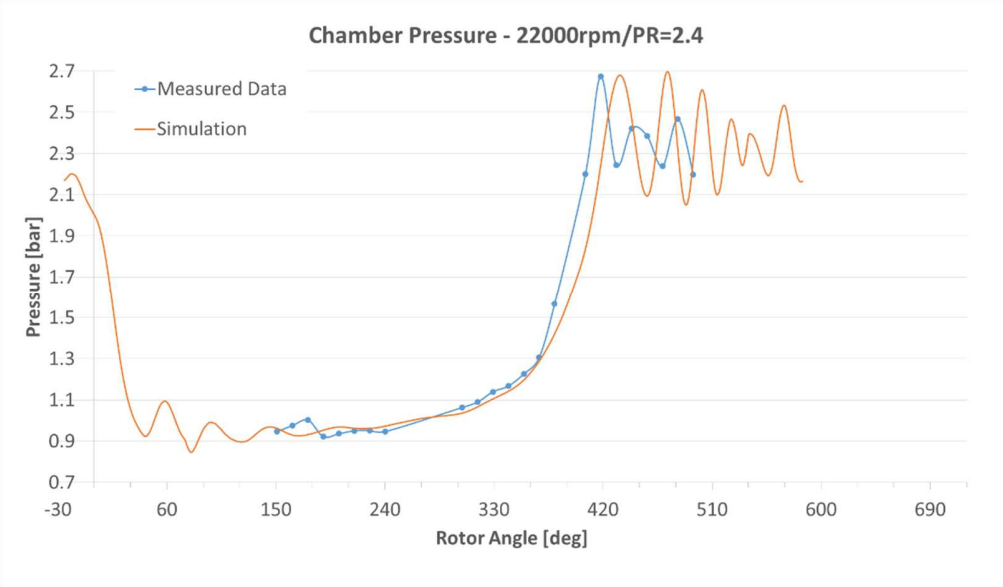
Chamber Pressure - 22000rpm/PR=2.4
Measured Data
Simulation
Pressure [bar]
2.7
2.5
2.3
2.1
1.9
1.7
1.5
1.3
1.1
0.9
0.7
-30
60
150
240
330
420
510
600
690
Rotor Angle [deg]

Appendix B

Simulation results and measured data of the M-type supercharger map are shown in this **Appendix B** for limited number of operating points considered during 1-D model calibration.

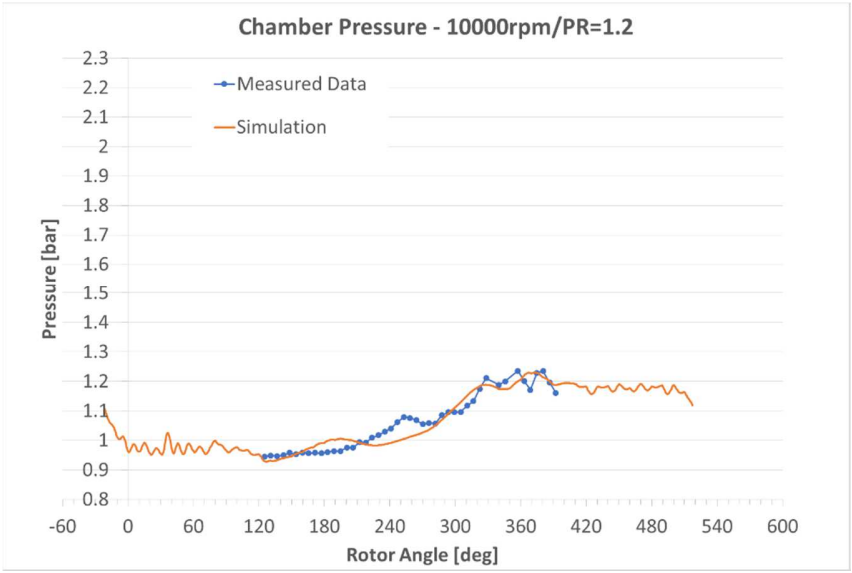

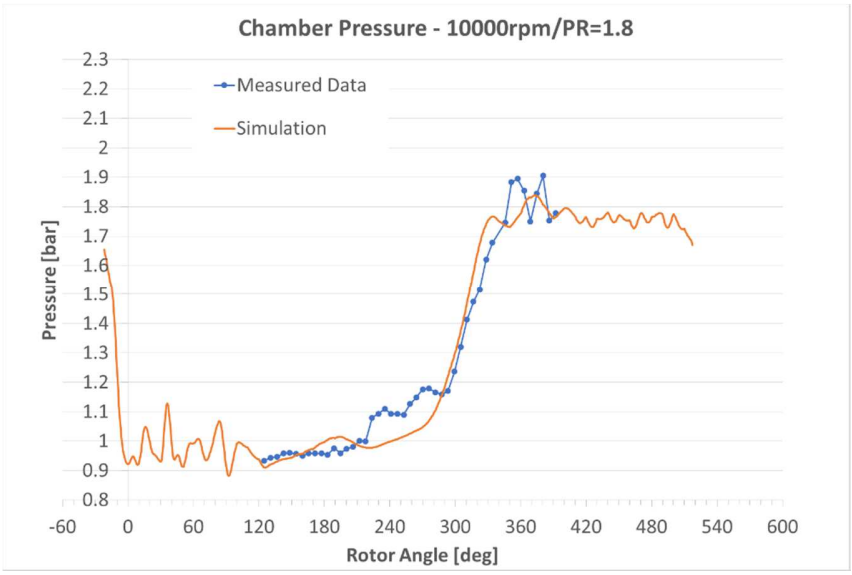

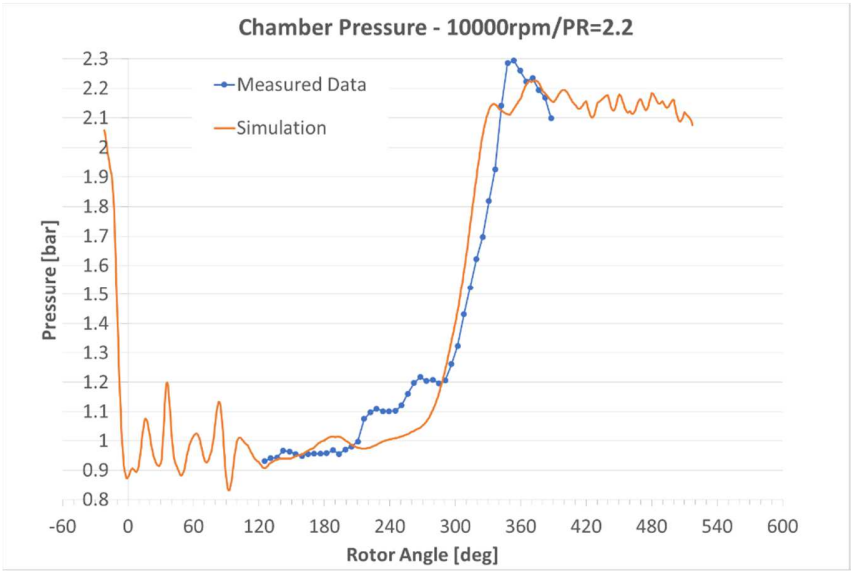
Chamber Pressure - 10000rpm/PR=2.2
Measured Data
Simulation
Pressure [bar]
Rotor Angle [deg]

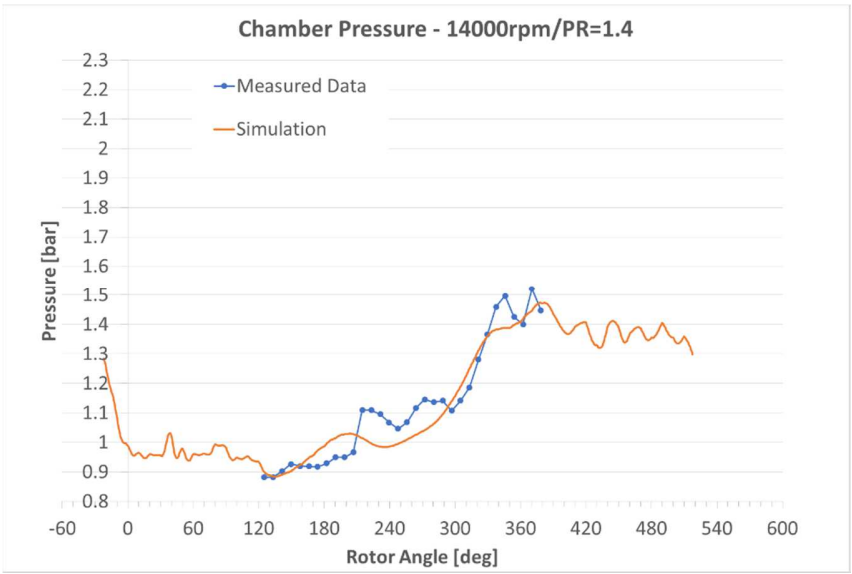
Chamber Pressure - 14000rpm/PR=1.4
Measured Data
Simulation
Pressure [bar]
Rotor Angle [deg]

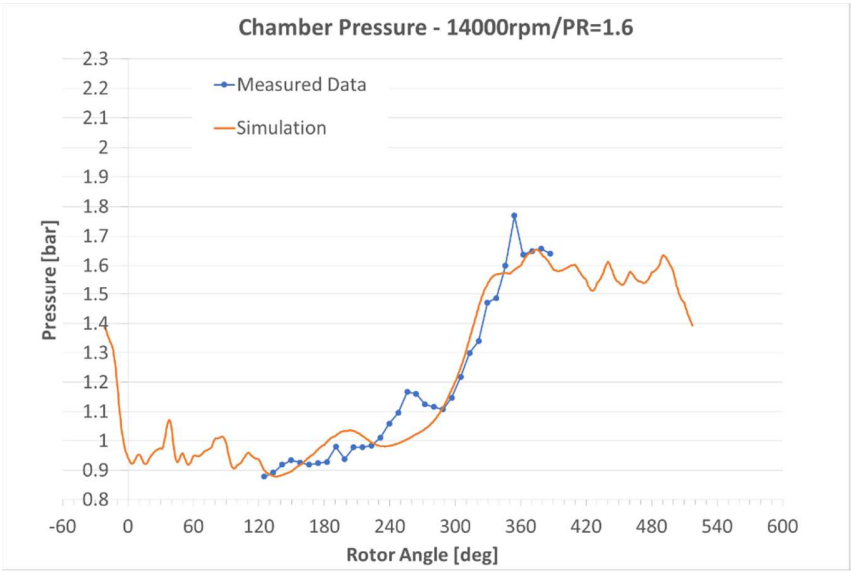
Chamber Pressure - 14000rpm/PR=1.6
Measured Data
Simulation
Pressure [bar]
Rotor Angle [deg]
2.3
2.2
2.1
2
1.9
1.8
1.7
1.6
1.5
1.4
1.3
1.2
1.1
1
0.9
0.8
-60
0
60
120
180
240
300
360
420
480
540
600

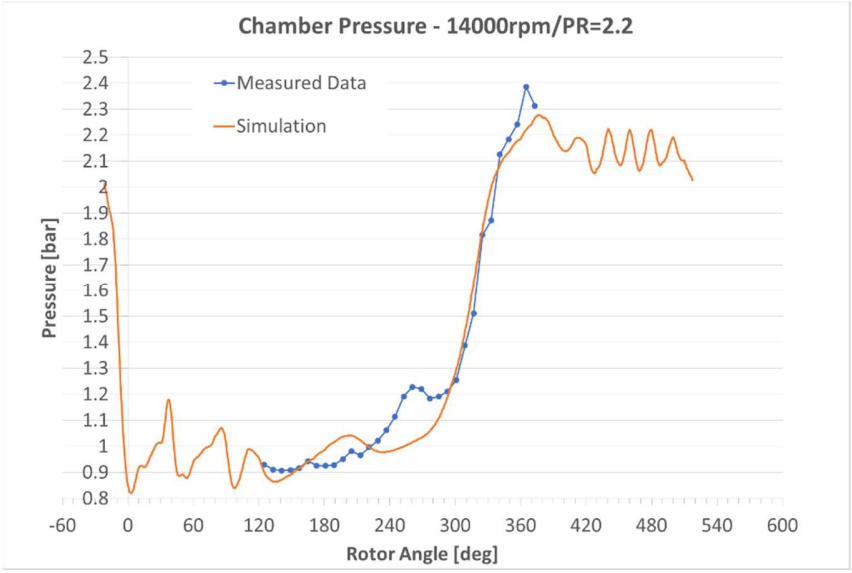
Chamber Pressure - 14000rpm/PR=2.2
Measured Data
Simulation
Pressure [bar]
Rotor Angle [deg]
2.5
2.4
2.3
2.2
2.1
2
1.9
1.8
1.7
1.6
1.5
1.4
1.3
1.2
1.1
1
0.9
0.8
-60
0
60
120
180
240
300
360
420
480
540
600

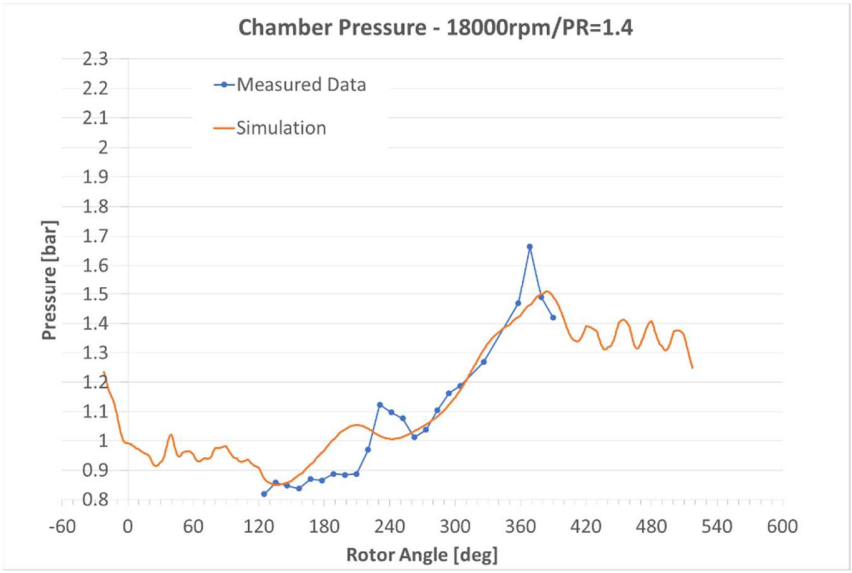
Chamber Pressure - 18000rpm/PR=1.4
Measured Data
Simulation
Pressure [bar]
Rotor Angle [deg]

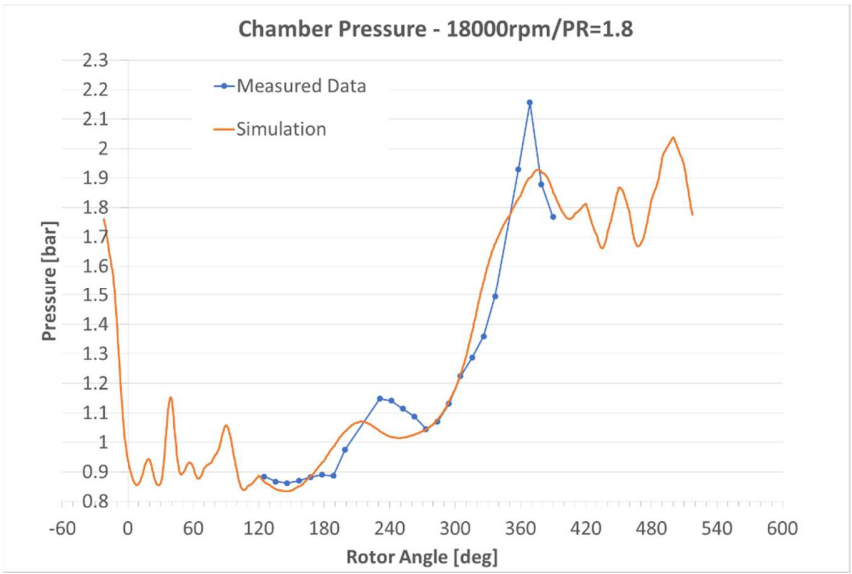
Chamber Pressure - 18000rpm/PR=1.8
Measured Data
Simulation
Pressure [bar]
Rotor Angle [deg]

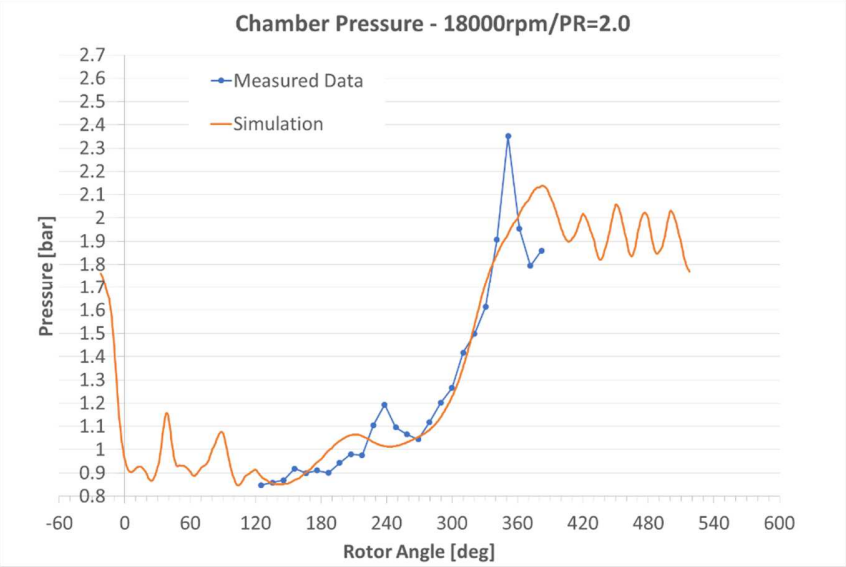
Chamber Pressure - 18000rpm/PR=2.0
Measured Data
Simulation
Pressure [bar]
Rotor Angle [deg]
2.7
2.6
2.5
2.4
2.3
2.2
2.1
2
1.9
1.8
1.7
1.6
1.5
1.4
1.3
1.2
1.1
1
0.9
0.8
-60
0
60
120
180
240
300
360
420
480
540
600